UNIVERSITA' DEGLI STUDI DI PARMA

Dottorato di ricerca in Scienza e Tecnologia dei Materiali

Ciclo XXIX (2014-2016)

TiO_2 based memristive devices towards controlling performances and interfacing

Coordinatore:

Chiar.mo Prof. Enrico Dalcanale

Tutor:

DR. Salvatore Iannotta

DR. Roberto Verucchi

Dottorando: Giovanni Giusti

to Roberto P.

I am always doing what I cannot do yet, in order to learn how to do it

— *Vincent Van Gogh*

Abstract

The main aims of this thesis are to evaluate suitability of TiO_2 thin films, synthesized by Pulsed Microplasma Cluster Source (PMCS), for realization of devices showing memristive response and that could be used in a neuron-memristor hybrid system, where biological system and electronics could interact each other. All research activities have been carried out at the IMEM-CNR laboratories of Trento, in the mainframe of a four-year project named Madelena where different partners are involved, with skills from materials science to electronics and biology. The PMCS deposition technique uses supersonic molecular pulsed beams seeded by clusters of the metal oxide synthesized in a plasma discharge. In order to achieve the film properties necessary for electronic applications, by a tough optimization of the deposition process it has been possible to synthesize TiO_2 thin films having suitable, controlled and reproducible properties. In general, all PMCS thin films showed an anatase TiO_2 structure, grain dimension size lower than 20nm, an average roughness of about 3nm and with the possibility to control oxygen stoichiometry, with a O/Ti ratio from 2 to 2.2 by changing the composition of the used gas carrier.

The inedited employing of the PMCS in memristive application showed promising results. Indeed, using as top electrode a Pt wire, all the PMCS TiO_2 have exhibited a significant memristive response, modulated by the intrinsic chemistry of the material. In particular by increasing of the percentage of oxygen in the matrix, both resistances (ON state and OFF state) and the voltage switch increases. Moreover, a MIM device has been realized showing same main electrical properties, with device life as long as 1000 cycles.

To achieve the proposed challenging final aims, an important study has been carried on the biocompatibility and neurocompatibility of TiO_2 grown by PMCS. All the films guaranteed consistent biocompatibility and a spontaneous absorption of poly-D-lysine (PDL) that has increased their neurocompatibility. Moreover, the electrical activities of the neural culture grown on the TiO_2 film can be modulated by changing of the surface chemistry.

Finally, starting with these significant and promising results, a prototype of PMCS TIO_2 based on memristor-neuron hybrid system was designed and realized, opening new perspectives for the realization of more complex bio-inspired devices.

Index

List of figures

List of tables

Chapter 1
Introduction

1.1 Memristors and memristive devices

The memristor, the missing electronic element predicted in 1971 by Leon Chua, has attracted a great deal of attention since 2008, when an HP, Hewlett Packard group claimed it. An essential property is the dependence of its resistance on the total charge that has passed through it. None of reported devices can be considered an ideal memristor so that the term "memristive device" has been suggested. HP memristors were made of TiO_2 where switching in conductivity is attributed to drifts of the oxygen vacancies under the applied electric field. Indeed, most of memristive devices to date are based on metal oxide layers, synthesized by different techniques but always characterized by thickness at the nanoscale. The majority of available patents on inorganic memristive devices still belongs to HP, mainly interested to realize non-volatile memories based on these passive elements, with low power consumption and intrinsic nanoscale dimensions. However, despite of the different examples that can be find in literature, as well as the great efforts developed by HP and important labs, memristive devices typically have strong lacks in reliability and reproducibility. These are major problems for electronics applications, and some first backward steps have been reported, especially from HP that removed memristors in “The machine” project, a new supercomputer. However, memristor would be a great step towards the so called post-Moore electronics, capable of overcoming the physical, technological, and economical limits of circuit integration and traditional electronics. This is particularly true if we consider that computers will be soon required to accomplish some goals in which the brain of man, and even of animals, is so skilled, but which are still undefeatable hurdles for artificial systems.

This applicative objective goes, in turn, hand in hand with another goal more oriented to basic science, i.e. setting up hardware models of (parts of) the brain to understand the way it works more easily than it can be done in terms of in vivo studies, possibly interfacing machines and nervous systems as seamlessly as possible.

It is clear that both goals are beyond the present computers' capabilities, as current electronic hardware works on a sequential basis and it cannot be modified, as opposed to the natural "nervous hardware" which is highly parallel and plastic. Efforts have been made in the past decades to partly mimic nature (i.e. by neural networks), but results have been comparatively poor, because all learning and processing is curbed within software which, in turn, is designed for traditional hardware.

Having in mind this panorama, memristors could really be the key factor. Such devices can be made more or less conductive, and in this sense, they can be compared to natural synapses in neuronal network, where learning means, physically speaking, repeatedly activating the right connections to reinforce them over the wrong ones. Thus, memristors have adaptive learning ability and could be used as computing element able to perform both storage and processing of data, as in natural neurons. Their known poor repeatability could be overcome with redundancy, as actually occurs with neurons and synapses. However, new electronic architecture have to be developed and, nevertheless, more should be done to improve memristive material properties and reliability.

1.2 A different approach: from materials synthesis to biological interfaces

Development of memristive materials is a great task, and the constantly increasing number of publications on this topic suggests that, probably, it is not so difficult to achieve a reasonable level of performances but is still quite far the ability to properly control, reproduce it. New and challenging approaches are thus necessary.

In this thesis work, a different method to material synthesis will be exploited to grow TiO_2 thin films. It is based on supersonic pulsed molecular beams seeded by clusters of metals or

metal oxides: film growth is achieved by deposition of these aggregates that form a compact structure, typically characterized by a good degree of nanocrystallinity.

It has been widely used to grow active elements for gas sensing, with devices showing high performances and possibility to actively interface with organic molecules. The Pulsed Microplasma Cluster Source approach (PMCS) has never been proposed for development of memristive materials, a great challenge if we consider the highly different requirements and characteristics of an electronic device with respect to a gas sensor. Nevertheless, PMCS potentialities will be investigated and exploited for this purpose, synthesizing TiO_2 thin films towards achievement of memristive properties.

And further exploiting the known features of PMCS TiO_2 to create active interface with organic materials, a whole new class of bio-memristive systems could be developed, where the signals and information coming from a bio-system, in particular a neuronal tissue, is exchanged with and/or controlled by the interconnected memristive devices, systems and/or networks. This is a goal of great relevance, it could overcome the strong limitations that are facing the present approaches to study brain properties, based on biocompatible electrodes coupled to standard electronics.

The new proposed approaches represent a great deal, facing problems of materials science, realization of electronic devices up to interfacing of inorganics memristors with organic tissues. Such a challenging study can be developed only in an interdisciplinary framework, putting together different skills, from chemical/physical to biological and medical. This thesis work has pursued the proposed aims and objectives managing different techniques and expertise, trying to get rid of the intrinsic differences and difficulties to properly exchange information between different research areas by constantly connecting people and interfacing techniques.

The efforts required were well above the possibilities of a single PhD thesis, in fact this work has been developed within the Madelena project, that involves different groups in several research areas and has, within its final aims, the realization of memristive devices and their interfacing with neuronal tissues. Concurrently, the Madelena project has taken great advantage from the studies and knowledge here generated, in particular for the tight collaboration network that had this thesis work as center of gravity.

1.3 Thesis structure

In order to make the description of the results most effective, the different chapters of this work have been organized to focus on the different phases of the thesis work and report the main results obtained in each of them.

In Chapter 2 the basis of the memristors theory, as well as of the processes leading to the observed memristive effect will be presented.

Chapter 3 will focus the attention on the deposition technique (PMCS) for the synthesis of TiO_2 thin films, starting from the theory of supersonic molecular beams and most relevant examples of PMCS material synthesis in literature.

In Chapter 4 will be described the PMCS experimental apparatus, as well as the different techniques used for all material characterizations.

In Chapter 5 will be reported the developments of PMCS carried out at IMEM-CNR of Trento, focusing the attention on the upgrades provided to the deposition technique, as well as on the achieved synthesis protocols. Moreover, the results for analysis of morphology, structure and chemical/physical properties will be shown.

Chapter 6 will discuss the electrical response of PMCS TiO_2 thin films under different viewpoints, exploring the memristive properties and giving several interpretations about the formation and tuning of the conducting filament properties, which is indeed one of the aim of this thesis work.

Chapter 7 will report the study of the bio-neurocompatibility of PMCS TiO_2 films in biological environments, from organic cells to growth of complex neuronal tissues. This is the preliminary step toward the realization of a hybrid device, where inorganic/organic interfacing will be exploited to exchange signal from memristor to neurons and vice versa. Preliminary results will be presented in Chapter 8.

Final conclusions and perspectives, also considering the development of the Madelena project, will be finally presented in Chapter 9 .

Chapter 2
Memristor: theory and devices

2.1 History of the memristor

The concept of memristor (memory resistor) was first proposed by Chua four decades ago [1]. His observation of the symmetry between the three fundamental circuit elements – resistor, capacitor, and inductor – led to the proposal of a fourth element, connecting the missing link between charge and flux to complete the relationships between the four physical variables: voltage, flux, current, and charge (Figure 2.1). This element would behave as a nonlinear two-terminal resistor with memory, thus termed "memristor".

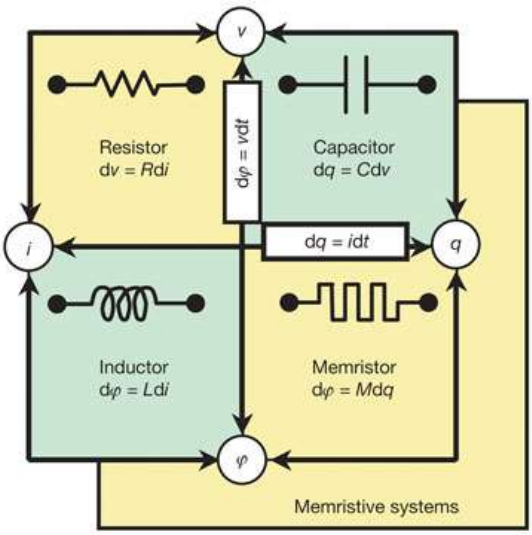

Figure 2.1: The four fundamental circuit elements and their respective relationships.

Chua and Kang [2,3] formulated the "*memristive system*" into a set of equations and generalized this definition to any two-terminal system that can be described by the theory when appropriate variables and expressions are chosen.

For a "voltage-controlled" memristor, this set of equations can be written as

$$v = R(w)i \tag{1}$$

$$\frac{dw}{dt} = f(w,t) \tag{2}$$

Where *w* can be an internal state variable, and *R* and *f* can in general be explicit function of time. Chua and Kang also pointed out that the "quasi-static" conduction equation that links the voltage across the device with the current through it at any particular time, and the dynamical equation that considers the state variable *w* as a time varying function of itself and possibly the current thought the device, are two critical equations to characterize memristive systems.

Notwithstanding the availability of the mathematic model, memristor has not received much attention from worldwide researchers until, in 2008, Strukov et al. [4,5] proposed a nanoscale TiO_2 device model to achieve the memristive behavior. Since then, massive research enthusiasm has been devoted to the exploration of the innovative memristor technologies, resulting in many technical publications and a large number of US patents. Under this circumstance, the necessity to strictly distinguish memristor from memristive system becomes unimportant, and Chua has therefore recommended to simplify the nomenclature by referring to both as memristors, since in fact the generalization is a 'trivial extension' [2]. In this work, Chua also gave a broader definition of memristor that includes all 2-terminal non-volatile memories based on resistive switching.

As the memristive behavior has been found on a wide variety of systems (unipolar and bipolar resistive switches, magnetic spin-torque transfer device and phase-change memories), Chua has further expanded the scope of the memristor to:

"Any 2-terminal device that exhibits a pinched hysteresis loop in the v-i plane when driven by any bipolar periodic voltage or current waveform, for any initial conditions" [6].

Such a definition is finally accomplished in Chua's most recent publications [7,8] so as to be suited for the original definition of the ideal memristor as well as of the generalized definition for memristive system:

"*any 2-terminal black box is called a memristor if, and only if, it exhibits a pinched hysteresis loop for all bipolar periodic input current signals (or input voltage signals) which result in a periodic voltage (or current) response of the same frequency in the voltage-current (v-i) plane".*

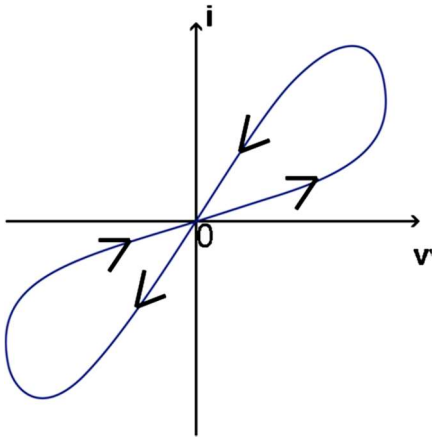

Figure 2.2: A typical pinched hysteresis loop of the memristor.

The most representative attribute of the memristor is its current–voltage (I–V) curve that exhibits a pinched hysteresis loop, as shown in Figure 2.2. Such a pinched hysteresis loop, which always passes through the origin, plays an essential role in characterizing the *v-i* relationship of a memristor excited by any periodic current source (resp., voltage source) that spans both positive and negative values over each period.

It is to be noted that the shape of the pinched hysteresis loop would vary along with the change of the frequency and the amplitude of the input waveform. In this case, the *v-i* locus will behave as a normal resistor by increasing frequency towards infinity, but still including the origin. It is instructive to realize that the pinched hysteresis loop is not derived from a mathematical model, but is an inherent feature of the memristor [8]; any device that exhibits a pinched hysteresis loop over any bipolar periodic testing input signals is considered as a memristor, regardless of the shape of the loop.

The reason that memristor has become one of the current scientific focus arises from its extraordinary properties. First, as suggested by Figure 2.2, if the memristor is in its equilibrium state at some certain moment, i.e., $v = i = 0$, the memristor does not lose the values of the magnetic flux and the electric charge when both voltage and current are zero

at the instant when the power is switched off, but rather makes the original values unchanged. This would enable memristor to remember its most recent state when facing a power-off, exhibiting the potential of being a non-volatile memory. In addition, the feasibility of scaling memristor to 10 nm and even below has been demonstrated [9], indicating a potential for much higher integration density than current non-volatile memories. More importantly, the attribute that the resistance dynamically changes according to the applied stimulus would allow memristor to imitate functions of brain synapse whose state can be changed via the interactive strength between two neurons. Therefore, memristor has been proposed to be utilized for a wide range of applications including non-volatile memory, dynamic load, neuromorphic system, and image processing, and a set of memristor devices have been designed at the laboratory level such as resistive memristor [10-17], polymeric memristor - [18-20], ferroelectric memristor [21,22]) and spintronic memristor [23,24] and much more.

Among the several scientific fields in which the memristor concept could be employed, recently works have proved their usefulness also in neuroscience, and in particular in Artificial Intelligence applications (A.I.). It has been shown that synapse action [16,25] is memristive and the ion channels involved in neuronal signal transport can be modelled as biological memristors. In fact, the time-varying resistors in Hodgkin-Huxley's electrical model of the neuron have been more properly identified as memristors [26,27]. In a computer neural net, the memristors can act as synapses where the conductivity of a memristor connection is taken as the synaptic weight of that connection. During the training period, the synaptic weight increases as the resistance of the memristor decreases. Some examples of memristive synapses in neural nets are [16,28-31]. Starting from this concept, Gale et al [32] proposed an innovative experimental setup in which memristors and neuronal culture grown on a Multi Electrode Array (MEA) device were able to actively communicate each other. The promising results pave the way towards the design of hybrid system which could interact with biological environment, mimicking their intrinsic behavior.

Nevertheless the great number and kind of memristor available, in this work the attention will be focused on a specific category of memristor, i.e. the resistance switching inorganic memristive devices, in particular based on TiO_2

2.2 TiO_2 resistance memristor

TiO_2 is a semiconducting oxide with a wide range of application such as photocatalyst [33], gas sensor [34-36] and electrode in solar cell devices. [37,38] In fact, several previous studies have shown that TiO_2 exhibits n-type semiconducting property with extra electron carriers generated by the formation of oxygen vacancies [39,40], as occurs for many electrical and chemical properties of most of transition metal oxide (TMO) that are affected by point defects[41].

From a memristive point of view, TiO_2 has been receiving a great deal of attention, in particular after the fundamental work of Strukov [4], in which demonstrated that a MIM (metal –insulator-metal) consisting of TiO_2 nanometric thin film layer (10nm) sandwiched by two platinum electrodes had a memristive electrical response. In the model proposed by Strukov, it was assumed that the memristor was composed of two resistors in series, one is undoped with high resistance and the other is doped by oxygen vacancies, thus having low resistance [4]. The total thickness of the film is given by that of the doped and undoped regions, and the total resistance is the sum of the two regions. The length of the doped region is taken as the state variable (w), which can be changed by moving the boundary between the two regions under external field due to the drift of oxygen vacancies (Figure 2.3).

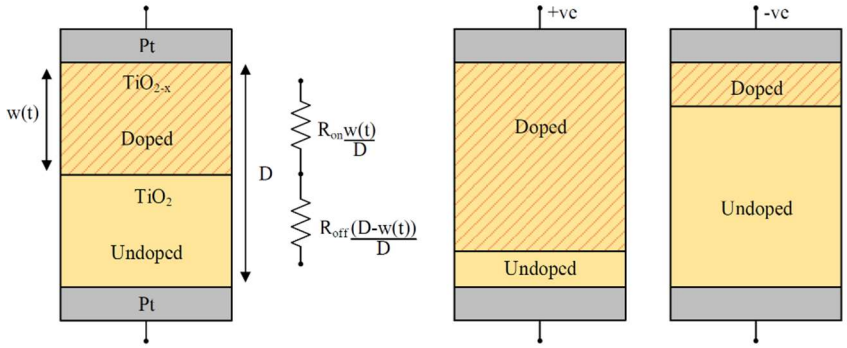

Figure 2.3: Cross section of Pt/TiO_2/Pt Strukov's memristor. Adapted from [42].

Several studies have been carried on TMO thin films according with this model [43-45], reported that the resistance switching is due to a local stoichiometric change by the migration of oxygen vacancies [10].

As donors in TiO_2, the accumulation/depletion of oxygen vacancies can cause an increase/decrease of the local conductance, which in turn results in the modulation of the overall device conductance. This important behavior was deeply study by Yang *et al* [5,10], who evaluated how the drift of oxygen vacancies towards the Pt/TiO_2 Schottky interface, driven by the external electric field, results in the accumulation of oxygen vacancies and the creation of conducting channels that shunt the barrier for electron injection.

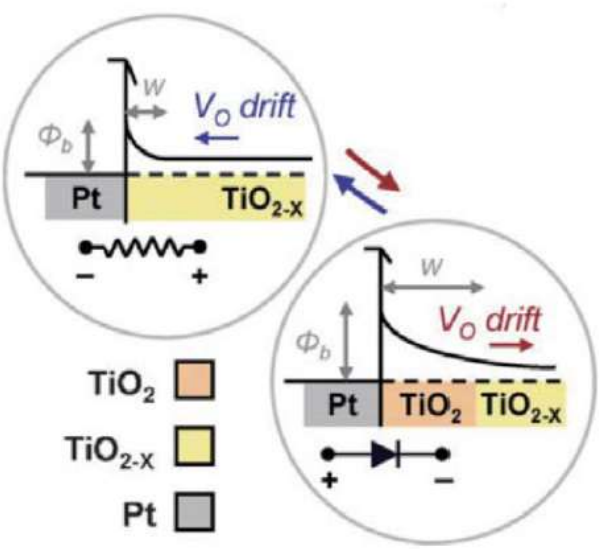

Figure 2.4: Schematics of the set/reset process in bipolar switching. Modulation of the Schottky barrier by oxygen vacancy movements [5].

When applying electric fields with a reverse polarity, the oxygen vacancies are driven away from the Schottky barrier, hence dissolving the conducting channels and switching the device back to OFF state. Later it was demonstrated that the aggregation of oxygen vacancies in TiO_2 in the conductive region may in fact lead to the formation of a new oxygen deficient Magnéli phase (Ti_4O_7) that is more metallic, as directly revealed by TEM studies [46,47].

It has to be highlighted that most of TMO devices, in particular those based on TiO_2, become memristive only after a specific procedure called electroforming (EF). Prior to this process, the metal oxide has a very large resistance, as long as the chemical composition is close to the stoichiometric value. However, under a large external voltage the device can enter into a low resistance state (LRS). During the forming process, some chemical and structural changes take place in the oxide layer caused by the movement of intrinsic defects. As already

mentioned, in Pt/TiO_2/Pt structure, the most common defects are oxygen vacancies, whose concentration and distribution can affect the electrical resistivity of the material. (see Figure 2.5)

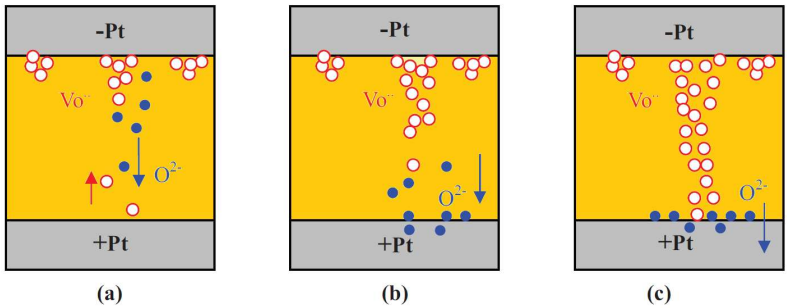

Figure 2.5: Scheme of the electro-forming process: the filaments grow by intrinsic ion migration under effect of the electric field.

The EF process is based on the formation of a first strong conductive filament (CF) composed of Ti_nO_{n-1} Magnéli phase. [46,47]. In this phase, the oxygen vacancies lead to an increase in the electric conductivity of the TiO_2 film due to the relatively higher concentration of free electrons emerged from dangling bonds[48]. Hence, the CF has a higher conductivity compared to the pristine TiO_2 and for this reason, during the EF process, it is important to limit the flowing current to what is termed compliance current (I_{compl}) otherwise the metal oxide film will experience a complete and irreversible dielectric breakdown [49].

After the EF, the resistance of the device can be switched back and forth between a low resistance state (LRS) and a high resistance state (HRS) by controlling the applied voltage. The switching process from HRS to LRS and the corresponding switching voltage are usually named 'SET' process an V_{set}, while the process from LRS to HRS and the required switching voltage are represented by 'RESET' process and V_{reset}. It should be noted that in bi-stable resistive materials, like some transition metal oxides, there are usually two switching modes, i.e., unipolar switching and bipolar switching, as shown in Figure 2.6.

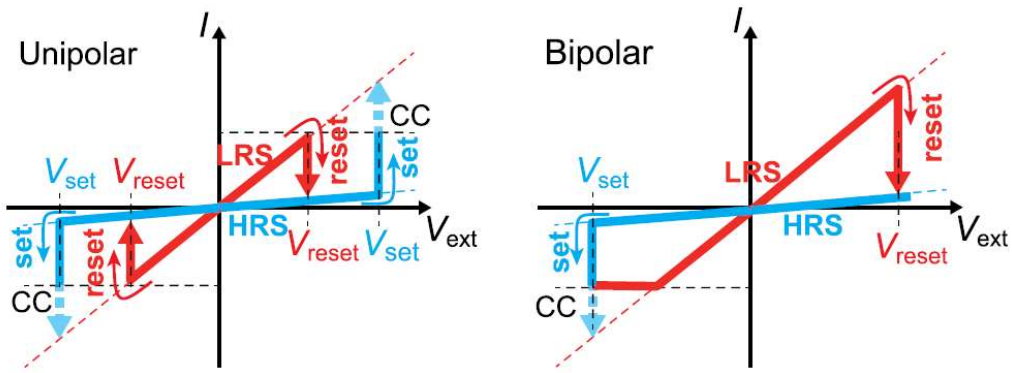

Figure 2.6: Schematic of a typical unipolar I-V curve, which is symmetric with respect to the polarity of an external voltage. Thus, set and reset can occur with a single polarity. (b) Schematic of a typical bipolar I-V curve, which is asymmetric with respect to the polarity of an external voltage [50].

Unipolar switching allows for a switching process that is independent of the voltage/current polarity. Therefore, the 'SET' process and the 'RESET' process can be achieved with the same signal polarity. However, the bipolar switching mode gives rise to an opposite signal polarity between the 'SET' and the 'RESET' process. The comparison between Figure 2.2 and Figure 2.6 clearly shows that the resistive material, when operated in the bipolar switching mode, exhibits an I–V curve analogous to that of the theoretical memristor. Even if several models and mechanisms are involved in the memristive response of TiO_2 memristive device, generally in bipolar mode the switching is typically associated with electric field inside the device. Widely used switching models are metal ion [51] injection from the electrodes, change of states of trap sites either in bulk or interface of the switching medium such as space charge limited conduction (SCLC) [52-56] and drift of oxygen vacancies [5]. More in details, such polarity-dependent operations can be described by two main models: the growth of a virtual cathode and the modulation of the Schottky barrier by oxygen vacancies movements.

The first one since the accumulation (depletion) of oxygen vacancies generally increases (decreases) the conductance, the migration of oxygen vacancies under an electric field can induce a polarity-dependent RS. This mechanism, depicted in Figure 2.7, is generally called the "virtual cathode" [57,58]

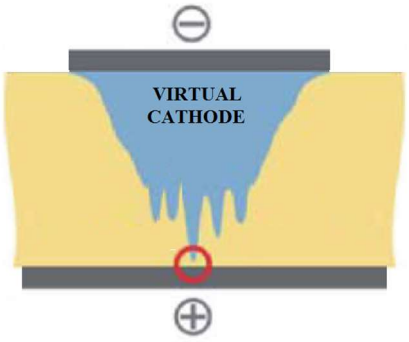

Figure 2.7: Schematic of a virtual cathode model. A virtual cathode grows from the cathode. When it touches an anode, the cell changes into a LRS [57].

The virtual cathode denotes a region with a high concentration of oxygen vacancies and thus exhibits a higher conductance compared with the surrounding matrix. Although not clearly stated in the literature, the virtual cathode should be closely related to CFs. The virtual cathode corresponds to the largest portion of the CFs and the regions of intermediate resistance states. When a virtual cathode is formed, it will grow from the cathode by oxygen vacancy accumulation because the oxygen vacancies are positively charged. After the forming process, the size of the gap between the virtual cathode and the anode becomes only a few nanometers wide. Thus, it is possible to control the percolating path of the virtual cathode by applying an external electric field, which induces bipolar switching. Such an operation should depend on the polarity. At a negative bias, the virtual cathode is attracted to an anode, the oxygen vacancy-rich region becomes percolated and the device enters the LRS. At a positive bias, the virtual cathode is repelled from the anode, the percolating channel becomes ruptured, and the memristive device enters the HRS.

As already described, the switching can therefore be achieved by modulating the Schottky barrier using the motion of the oxygen vacancies. Figure 2.4 shows the Schottky barrier modulation via oxygen vacancy migration in a Pt/TiO_2/Pt bipolar switching cell. [5] When a negative voltage is applied to the anode, positively charged oxygen vacancies are attracted toward the electrode, thereby narrowing the Schottky barrier width and inducing HRS to LRS switching. When a positive voltage is applied at the anode, oxygen vacancies are repelled from the electrode, thereby recovering the original width of the Schottky barrier and inducing LRS to HRS switching.

In case of unipolar devices, switching depends only on the magnitude of the applied bias. Hence switching typically involves Joule heating inside the device [50,59] and is controlled by adjusting the current levels used to program the device. For examples, to switch off the device, no current compliance is necessary to generate enough heat to break the conducting local path inside the device, while the current must be limited to prevent the switching medium from generating excess heat so that the local conducting path is created to turn on the device.

To study and understand the memristive response in TiO_2 thin films, several and different deposition techniques have been employed. According to the recent research reports [60, 61], it can be envisaged that atomic layer deposition (ALD) and plasma enhanced ALD (PEALD) are most reliable and suitable processes for resistance memristive devices owing to its excellent controllability. By these processes, layer by layer deposition of ultrathin film is possible which eventually leads to extremely fast electron transport (switching). Thermal oxidation of titanium thin films [62] and radio frequency Magnetron sputtering [63,64] TiO_2 are recently reported to be efficient methods to synthesize uniform, stable, highly crystalline and stoichiometric TiO_2 film yielding reproducible and endurable resistance switching devices.

Despite the more reference method to synthesize metal oxides for memristive applications, as reported, in the last decade increasingly new and exotic growth techniques have been employed in this direction, such as drop-coated titanium [65], electro-hydrodynamic inkjet printing [66], assembled nanoparticles [67,68] and so on. In particular, the researches focused the attention on methods that enable very controllable growths, nanostructured thin films having no limitation concerning the materials of the substrate. For instance, sol gel grown TiO_2, owing to the simplicity of the process technology, low cost and fast deposition of the film on a wide varieties of substrates, has been employed [69].

In this work, an innovative growth technique is proposed based on supersonic cluster beams as good candidate for the synthesis of TiO_2 thin film for memristive application.

Chapter 3
Supersonic cluster beam for thin film growth

Introduction

Supersonic beams is based as a method to grow films and interface. Molecules and aggregates in non-thermal equilibrium, controlling their kinetics parameter and properties [70]. For a proper understanding of the supersonic molecular beams generation and their applications, two books by G. Scoles [71] and P. Milani and S. Iannotta [72] can be considered as main references. This chapter gives as an overview of the supersonic molecular beam approach and its use as a technique for thin film growth. More detailed information of film growth of specific inorganic materials will be given in the following chapters.

3.1 Fundamentals of supersonic molecular beam approach

The earlier studies about the potentiality of supersonic beams in molecular and surface physics were carried out by Stern and Gerlach [73] in the 30's: for the first time they investigated a number of physical phenomena, ranging from the measurement of electric and magnetic moments of atoms and molecules by beam deflection in applied fields, to evaluation of intermolecular forces in scattering experiments. In 1951, Kantrowitz and Grey [74] developed a design of an asymmetric converging-diverging nozzle, together with a cone shaped skimmer, in order to obtain a well defined molecular beam and to solve the so called problem of the "scattering cloud". The resulting molecular beam improved indeed the overall performance showing intensities that could be considerably higher than those achieved by conventional effusive sources. As a matter of fact, these studies can be considered as the

foundations of modern supersonic molecular beams. However, the basic vacuum requirement has long limited their use, preventing the demonstration of their effectiveness and potential.

Becker and Bier [75] in 1956 were able to confirm the predictions of Kantrowitz, developing a system with a pumping speed high enough to produce and maintain a reliable supersonic beam. In a following work, Becker and co-workers [76] found the narrowed velocity distribution of an argon beam as predicted in the previous paper. It was not possible to make a direct comparison between theoretical assumptions and experimental results, since at that time the skimmer interference on supersonic beam properties was not fully understood. These studies, which demonstrated the high intensity and narrow velocity spread of a supersonic beam, were the starting point in the knowledge of supersonic beams. In fact Hagen in 1970 [77] showed the relaxation of internal degrees of freedom of carbon dioxide in a supersonic free jet, followed by Anderson [78] who studied the process of "running out of collisions" in the supersonic expansion.

To better understand which are the physical processes leading to the properties of supersonic molecular beams it is possible to start from the study of a "classic" effusive source: the Knudsen cell.

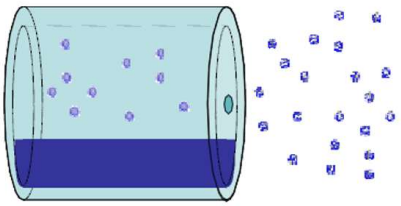

Figure 3.1: Schematic view of an effusive Knudsen cell.

It is essentially an oven in a vacuum chamber, opened to the external environment through a small orifice (nozzle), where the desired material can be heated (see Figure 3.1). The evaporating/sublimating material, characterized by a temperature T_0, is in thermal equilibrium with its vapors at a pressure P_0 ($P_0 \sim 10^{-3}$-10^{-1}torr, $T_0 \sim 10^2$-10^3K). The nozzle aperture is smaller than the mean free path (λ) of the particles (usually some cm) so the outgoing flux is molecular and can be fully described by the classical gas kinetic theory as

an effusive flux. Its internal degrees of freedom (the roto-vibrational modes) are those typical of a gas in thermal equilibrium at the specific temperature, leading to a cosinusoidal spatial distribution of the particles and a Maxwellian energy distribution, centered at the energy corresponding to the temperature T_0 of the evaporated species.

From an experimental point of view, the oven is heated by an external heating element and thermally stabilized by a temperature sensor (usually a thermocouple), with a feedback system acting on the power supplier. In the following are reported some basic expressions to describe the characteristics of an effusive beam and necessary to introduce those of a supersonic one. The mean free path (λ), the intensity N, the average molecular velocity ($\bar{v}$) and the normal velocity distribution ($f(v)dv$) of the particles in the beam are given by the following relationship:

$$\lambda_{[cm]} = \frac{7.321 \times 10^{-20} \mathrm{T_0}}{\mathrm{P_0}\ \sigma} \tag{3}$$

(σ is the collision cross-section in cm^2)

$$dN = \frac{d\omega}{4\pi} n_0 \bar{v} A \cos\theta \tag{4}$$

where n_0 is the number density in the source, in atoms/cm^3, A the orifice area and $d\omega$ the solid angle;

$$\bar{v} = 1.4551 \times 10^4 \sqrt{\frac{T_0}{M}} \tag{5}$$

(in $cm \times s^{-1}$, M is the mass in atomic units)

$$f(v)dv = \frac{4}{\sqrt{\pi}} \mathrm{v}^2 \mathrm{e}^{-\mathrm{v}^2} \mathrm{dv} \tag{6}$$

In the classical effusive molecular regime, the particles leave the oven though the nozzle without collisions, and the Knudsen number is $K=\lambda/d>1$ (d is the nozzle diameter). A supersonic beam is obtained by increasing the pressure P_0 so that the Knudsen number

$K=\lambda/d<<1$, a regime in which the particles will undergo a large number of collisions, giving rise to the free jet expansion driven by the pressure gradient between the source and the external vacuum. To maintain the pressure gradient also in presence of high gas loads, an adequate much larger pumping speed is needed, due to typically five order of magnitude larger P_0. From an experimental point of view, a supersonic beam source consists essentially of a closed heated vessel, with a micrometric nozzle, inside of which is injected a high-pressure gas. To give a description of the generation of a supersonic beam, the expansion process (and subsequent beam's extraction) for a short converging nozzle will be taken into account.

We will see, in the following, how the nozzle's shape affects the beam formation.

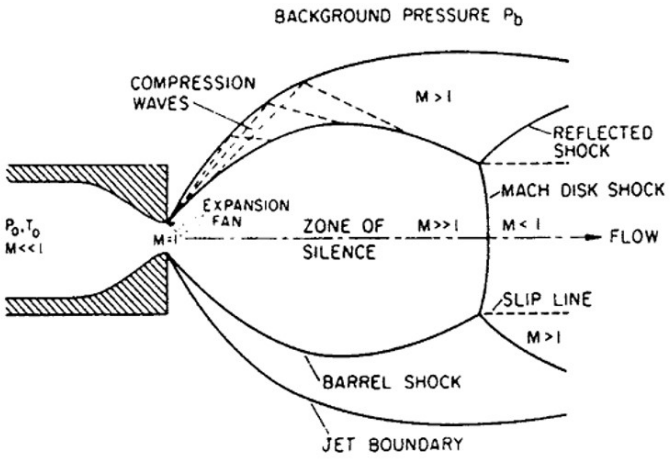

Figure 3.2: Diagram of the free jet expansion describing schematically the different regions [72].

Figure 3.2 shows the general scheme of the free jet expansion in steady-state conditions, assuming an isentropic expansion with negligible heat conduction and viscous effects. Within the oven, the physical parameters, P_0 and T_0, are representative of the chemical-physical state of the source, the so-called *stagnation state*. It is a thermalized condition where the gas particles have a statistical thermal velocity distribution that depends on P_0 and T_0, but showing a quasi-static drift towards the nozzle. Because of the much lower outer pressure P_{out}, as they flow towards the throat, particles accelerate increasing their speed up to the sonic speed corresponding to a Mach number $M=1$, where the ratio between the velocity of gas particles and the local velocity of sound propagation, $M = v/vs$.

The onset of the supersonic expansion depends on the pressure difference between the source and the outside, which should be kept low enough to drive the expansion itself.

The critical P_{out} value can be calculated by the following expression:

$$\frac{P_0}{P_{out}} = \left(\frac{\gamma + 1}{2}\right)^{\gamma/(\gamma-1)} \tag{7}$$

where $\gamma = c_p / c_v$ is the ratio between the specific heats at constant pressure and volume.

At the stationary state, the gas flow outside of the source will be characterized and confined by a matching between the expansion zone and the vacuum environment. The pressure just outside the nozzle is about $P_0/2$ (typical of an *underexpanded* flow), reaching $M = 1$ at the nozzle exit and $M > 1$ in the portion of beam just outside the nozzle. This region is the so called *sonic region*, while the following larger region is the *core of the expansion*, called the *zone of silence* just because the beam does not "feel" the presence of the external environment (Figure 3.2). The border of the supersonic beam's portion (*Mach disk*), in the forward direction, is outlined by shock waves outside of which the supersonic properties are strongly depleted and lost. Differently, on the side portions the flow loses the isentropic, not viscous behavior with $M > 1$ by means of compression waves. The distance between the Mach disk and the nozzle (x_M or δ_M) can be estimated in terms of nozzle diameter d, using an empirical, experimentally tested rule:

$$\delta_M = \frac{x_M}{d} = 0.67\left(\sqrt{\frac{P_0}{P_{out}}}\right) \tag{8}$$

In the zone of silence the particles are extracted by an interfering conical collimator (*skimmer*), in order to obtain a well defined supersonic molecular beam. To reduce to a minimum the interference of the skimmer in the zone of silence, a specific geometrical shape is necessary, i.e. a sharp edge skimmer with a hyperbolic profile. Moreover, the skimmer decouples of different vacuum zones and thus pumping independence between the chamber where the beam is generated and the chamber where the beam itself will be used.

3.2 Supersonic expansion properties

The thermodynamic approach to the beam properties can be simplified by assuming an isentropic flow, without any heat conduction effect (the unperturbed zone of silence satisfies these assumptions). The energy equation for such a flow can be written as:

$$h_0 = h + \frac{v^2}{2} \tag{9}$$

where h_0 is the enthalpy per unit mass considered as a constant along any streamline. This relationship does not take into account the internal energy, that it is not relevant since the driving force for the particles acceleration is the pressure gradient. It shows that when the enthalpy decreases, because of expansion process, the mean velocity of the particles must increase. Taking into account that $dh = C_p \cdot dt$, for an ideal gas equation (9) gives:

$$v^2 = 2(h_0 - h) = 2\int_T^{T_0} C_p dt \tag{10}$$

Under the assumption that C_p is constant over the range of interest ($T_0 \rightarrow T$):

$$v = \sqrt{2C_p(T_0 - T)} \tag{11}$$

the limiting velocity is hence calculated as:

$$v_\infty = \sqrt{\frac{2k}{m}}\left(\frac{\gamma}{\gamma - 1}\right)T_0 \tag{12}$$

where the subscript ∞ means that we are considering the terminal or maximum beam's velocity, that is at the end of the free jet expansion. v_∞ can be obtained considering a large cooling, that is $T \ll T_0$, and using the relationship $C_p = k_B/m(\gamma/\gamma\text{-}1)$, that is the case of an ideal gas (k_B is the Boltzmann constant).

The supersonic expansion is characterized by its temperature, pressure and density. They can be written as a function of the Mach number, defined as

$$M = \frac{v}{v_s} \tag{13}$$

where *v* is the speed of the particles in the beam and

$$v_s = \sqrt{\gamma KT/m} \tag{14}$$

is the speed of sound.

Taking in account these parameters, we obtain:

$$\frac{T}{T_0} = \left(1 + \frac{\gamma - 1}{2} M^2\right)^{-1} \tag{15}$$

$$\frac{P}{P_0} = \left(\frac{T}{T_0}\right)^{\gamma/(\gamma-1)} = \left(1 + \frac{\gamma - 1}{2} M^2\right)^{-\gamma/(\gamma-1)} \tag{16}$$

$$\frac{\rho}{\rho_0} = \frac{n}{n_0} = \left(\frac{T}{T_0}\right)^{1/(\gamma-1)} = \left(1 + \frac{\gamma - 1}{2} M^2\right)^{-1/(\gamma-1)} \tag{17}$$

Therefore, once the value of M along the beam axis is known, equations (14),(15) and (16) give a complete thermodynamic description of the beam. The exact solution of these equations is not simple for the supersonic expansion region of the beam, due to the dependence of *M* versus the distance from the nozzle along the beam axis. However, by using a numerical method like the so-called *Methods of Characteristic (MOC)*, the analytical expressions can be derived through a fitting procedure on the calculated values.

The detailed description of this method [71] goes beyond the aim of the present thesis; however, its main result gives the following relationship:

$$M = A\left[\frac{x - x_0}{d}\right]^{\gamma-1} - \frac{\frac{1}{2}\left[\frac{\gamma+1}{\gamma-1}\right]}{A\left[\frac{x - x_0}{d}\right]^{(\gamma-1)}} \tag{18}$$

where A is the nozzle cross section.

The typical behavior of the thermodynamic variables, as a function of the distance and in terms of number of nozzle diameters, is shown in Figure 3.3, for the case of a gas with γ=5/3 and in regime of isentropic flow, ideal gas behavior, C_P constant, continuum flow. All the variables, except the terminal velocity v_∞, show a continuum decrease from their initial values. v_∞, on the other side, rapidly increases its initial value until it reaches the 98% of the asymptotic limit in a few nozzle diameters (x/d, see Figure 3.3).

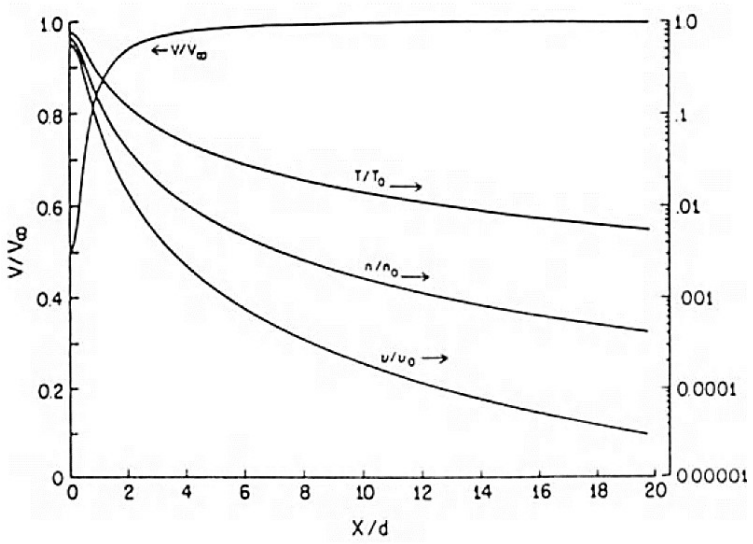

Figure 3.3: Evolution of velocity V, temperature T, density n and ν (collision rate for binary hard spheres) normalized to the corresponding values in the stagnation conditions (T_0 and n_0) and to the limit velocity (V_∞), plotted against the parameter x/d [72].

The collision frequency decreases rapidly, so that the continuum flow regime cannot be maintained and there is the transition to free molecular flow (see Figure 3.3): this happens beyond reaching 98% of v_∞, so that the molecular velocity is not significantly affected by this transition. Its spread, on the other side, depends on T which is affected by this transition: this is at the origin of a change in the beam energy distribution that results proportional to the ratio T/v^2.

In the sonic and subsonic part of the beam, thermodynamics provides an approximation to calculate the beam's properties: the flow, in fact, can be treated as a quasi one-dimensional compressive flow, with M constant across any nozzle cross section. Using this approximation, we can calculate the mass flow rate $\dot{m}$ related to M, in particular regarding the nozzle's shape. For converging nozzles, in fact, the sonic and subsonic regions are characterized by viscous effects that generate boundary layers, but in the regime of fast flow rates and sonic nozzles the quasi one-dimensional approximation can be used. Therefore we have:

$$\dot{m} = \rho v A = P_0 A^* \left(\frac{m}{kT_0} \gamma \left[\frac{2}{\gamma + 1} \right]^{\frac{\gamma+1}{\gamma-1}} \right)^{1/2} \tag{19}$$

where A^* is the nozzle cross section at the throat, thus at the minimum diameter.

Each other cross section area can be calculated by the following relation:

$$\frac{A}{A^*} = \frac{1}{M} \left[\frac{2}{\gamma + 1} \left(1 + \frac{\gamma - 1}{2} M^2 \right) \right]^{(\gamma+1)/2(\gamma-1)} \tag{20}$$

The intensity of a supersonic beam, in terms of molecules per radiant per second, can be evaluated to be

$$I_0 = \kappa N / \pi \tag{21}$$

where the molecule flow rate N at the nozzle is

$$N = n_0 F(\gamma) \left(\frac{\pi d^2}{4}\right) \sqrt{\frac{2kT_0}{m}} \tag{22}$$

and

$$F(\gamma) = \left(\frac{\gamma}{\gamma+1}\right)^{1/2} \left(\frac{2}{\gamma+1}\right)^{1/(\gamma-1)} \tag{23}$$

The parameter κ is the *peaking factor*, and its values can range from 1 to 2 as a function of γ (1 is referred to the ideal effusive source). The forward intensity of a supersonic beam is much higher than for a classical Knudsen source, mainly due to the higher values of *N* and of the peaking factor (κ >1).

Up to now, we have discussed the beam properties when the flow is in the continuum region, approximating it to an ideal gas, but it is necessary to take into account the non-equilibrium processes in a supersonic expansion, leading to fundamental kinetics effects. Molecular collisions provide an efficient mechanism of cooling the internal energy states: after the expansion, the collision rates fall down rapidly and the internal states "freeze", so that the particles molecular flow extracted by the skimmer in this zone will remain in a "frozen" configuration. Assuming that the typical number of collision in free-jet expansion is $\approx 10^3$, it is clear that vibrational and rotational modes of large polyatomic molecule can be efficiently cooled down, considering that a molecule needs only about 10^1-10^2 collision to relax. Energy is exchanged during the expansion and the molecule enters the collision-less flow zone in a "cooled" internal state.

In addition to the properties of supersonic beams, other predictions can be made about the distribution of the final velocity. Its evaluation can be performed with sufficient accuracy in the continuum region, while in the non-continuum regime the solution of the Boltzmann equation have to be carried out via a model. The resulting distribution has a Gaussian profile of the mean velocity and of its components in the two directions, perpendicular and parallel to the beam propagation axis

$$f(v) = n\sqrt{\frac{m}{2\pi kT_{II}}}\left(\frac{m}{2\pi kT_{\perp}}\right) exp\left(-\frac{m}{2kT_{II}}(v_{II} - V)^2\right) - \frac{m}{2kT_{\perp}}v_{\perp}^2 \quad (24)$$

It is useful to introduce another parameter to characterize the beam energy dispersion: the speed ratio *S*, defined as the ratio between the mean velocity *V* and the velocity thermal spread

$$S = \frac{V}{\sqrt{\frac{2kT}{m}}} = M\sqrt{\frac{\gamma}{2}} \quad (25)$$

High *S* values correspond to highly-monochromatic beams, a goal that can be achieved by means of a high degree of cooling in the supersonic beam. In a pure helium beam source, for example, the gas pressure can be increased to very high values without producing any condensation, the heat of which would deplete the supersonic expansion. The very high degree of cooling that can be achieved gives rise to *S* values as high as 150 and velocity spreads $\Delta V/V<1\%$. As a matter of fact, a He supersonic beam is an ideal source of a velocity/energy monochromatic beam to carry out scattering experiments on surfaces and atomic diffraction [79].

3.3 Supersonic expansion of gas mixture

Let we consider the interesting case of the expansion of a gas mixture, particularly relevant for thin film deposition and for this thesis work. *Seeded beams* are supersonic beams where the main carrier gas is “seeded” by a small amount of an evaporating/sublimating species or by aggregates, so that highly diluted beams are obtained.

As far as gas mixtures are concerned, the heat gives by the weighted contribution of the different species constituting the flow. Thus we have

$$\overline{C_p} = \sum_i X_i C_{pi} = \sum_i X_i \, k_B(\gamma/(\gamma - 1)) \tag{26}$$

where X_i is the molar fraction of the *i*-component. The average kinetic energy (KE) of the particles in the beam depends on $\overline{C_p}$ and T_0: each species will be characterized by an energy above or below the average, in dependence of their mass with respect to the weighted averaged beam's mass. There is hence an inverse relationship between the molar or average molecular weight of the mixture and the mean velocity, thus the *i*-component, which is one of the "seeding" species in the beam, can increase or decrease its velocity if it is the heavier or lighter gas in the mixture respectively.

This process is usually denoted as *aerodynamic acceleration* and the energy of the individual species (assuming $\overline{C_p}$ and T_0 constant over the range of expansion temperatures) can be roughly written as:

$$E_i \approx \left(\frac{m_i}{\overline{m}}\right) T_0 \tag{27}$$

here $\overline{m} = \sum_i X_i \, m_i$.

The dilution process is briefly called "seeding", while the difference in velocity between the carrier gas and the seeding species is called *velocity slip*. Just to quantify the effect of the dilution, let's consider the case of a binary mixture, in which the seeding particles are less than 1% of the mixture, while more than 99% is the carrier gas. Helium can be taken as the example of the light carrier gas while, as seeding particles we can consider a polyatomic molecule of large mass, about 700 amu for instance (i.e. the TetraPhenylPorphyrin H_2TPP): applying the relationship (27) the KE of beam particles increases up to about one hundred times (at a given temperature) with respect to the energies in classical molecular beams. This means, for examples, that the H_2TPP seeding particles in a helium carrier gas can reach kinetic energies as high as few tens of eV.

In the case of aggregates or cluster species, their KE depends on the ratio between clusters' mass, M_c, and carrier gas's mass, M_g, so that:

$$E_{kin} = \left(\frac{\gamma R T_0}{\gamma - 1}\right)\frac{M_c}{M_a} \tag{28}$$

where M_a is the average molecular weight. It is clear that the highest KE is achieved by employing hydrogen as a major component of the mixture (carrier gas), which gives rise to the highest $\gamma/(\gamma - 1)$.

Another important feature of highly diluted beams is the effect of confining of heavier and lighter species in different parts of the molecular beam, after the skimmer selection. If we assume that the composition of the beam impinging on the skimmer is approximately the same of the gas mixture coming out from the nozzle, after the skimmer the heavier species will be concentrated on the centerline of the supersonic molecular beam flux, while the density of the lighter species increases at the border. Taking into account that the perpendicular component of velocity, after the skimmer selection, depends on the factor S and can be written as:

$$S_\perp = \frac{V}{\sqrt{\frac{2kT_\perp}{m}}} \tag{29}$$

for given V and $T_\perp$, it is evident that the lighter species get a low $S_\perp$ and consequently a large perpendicular component of the velocity, leading to a centerline density of lighter species lower respect to that of heavier ones.

3.4 Supersonic vs effusive molecular beams

The two kinds of molecular beams differ in several aspects, mainly velocity spread, spatial distribution and thermodynamic properties. The framework conditions for the two cases are dramatically different: while Knudsen cells are characterized by processes at thermal equilibrium, supersonic beam sources are highly non-equilibrium systems.

Parameters like the Knudsen number K_n, the evolution of temperature (from T_0 to final value T_f) and pressures (from P_0 to the final P_f) show distinct behaviors:

- K_n is less than unity for supersonic beams: the gas is underexpanded and a large number of collisions occur during the expansion. For K_n larger than 1, as for Knudsen cells, the flow is molecular and effusive: in supersonic beam, this occurs over a distance of few nozzle diameters.
- In supersonic beam, T_f and P_f are considerably smaller with respect to their initial values. The expansion can be assumed isentropic. Knudsen cells, operating in thermal equilibrium, show no significant differences between initial and final temperatures.
- An isentropic expansion leads to final velocities in supersonic beams considerably larger than initial values, while the velocity distribution from Knudsen cells is essentially that of the oven (Maxwell distribution).
- The free jet expansion induces the cooling down of the ro-vibrational modes, the efficiency of which depends from the energy spacing of the molecular states. Such effects are not present in Knudsen cells, where the state population is given by the standard distribution at the temperature of the source. Diluted or very diluted insemination (seeding) of the species under study in lighter non condensable gases gives on way to control the KE and the molecular ro-vibrational cooling.
- Clustering is promoted by the use of constrained nozzles and by seeding in carrier gases, while in Knudsen cells the process can be achieved only by external cooling and gas aggregation [72].
- As far as velocity spread is concerned, Figure 3.4 reports a comparison between the velocity distributions of the two types of sources: the supersonic source shows a narrower spread (it is proportional to$\left((2/\gamma)^{1/2}/M\right)$, while a Knudsen cell gives rise to a Maxwellian considerably larger (thermal) velocity distribution.
- In Figure 3.5 shows the angular distribution has a typical cosine-like angular intensity distribution in effusive molecular beams while for supersonic molecular beams a very high forward intensity narrowly peaked along the beam axis.

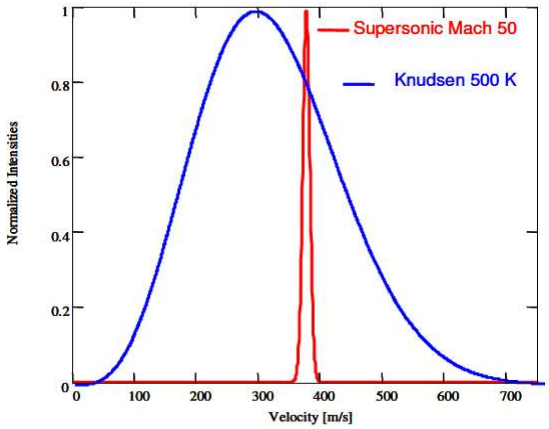

Figure 3.4: Velocity spread for a molecular beam produced by two sources (supersonic and effusive) [72].

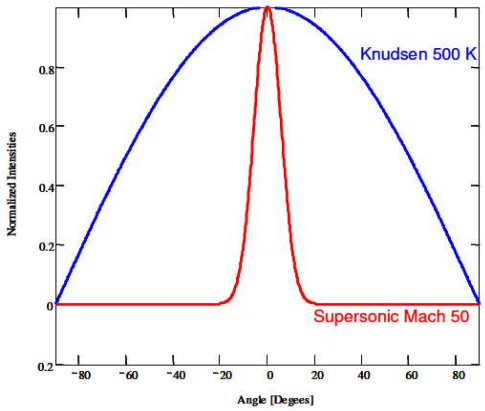

Figure 3.5: Angular distribution for a molecular beam produced by two sources (supersonic and effusive) [72].

All these features make supersonic beams ideally suited for the controlled growth of thin films with innovative properties.

3.5 Clustering process in supersonic beams

A very important effect that can be activated during the supersonic expansion is the condensation and the formation of clusters, which is widely used in this work.

The clusters nucleation typically occurs when the heat of condensation is efficiently taken away from the forming aggregates: this is the main reason, because of the rapid and very large cooling effects induced by seeding supersonic expansion the ideal environment to produce and control the cluster formation [80,81]. The density of the formed clusters as well as their average size are primarily depending on pressures and temperatures of both seeded and carrier gas. In particular, low source temperatures promote the supersaturation onset (so the higher is T, the smaller is cluster size and density), while high carrier gas pressures enhance clusters formation by increasing the number of collisions. Moreover, the final mass distribution is also depending on the type of carrier gas and the degree of seeding, as the large clusters are stabilized by the collisions between carrier gas particles and those of the seeding species, that is the basic mechanism to carry away the condensation energy.

The nozzle geometry and size is a further critical parameter to control the beam properties including clustering phenomena. Large nozzle diameters typically enhance cluster formation, while the expansion coming from smaller where collisions runs out rapidly, produce smaller and fewer clusters. Moreover, a constrained expansion induces higher number of collisions, increasing the formation of clusters. The nozzle geometry can be hence conveniently designed and selected to promote or inhibit particles aggregation.

Following the notation of Hagena and Obert [82], three different configurations can be defined to produce an axial symmetric free jet: the sonic, the conical and the Laval nozzle (Figure 3.6). Among them, the first geometry is specifically designed to minimize the collisions number as well as the expansion time, in order to reduce clustering, while conical, cylindrical and converging/diverging nozzles are specifically suitable for particles aggregation.

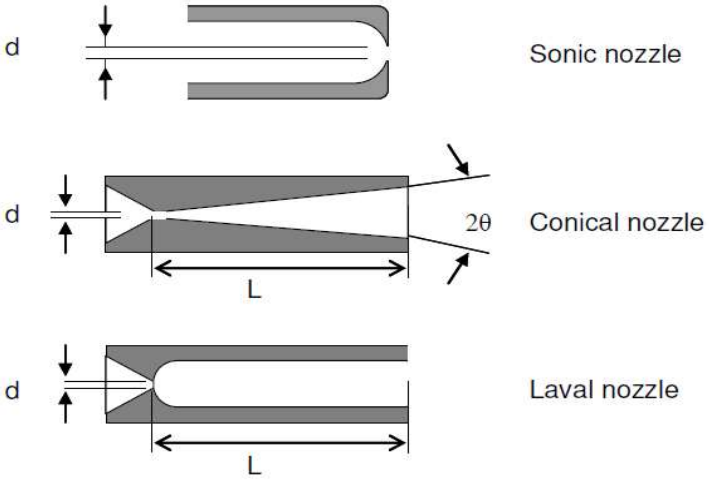

Figure 3.6: Schematic representation of three nozzle geometries, axially symmetric.

3.6 Supersonic pulsed sources

This kind of source is particularly well suited when the material to be seeded can hardly be sublimed (metals such as titanium, carbon in graphite form, etc...). In this case the vaporization of refractory materials can be achieved through the ablation by plasma, activated by a high voltage discharge. The sputtered material and the carrier gas then thermalize in the source chamber; subsequently the seeded gas formed in such a way expands in vacuum through the nozzle producing a supersonic beam.

The source will be better described from a technical point of view in the next chapter.

PMCS technology has been involved on several studies concerning the growth of nanostructured thin films [83]. It was used for the production of carbon based materials [84] refractory material clusters and in particular of transition metal-oxides. Moreover, using different cathode materials and different carrier gases mixed clusters can be obtained in order to deposit thin films, with suitable and tunable properties.

Milani *et al* proposed the PMCS technique in several multidisciplinary works. An innovative deposition setup was developed in order to improve the quality of the thin film deposition, by employing of a focuser device [101] or aerodynamic lens [102]. Moreover, import studies were carried on using different materials, from carbonaceous target to metal oxide system. Indeed, thanks to the peculiarity on the control of clusters, PMCSs could find application in several scientific applications as supercapacitors [85], optical devices [86,87], sensor arrays [35,38,80,88,89] or in biology [90-94].

Among devices based on film synthesized by PMCS, a great interest was for the realization of innovative PMCS TiO_2 gas sensors, also combined with organic molecules. Iannotta *et al* [88] demonstrated an improvement of the efficiency of hybrid n-TiO_2-CuPc gas sensors due to the active interaction between inorganic and organic systems. Concerning the hybrid system and especially the interaction in the biological environment, Carbone *et al* [93] demonstrated the no toxicity and good biocompatibility of PMCS TiO_2 thin films used like scaffold for primary cellular lines.

Despite the extend works on PMCS thin films in different applications, no study has been carried on yet in the realization of memristive devices or towards a hybrid system that can be used like an active interface between the electronic system and the biological environment. Here, for the first time, in the mainframe of the MaDEleNA Project, a PMCS system was developed and employed for this purpose.

3.7 MaDEleNA project

The present work is involved in a wider and multidisciplinary project named MaDEleNA (Materials and Devices towards adaptive Electronics and Neuroscience Applications). It proposes a strongly innovative approach to study and solve relevant demands from modern science and technology, in fields apparently far apart such as electronics and neurosciences. MaDEleNa addresses a hybrid area, where electronics and neuroscience are inevitably going to meet and possibly develop in symbiosis in the next few years, with a twofold objective:

implementing new neuro-bio-inspired computing systems and setting up hardware models of the brain.

In this framework, the project aims at the very challenging aim of the development of a new technology where brain and computing can actively communicate with each other, overcoming the present limits essentially based on the concept of biocompatible electrodes.

Within the MaDEleNA, this thesis, as it is true in the whole project, involve several different disciplines this thesis will involve different disciplines all of which are essential to reach the final objectives. Besides, the role of the author has been to collaborating on multiple activities and groups involved in the project, hence acquiring an overall perspective on its development and current challenges.

Chapter 4
Experimentals

In this chapter, after a detailed description of the deposition technique for the synthesis of TiO_2 thin films, an overview of the main experimental techniques used for their characterizations will be carried out.

4.1 The deposition system: PMCS source and apparatus

As it was briefly described in paragraph 3.6, the Pulsed Microplasma Cluster Source (PMCS) apparatus, schematically shown in Figure 4.1, is based on a two stages (chambers) high vacuum system, the cluster source and the samples holder, where the substrate is placed for the deposition

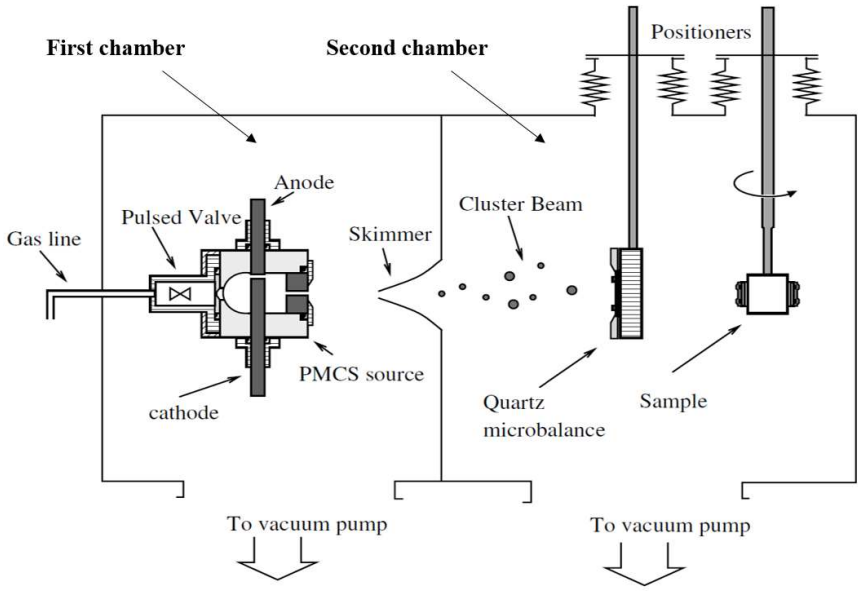

Figure 4.1: Deposition system.

The vacuum system has been designed to maintain a high level of vacuum in both the chambers during operation (material growth) that is when the high intense supersonic beam is working. 10^{-7} and 10^{-8} mmbar are typically the level of vacuum in the source and substrate chambers, respectively. In particular, in the first chamber was installed a diffusive pump with 2000L/s pumping speed while the second chamber is evacuated by turbomolecular pump with 700L/s pumping speed. The primary pumping system is composed of an 80 m^3/h rotary pump equipped with a mechanical booster (250 m^3/h) to improve pumping speed for light gases.

The Pulsed Microplasma Cluster Source (PMCS) is schematically represented in Figure 4.2:

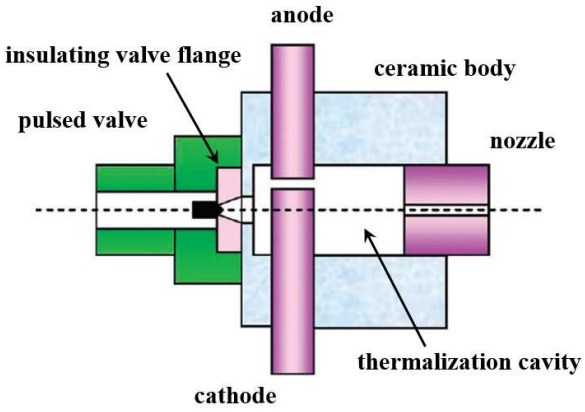

Figure 4.2: Schematic representation of PMCS source.

It consists of a cubic shaped ceramic body, 40mm side length, made from machinable ceramic such as Shapal-M or Macor, where a 1.8cm^3 cylindrical cavity is drilled. At the end of which are placed the input of the gas (pulsed valve) and the nozzle from which the beam is formed. (Figure 4.3). A channel of 6 mm diameter is drilled perpendicular to the axis of the cavity and hosts two titanium electrodes (Sigma Aldrich 266051-25G), facing each other and separated by a gap of 0.7mm. In the front end a removable titanium nozzle with cylindrical shape, 2mm in diameter and 8mm long, closes the front of the source itself. It is worth nothing that a graphite nozzle has been previously used: however, in order to reduce possible presence of carbon contamination in the deposited film, it was decided to use a nozzle made of the same material being synthesized, i.e. titanium in this case.

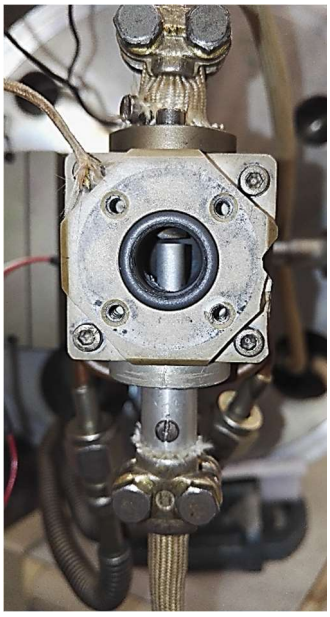

Figure 4.3: PMCS chamber.

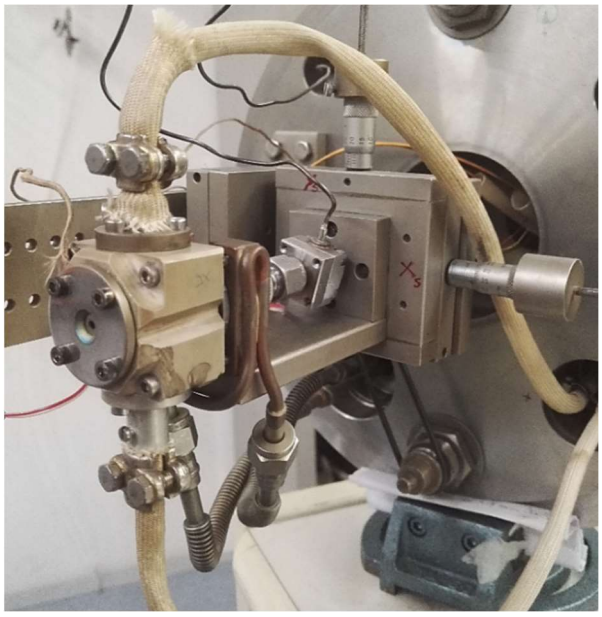

Figure 4.4: PMCS system.

The carrier gas inlet is supplied by a pulsed electro-valve driven by a solenoid [95] that in a pulse of few hundreds of second generate a gas jet with rising the pressure of several tens of bars. This valve is controlled by an external power supply that, by proper feedback from the vacuum gauge, stabilizes the shape and reproducibility of each pulse. In this way, the carrier gas is injected at 30 bar through an insulating ceramic nozzle on the back of the cavity and expands in the source chamber and along the cathode surfaces After the injection of the carrier gas pulse, a short (few tens of ms) and very intense (hundreds of amperes) discharge is fired between the electrodes by applying a voltage ranging from 500 up to 1500 V. Ionized helium sputters a small area of the cathode surface, causing the vaporization of the rods atoms and triggers cluster nucleation. The peculiar source cavity configuration allows the efficiency enhancement of the ablation process, that is localized in a very small region of the target/cathode. The clusters are then carried out through the nozzle by the supersonic expansion, where further clustering phenomena can take place.

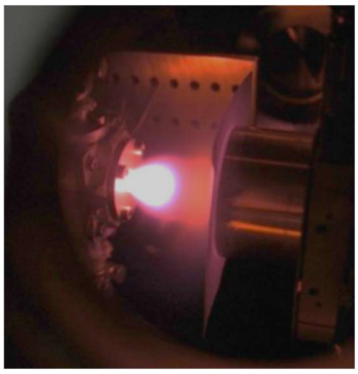

Figure 4.5: Supersonic expansion.

As a carrier gas, it was adopted pure helium or a mixture of helium and oxygen. It was realized that, as expected, critical growth parameter is the composition of the carrier gas mixture, since the presence of specific percentages of O_2 induces the formation of oxides clusters directly into the plasma source, thus determining the final stoichiometry. This aspect is obviously crucial for the control of final properties of the metal oxide, e.g. stoichiometry, as it will be discussed in detail in paragraph 5.3.

The PMCS is mounted on ultra-high vacuum (UHV) compatible manipulator that allows precise movements along the three perpendicular axes (X-Y-Z) (Figure 4.4) This setup was used to improve the quality of the final deposition as described in details in paragraph 5.1.

A metallic skimmer with 2.2mm hole (Figure 4.6) is installed and aligned with the PMCS and it is used to select only a specific portion of the beam and collimate the flux on a smaller area.

Figure 4.6: Metallic skimmer.

In the second chamber, a removable quartz microbalance placed between the skimmer and the sample holder was installed and used to check and monitor the deposition rate. Behind the skimmer, the sample-holder holds the suitable substrate

As it will be widely described in the paragraph 5.1, during this work important developments have been made on this part of the deposition setup. This has been necessary to the overcome difficulties in obtain a reliable, reproducible and controllable performance of the PMCS source. These difficulties are basically related to form of a stable and well defined gas pulse, a reproducible discharge between electrodes and thus plasma giving rise to the material ablation, sputtering that will seed the carrier gas and create the final supersonic beam. This is particularly true when a helium-oxygen gas mixture is used. The very stringent characteristics of the TiO_2 films used in this work have required a large tuning range of the PMCS source technical characteristics and working parameters as described in the next chapter in more details.

4.2 Investigation techniques and methods

The intrinsic multidisciplinarity of this work required a series of different characterization tools and approaches in order to investigate the different relevant material properties and interfaces. In this chapter, it will be first devoted attention on the techniques that it was used for studying of physical/chemical, morphological properties of the TiO_2 thin films deposited on different and suitable substrates. Characterization of electrical performances of memristor devices will be also presented, and finally all the techniques employed in the biological investigations will be reported.

4.2.1 X-Ray Photoelectron Spectroscopy (XPS)

The X-ray Photoelectron Spectroscopy (XPS) is based on the photoelectric effect: when X-ray photons hit a solid surface, their energy (from few hundreds to thousands of eV) can be absorbed by an electron of a core level, causing its escaping from the surface sample.

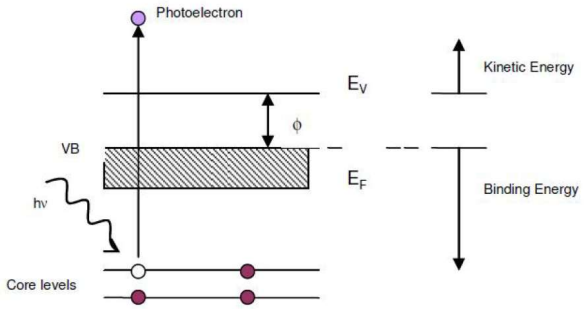

Figure 4.7: Photoemission process.

This process is sketched in Figure 4.7: the electrons generated from a core level leave the surface with a kinetic energy that depends, in a first approximation, from the initial photon energy, the binding energy and the work function of the solid. The fundamental relationship that describes the photoemission process is:

$$KE_{el} = h\nu - BE - \phi \tag{30}$$

where KE_{el} is the electrons kinetic energy, BE is the binding energy of core level from which they were ejected and ϕ is the work function of the system (considering the sample in electric contact with the analyzer, and at the same ground potential). This relationship is based on the so called one-electron approximation. A more accurate description requires to take into account other phenomena, including the relaxation processes occurring in the excited parent atom and the energy loss processes experienced by electrons in the solid

(electron-phonon coupling and plasmon losses). All these processes lead to a final energy distribution composed of main features, reflecting the core level density of states, and secondary peaks, due to transport processes. As the system can not reach the equilibrium state prior to the photoemission, thus the final state can show two configurations (the so-called "sudden approximation"): in the first one, the electron lies in one atomic excited state, while in the second one the electron is ejected, leaving the atom double ionized.

These processes decrease the kinetic energy of the photo-emitted electron and give rise to satellite peaks, such as the so-called shake-up and shake-off features. A detailed description of these processes is beyond the aim of this thesis, and can be found in [96]. The photoelectron spectrum is obtained by measuring the kinetic energy of photo-emitted electrons and plotting the intensity (usually expressed as counts per seconds) versus the kinetic energy.

It consists of several features: core-hole lines, shake-up and shake-off excitations, Auger peaks, valence band peaks and secondary peak due to minor physical processes. XPS is a powerful technique since allows the observer to get information about the chemical properties and the elemental composition of the studied surfaces and interfaces. Elemental characterization is possible due to the intrinsic uniqueness of each atom electronic configuration, just by evaluating the Binding Energy. Quantitative analysis can be performed measuring the peak area associated to an element, weighted by a sensitivity factor that takes into account the excitation efficiency of each element. For a homogeneous sample with an isotropic elastic diffusion of the photo-emitted electrons, the photocurrent intensity can be expressed as:

$$I_i(KE_{el}, i) = I \cdot N_i \cdot \sigma_i(k) \cdot \lambda(KE_{el}) \cdot H \tag{31}$$

where I is the incident photon flux, N_i the atomic concentration of the i-species, σ_i the ionization cross section referred to the level i and to the incident photon, $\lambda(KE_{el})$ the escape depth length at the kinetic energy KE, H an instrumental factor. Since ab-initio calculation of some of the factors in Equation (31) is quite difficult, the general procedure for this type of analysis is the use of calibrated quantities and the atomic sensitivity factors (ASF), which takes into account the excitation probability of the element i, for a certain impinging photon.

In such a way the relative atomic concentration of the element i can be expressed as:

$$N_i = \frac{A_i}{ASF} \tag{32}$$

in which the peak intensity is its integrated area Ai. The ASFs which are also defined for the AES peaks, are tabulated taking as a reference the element i in a standard state [97].

The chemical analyses were performed at the IMEM-CNR laboratories in Trento by Dr. L. Aversa as well as the elaboration of the obtained spectra by Igor Pro software. The investigations give the stoichiometries of the different TiO_2 thin films both on platinum substrates and on glass coverslips. A deep study was performed on the different oxidized species on the TiO_2 surfaces, which have a primary role in the biological interfacing. Concerning XPS, analysis have been performed at normal electron acceptance using acquisition conditions ideal for quantitative and high resolution studies (Passing energy, PE, of 20eV and 10eV). The photon emission was a Mg Kα with an energy of 1253.6eV, achieved from a magnesium anode. Total maximum energy resolution is 0.86 eV. All the core level binding energies (BE) were normalized to the Au 4f7/2 core level signal (at 84.0 eV), obtained from a sputtered gold surface. The core level analysis has been performed by Voigt line-shape deconvolution after the background subtraction of a Shirley function. The typical precision for each component's energy position is ±0.05 eV. The uncertainty for the full width at half-maximum (FWHM) is less than ±2.5%, while for the area evaluation it is about ±2%.

4.2.2 Micro Raman Spectroscopy

Micro Raman spectrum of TiO_2 thin films were performed at the Physics Department in Trento by a microprobe set-up (Horiba-Jobin-Yvon, model Aramis) using a He-Ne laser operating at 632.8 nm (power 10mW). This spectroscopy technique is based on inelastic scattering of monochromatic light, usually from a laser source. Photons of the laser light are absorbed by the sample and then reemitted with a frequency shifted up or down in comparison with the original monochromatic frequency (ν_0). When the incident radiation is shifted to a lower frequency, the scattered light is called Stokes scattering. In this case the energy is transferred to the vibrational mode of the molecule which ends up in a higher vibrational energy state. Besides, when the incident radiation is shifted to a higher frequency , in the so called anti-Stokes scattering, the energy is transferred from a vibrationally excited molecule, which ends up in a lower vibrational state after the scattering event. Moreover, a substantial number of the scattering photons are not shifted in frequency. These photons are generated in a process called Rayleigh scattering, where the excited molecule returns back to the same basic vibrational state and emits light with the same frequency ν_0 as an excitation source. displays the energy levels and transitions that are responsible for Rayleigh, Stokes, and anti-Stokes scattering [98].

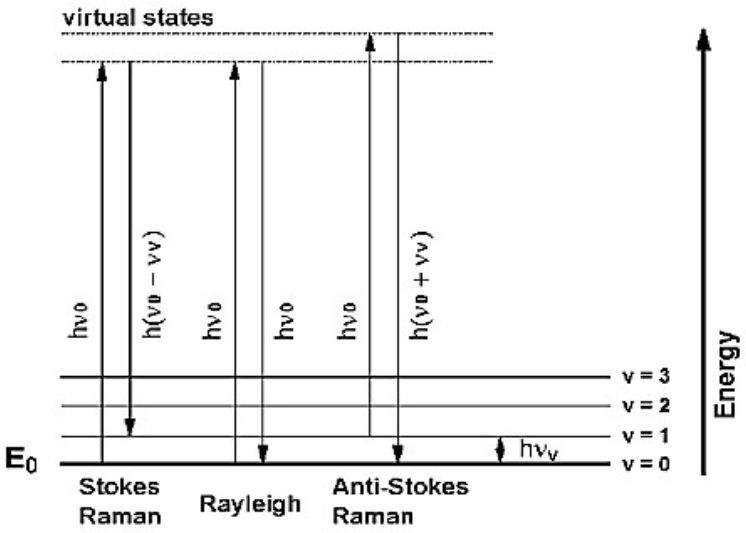

Figure 4.8: Energy-level diagram displaying Raman Scattering [98].

A Raman spectra is obtained by exposure of a sample to a monochromatic source of exciting photons and measuring the frequencies of the scattered light. The intensity of the Raman scattered component is much lower than the Rayleigh scattering, so that a highly selective monochromator and a very sensitive detector are required. A typical Raman apparatus consists of four major components: i) Excitation source (Laser); ii) Sample illumination system and light collection optics; iii) Wavelength selector (Filter or Spectrophotometer); iv) Signal processing system (detector, amplifier and output device).

The scattered light is collected with a lens and sent through an interference filter or spectrophotometer to the detector in order to obtain the Raman spectrum of the sample.

4.2.3 NEXAFS (Near Edge X-ray Absorption Fine Structure)

Part of the surface photoelectron experiments have been performed at the BEAR beamline - ELETTRA (Trieste) by Dott. M.V.Nardi, in order to take advantage of high photon flux and resolution. The BEAR beam-line is particularly suitable for this studies as X rays absorption measurements (XAS) and photoelectron emission spectroscopies (PES) can be performed with the needed resolution. Concerning XAS, the region very close to the absorption edge of single core levels is characterized by transitions of the photoelectron to unoccupied bound states and, in this case, this technique is also referred to as near edge X-ray absorption fine structure (NEXAFS). NEXAFS is therefore sensitive to the chemical bonding, exhibiting for example characteristic features for different oxidation states of the absorbing atom [99].The XAS features are also influenced by strong multiple scattering effects which depend on the three-dimensional geometry of the crystal structure. This provides a means of distinguishing between different crystal phases [100] by comparing with known standards. The BEAR beam-line optics is based on a couple of parabolic mirrors and two in normal and grazing incidence, respectively monochromatizing sections working in parallel light. The design allows to collect emitted radiation from the bending magnet in the 4mrad horizontal and +/- 1mrad vertical solid angle. The delivered photons cover the 4-1400 eV energy range, with a spot size at the sample of the order of 300x30 μm x μm (horizontal x vertical). The

hemispherical electron energy analyzer has a radius of 66mm, with an energy resolution of 10 meV.

4.2.4 AFM (Atomic Force Microscope)

Atomic Force Microscopy (AFM) is a technique of surface characterization based on interatomic forces. The instrument uses an "atomically" sharp probe (a tip), integrated to the end of a spring cantilever, to scan across the sample's surface in a raster pattern spawning an area of few nm^2 to some tenths of μm^2 large. The tip-sample interaction has a very low intensity with a force in the 10^{-9} N range: the detection system does not detect directly this force. By measuring the cantilever deflection, the morphological features of the surface can be mapped.

According to the tip-sample interaction mode, three AFM methods are definied: i) contact mode, the tip scans the surface in close contact (tip-sample separation of the order of Å) and the force on the tip is repulsive; ii) non-contact mode, using Van der Waals forces with a tip-sample separation of 10-100 nm; iii) tapping mode, suitable for soft samples, is gained by alternating placing the tip in contact with the surface and lifting it off to avoid dragging the tip across the surface.

AFM advantages such as high lateral resolution (few nm, limited by the tip dimensions), possibility of mapping several materials (conductive, insulating, biological samples as well as liquid samples) and operation in air or UHV, make it a technique of choice for a fast morphological characterization of surfaces.

It is worth nothing the possibility to analyze also surface magnetic properties, electrical conductance by using proper materials for the probing tip and applying specific scanning procedures.

The TiO_2 thin films (on platinum substrate) AFM studies were performed in collaboration with DR. P. Bettotti at the Department of Physics, University of Trento. The sample morphology was studied by a SFC100SEMI Universal SPM scanning Head 1, acquiring the images on a 1x1μm area with a 256x256 sampling points. Moreover, TiO_2 thin films on

microscope glass coverslips were analyzed by a Thermomicroscope Autoprobe CP-R in contact mode, in collaboration with DR. L. Lunelli.

4.2.5 SEM (Scanning Electron Microscopy)

The Field Emission Scanning Electron Microscope (FE-SEM) has been used to characterize the nanocomposite morphology. A FE-SEM employs a scanned electron beam and electromagnetic lenses to focus and direct the beam on the specimen surface in an identical way as a conventional SEM. A very small focused electron spot is scanned in a raster form over a small specimen area. The beam electrons interact with the specimen surface layer and produce various signals that are collected with appropriate detectors. The output of these detectors modulates, via appropriate electronics, the screen of a monitor to form an image that corresponds to the small raster and information, pixel by pixel, emanating from the specimen surface.

The TiO_2 thin films on platinum substrate were performed at IMEM-CNR in Parma. The sample morphology was studied by high-tech AURIGA Compact FIB-SEM.

4.2.6 Electrical characterization

In order to study the electrical response of the PMCS TiO_2 thin films, a source measure unit NI PXIe-4138 has been employed and connected to a dedicated probe station. A Labview interface was programmed and used to control the electrical measurements. By means of this interface, it was possible to tune different parameters, such as the range of the applied voltage, the current compliance, the number of the loop cycles and rate of the applied voltage. Moreover, the accurate control of the tip was performed using manual micrometric manipulator and an optical microscope.

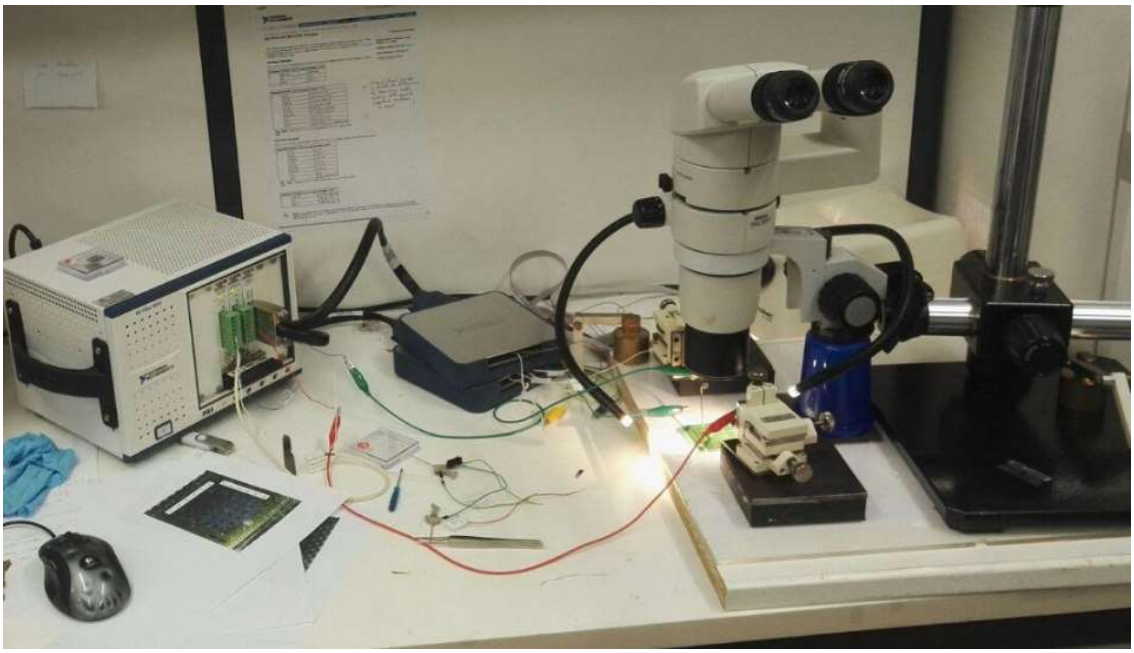

Figure 4.9: Experimental setup for electrical measurements.

With respect to the type of sample, two different configurations were used. In a first one, the investigation was performed by Ø50µm platinum wire employed as top electrode. Whereas in case of top metal electrodes deposited on the PMCS TiO_2 thin film, a steel spring contact tip was used. The bottom electrode of all samples was always grounded.

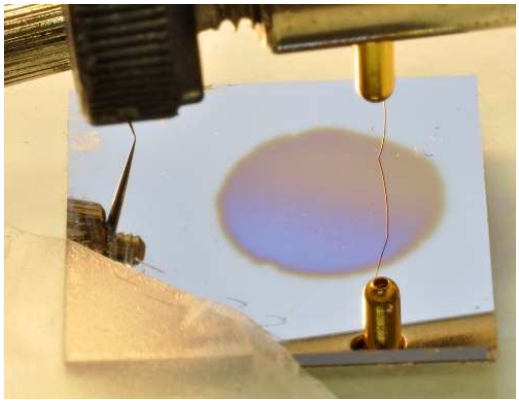

Figure 4.10: Configuration with platinum wire as top electrode.

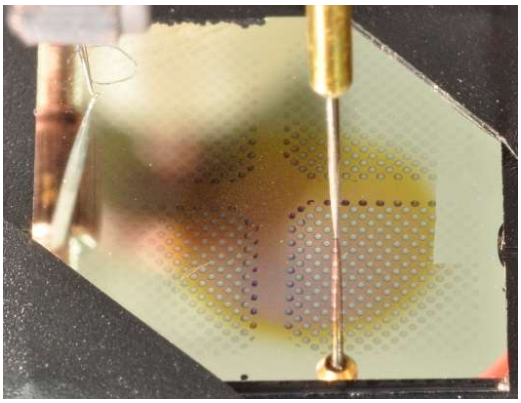

Figure 4.11: Configuration with steel spring contact tip.

Chapter 5
Synthesis and characterization of TiO_2 thin film by PMCS

As it has been mentioned in the previous chapter, a great attention was devoted to the development of the PMCS deposition technique. This step was fundamental to synthesize TiO_2 thin films having the requested properties for all applications, as well as achieve the necessary level of film performances repeatability. In fact, several morphological and structural characteristics achieved in the past (for other final applications) are not fully suitable for realization of memristive devices. Here, both the main improvements of the deposition setup, that was designed and installed by the author, and their impact on the metal oxide thin films, are reported.

Thanks to these developments, it is indeed possible to control the different properties of the TiO_2 thin films, as the average grain size and the homogeneity of the film thickness. The higher control and reproducibility of the growth conditions increased the ability to tune the deposition process in order to realize a large number of films with specific features, as requested by different research activities in this Thesis work and in the Madelena project.

5.1 Reliability and repeatability of the process

As previously shown in paragraph 4.1, the PMCS deposition apparatus is composed of a first main high vacuum chamber, where the source is located and the supersonic expansion occurs, and a second high vacuum chamber, connected with the former by a skimmer, where

the substrate for film growth is installed. Having in mind this scheme, several developments have been introduced.

The reliability of the deposition process during the growth process has an important role to ensure the stability of the deposition properties, as well as the in depth homogeneity of the deposited film. Similarly, the repeatability is mandatory when a number of films are necessary to test other processes and results will be reliable provided the analysis. Tests have been performed on films having the same characteristics. Different deposition process parameters affect reliability and repeatability, and efforts have been devoted to improve them facing several PMCS process and source issues. While in other applications, developed in the past, the necessity to achieve such a high repeatability was not crucial (e.g., for gas sensing), for realization of memristors this is mandatory.

The PMCS process requires several vacuum chamber openings to change electrodes, place/remove deposited films, and each opening is highly time consuming. In order to solve these technical requirements, several improvements have been introduced in the experimental system.

To increase the productivity of the deposition system, a six positions samples holder was installed in the second chamber of the apparatus. In this way, it has become possible to grow six TiO_2 thin films, avoiding to replace the substrate after every single deposition and improving the duty cycle.

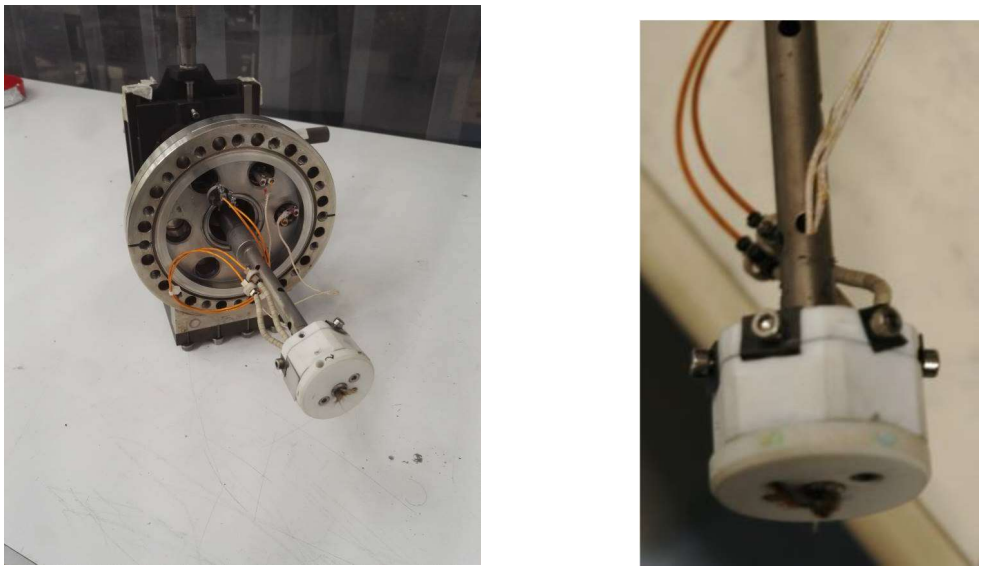

Figure 5.1: Six positions samples holder.

Furthermore, it was designed a new electrode shape (Figure 5.2).

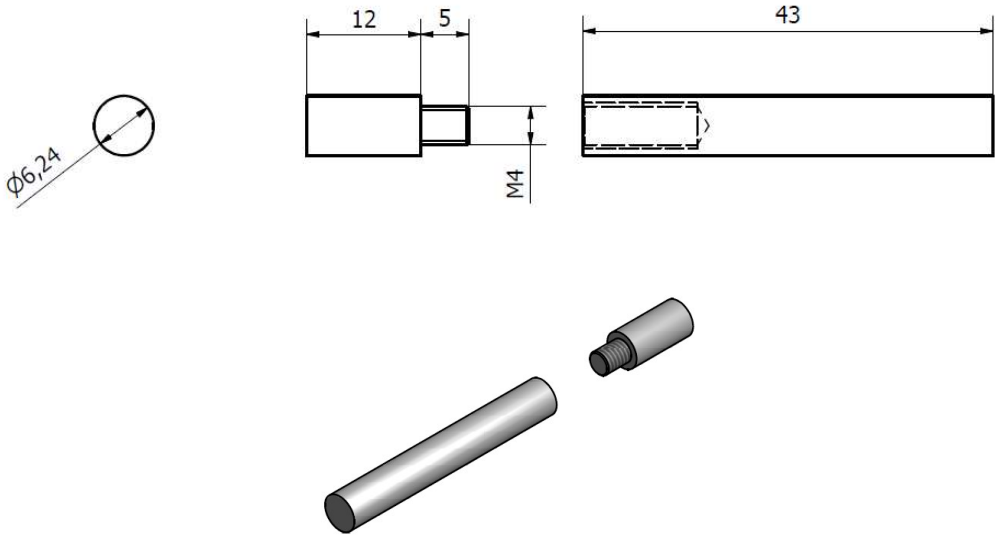

Figure 5.2: New electrode design.

Machine tools are often designed with a tool holder and a replaceable part, the one that is directly involved in the real machining process, and thus is gradually consumed requiring to be replace from time to time. As described in the previous chapter, the titanium rod must be replaced after the deposition process, due to the strong ablation processes that reduces its mass and change its shape The new model, as shown in Figure 5.2, allows for a partial replacement of only the ablated area, which is fixed to the main titanium rod through a screw thread.

Figure 5.3: Ablated area of a metallic Ti cathode.

The main advantages of this development can be summarized as follows:

- Higher control of the ablated area on the cathode,
- Decrease in the overall component consumption
- Decrease of the downtime between each deposition session

Moreover, the position of the cathode with respect to the carrier gas jet is more easily controllable and does not require a recalibration at each substitution (Figure 5.3).

In the growth process, the pulsed beam coming from the source is a highly supersonic flux seeded with clusters of Ti or TiO_x. During the first path (a few nozzle diameter long) the clusters are further formed and cooled down by the large number of collisions with much faster and numerous helium atoms. The collisions accelerate the cluster up to the limiting velocity of the helium atoms. After the free jet expansion, the beam passes the skimmer and reaches the so called free flight (molecular regime) and hence the atoms/aggregates reach the substrate leading to the deposition of a nanostructured thin film (Figure 5.4).

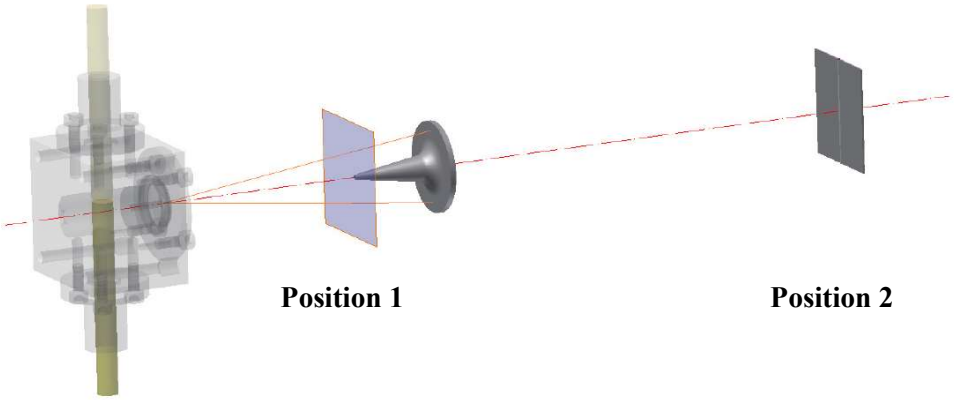

Figure 5.4: 3D scheme of the deposition technique.

In the initial configuration, the source nozzle, the skimmer and the sample holder were placed perpendicularly and coaxially along the same line. However, it was observed that the radial distribution of the deposited material was not homogenous, as shown in Figure 5.5, reflecting an intrinsic inhomogeneity of the supersonic pulsed beam.

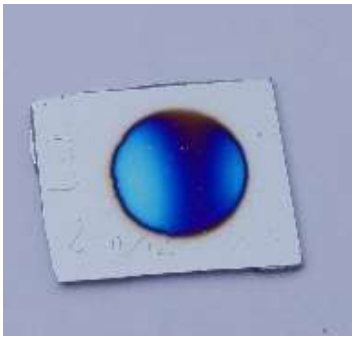

Figure 5.5: Radial distribution of the cluster density: deposited film spot of TiO_2 from PMCS using standard experimental setup.

In order to properly study the different distribution of the material in the pulsed beam, an experimental setup without the metallic skimmer was employed. In this way, it was possible

to evaluate a larger section on the beam in position 2 (Figure 5.4), obtaing more information about the distribution of the material seeding the supersonic beam (Figure 5.6).

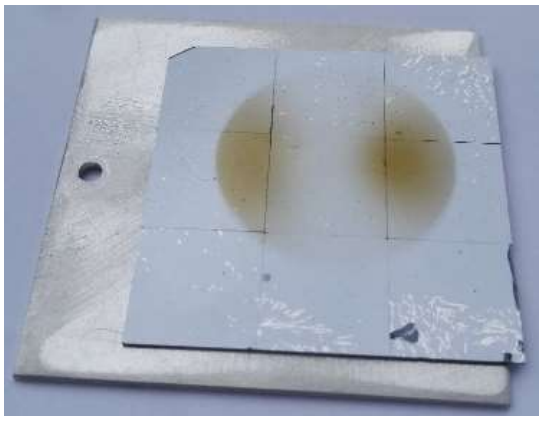

Figure 5.6: Radial distribution of the cluster density: deposited film spot of TiO_2 from PMCS without metallic skimmer.

Both conditions showed two distinctive areas having higher concentrations of the deposition materials (white areas in Figure 5.5 and intense orange in Figure 5.6). Same material distribution can be observed directly on the skimmer surface (position 1 in Figure 5.4), where the typical radial rings due to the different film thickness once more reveal the butterfly distribution. To get rid of this phenomenon and improve the morphological film homogeneity, it was proposed to shift the cluster source so that it would match the trajectory of only “one wing” of the butterfly shape (Figure 5.8). In this way, the homogeneity of the deposition thickness has been highly improved, at least from a quick optical analysis as clearly shown in Figure 5.9. composed of two lateral main areas where there is a cluster density significantly higher than in main axis line.

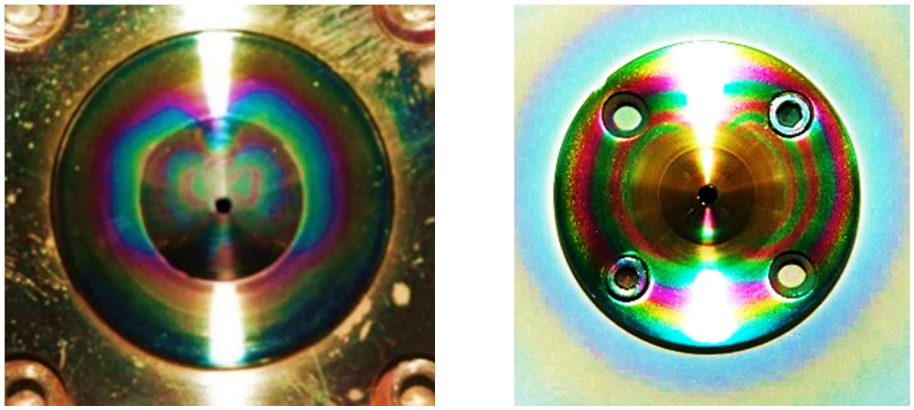

Figure 5.7: Two examples of butterfly shape effect on the metallic skimmer. Perfect alignment of source and skimmer (modified color).

A possible explanation of this phenomenom was provided by Milani *et al* [101,102]. The butterfly shaped distribution is due to a depletion of the gas flow-lines close to the cathode surface by the effect of particle diffusion and re-deposition on the rod-shaped cathode. The deposited film presents some dishomogeneities that are reminiscent of the internal geometry of the source cavity so that the thin film reflects the cluster distribution in the source prior to expansion. To get rid of this phenomenon and improve the morphological film homogeneity, it was proposed to shift the cluster source so that it would match the tragectory of only "one wing" of the butterfly shape (see Figure 5.8). In this way, the homogeinity of the deposition thickness has been highly improved, at least from a quick optical analysis, as clearly shown in Figure 5.9.

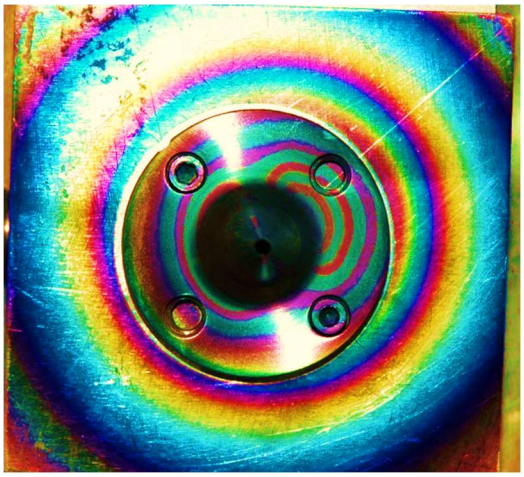

Figure 5.8: Butterfly shape effect on the metallic skimmer. Deviated alignment of source and skimmer (modified color).

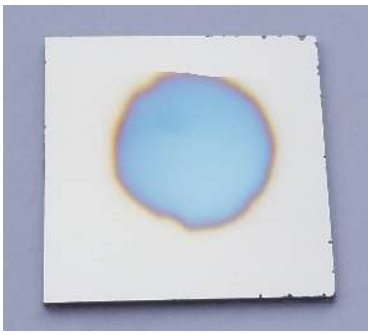

Figure 5.9: PMCS TiO_2 thin film with improved homogeneity thickness.

The improvements can be better qualified when film morphology is analyzed by AFM (Figure 5.10). The roughness (± 0.2nm) decreases from 4.5 to less than 2.6nm, and the main grain size is reduced from 30nm to 10nm, with a narrow size distribution. The improved control of the morphological properties of the TiO_2 thin films is crucial for a better performance such as electrical response, deposition of metal electrodes and hence for the applications of interest here.

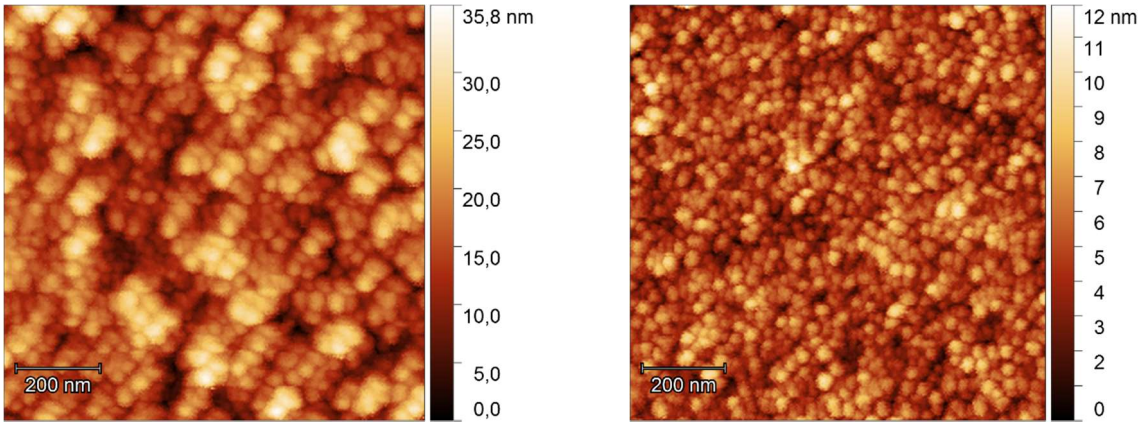

Figure 5.10: AFM images of PMCS TiO_2.

Another advantage was also observed from the realignment of the cluster source,. The metal oxide depositions did not show anymore the presence of undesired micrometric clusters. Those particles are concentrated on the main axis of the beam itself, i.e. between the two butterfly wings, being the heaviest species in the gas mixture.

Thus, the new skimmer/source configuration allows for a dramatic decrease of the probability of the bigger clusters to get channeled into the skimmer and reach the final substrate. (Figure 5.11).

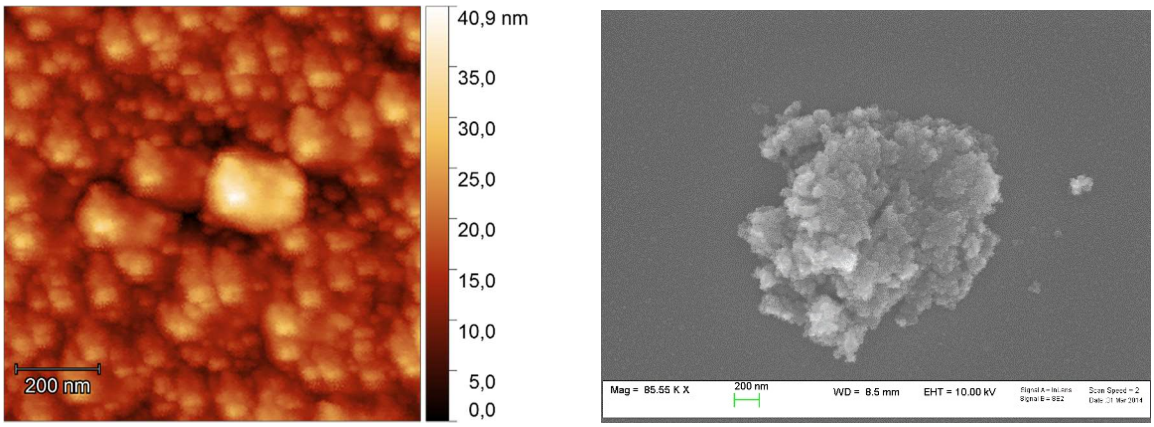

Figure 5.11: Presence of bigger cluster on the sample surface.

Their removal is particularly important. In fact, these large aggregates, microclusters, when other layers are deposited over the films, e.g. metallic top electrodes deposited on the TiO_2 surface to realize memristive devices, could deeply reduce their adhesion. This is due to their lower mechanical grip to the surface and their abnormal height, which could be even greater than the average top electrode thickness.

5.2 Final TiO_2 synthesis protocols

With respect to the specific experiment, the TiO_2 thin films were grown on different substrates. In this work, with the exception the NEXAFS studies in which the different TiO_2 thin film were deposited on a 10x10mm silicon oxide wafer, two main substrates were employed: a 15x15mm square platinized quartz for all memristive characterization, and a 15mm diameter microscope glass slide (Marienfeld 01 115 50) for the biological tests.

Before the deposition process, both kinds of substrates were cleaned in ultrasonic bath to remove all the possible impurities and organic/inorganic contaminations. The employed protocol was following:

- 10 minutes in acetone
- 10 minutes in isopropyl alcohol

Afterward, a drying step is carried out under a standard nitrogen flux at room temperature.

The substrates were fixed on the sample-holder, that was previously aligned along the beam path in order to have a deposition spot as centered on the substrate as possible. After the correct installation of the sample-holder, high vacuum is achieved in the deposition system, and the growth is started when the pressure is lower than 10^{-8} mbar.

The principle of operations of the cluster source is schematically summarized as follows: after the injection of the carrier gas pulse, a very intense discharge occurs by the application of 1200V between the electrodes, with a delay time of 700µs with respect to the trigger of the pulsed electro-valve. The opening time of the latter has been kept at about 700µs, in order to keep the first and second chamber pressure at 10^{-5} mbar and 10^{-7} mbar, respectively, with a carrier gas pressure of 30 bar. Plasma formation in helium gas occurs and the ionized gas sputters part of the cathode surface, creating atoms and aggregates. The helium pulse vaporized atoms quenches the plasma and cluster nucleation takes place. The cluster are then carried out through the nozzle by the supersonic expansion. The frequency of the pulsed electro-valve (and thus of the supersonic beam) for all the experiments was kept at 4Hz.

The choice of the numerical values of the main parameters is the result of an intense study led for almost 3 years. Particular attention required the tuning of the pulsed valve opening time and of the delay time for the discharge, with the proposed values the PMCS source is by far more stable than previously in terms of deposition rate and activation of the plasma. It is worth noting that the achievement of these deposition protocols has been possible thanks to the improvement of the skimmer/source position and to the design of the replaceable cathode, technical choices that sped up every system tuning operation.

Finally, the typical experimental conditions used for the TiO_2 depositions are summarized in the following table:

Carrier gas (He/O_2+He)	Opening time µs	Delay time µs	Voltage discharge V	Frequency Hz
0%, 0.1%, 1.0%	700	700	1200	4

Table 5.1: Standard experimental condition.

In Figure 5.12 two examples of TiO_2 thin film on different substrates are shown.

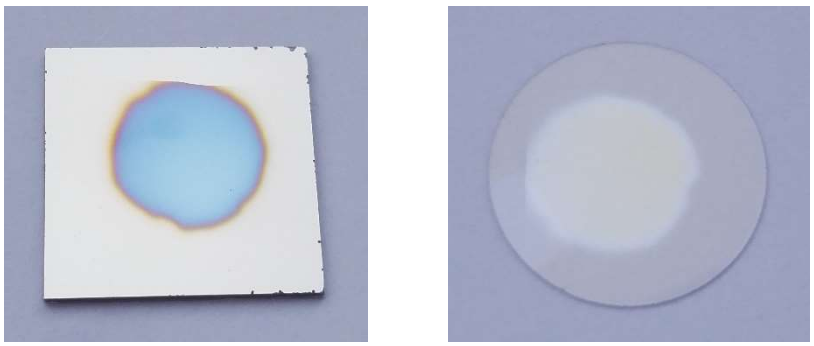

Figure 5.12: TiO_2 thin film on different substrates (platinized quartz on the left and coverslips glass on the right).

The thickness of the PMCS TiO_2 thin film was tuned by controlling the deposition rate (by means of a quartz micro balance) and the deposition time. Typical deposition rate was 0.5 nm/min. In general, for the memristive characterization the thickness was 30 – 100nm, whereas for the biological test the value of thickness was typically lower than 50nm.

The study of physical-chemical properties of the PMCS grown TiO_2 thin films has been carried on using as substrate 15x15mm square platinum (on quartz), and also glass for biological studies (Marienfeld 01 115 50). The former substrate has been used as an electrode for all electrical testing of the TiO_2 thin films also from an electrical point of view, which could not be done with the use of standard silicon wafers. The second substrate was used for all biological tests. Thus, all physical-chemical properties of TiO_2 film have been tested in same conditions of their final application, giving rise to results with higher reliability.

5.3 Properties of TiO_2 film grown by PMCS

As mentioned in paragraph 4.1, using the PMCS technique it was possible to control the final stoichiometry of the thin film simply by changing the carrier gas composition injected in the system. In this work, three different mixtures of gases with an increasing percentage of oxygen are used:

0%	0.1%	1.0%
Helium, pure	Helium + 0.1% O_2	Helium + 1.0% O_2

Table 5.2: Composition of mixture gas employed in the TiO_2 growth.

It is clear that using mixtures including O_2 triggers the oxidation process already in the source forming TiO_2 cluster during the deposition, while the first gas mixture with no O_2 leads to deposition of pure metal films. Thus, without no oxygen in the chamber the oxidation process must be carried out in a second step i.e. by exposing the titanium thin film to air at room temperature.

The structural properties of the thin films have been studied by micro-Raman and NEXAFS analysis.

In Figure 5.13, the micro-Raman spectrum shows how the TiO_2 thin film grown by PMCS has the typical peak of the anatase crystalline structure, independently from of the stoichiometry. The small shift of the main peaks (152, 398, 510, 625 cm^{-1}) with respect to the reference in literature is due to the very fine nanostructured texture [103].

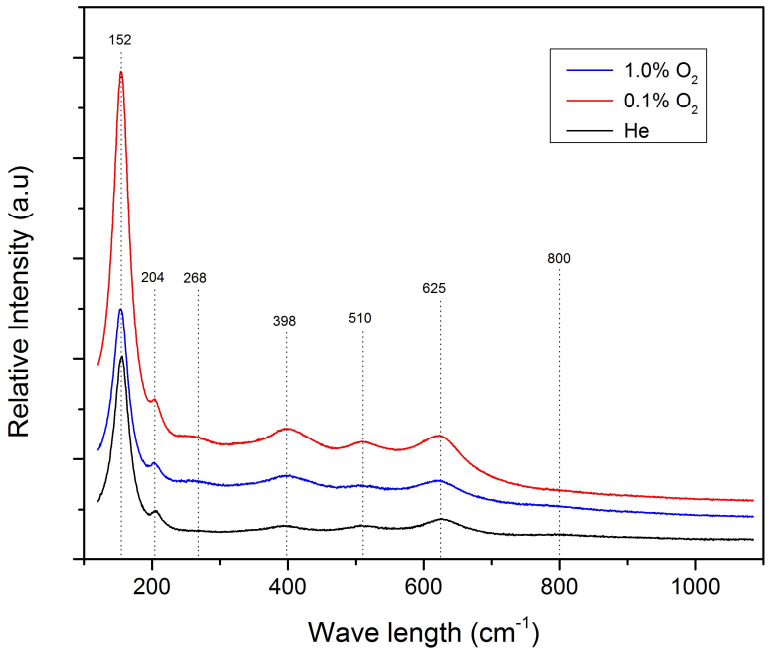

Figure 5.13: Micro Raman spectrum of PMCS TiO_2 thin films grown using different mixture gases.

XPS analysis have been performed on TiO_2 thin films deposited by PMCS on different substrates, namely Platinum film on glass and glass for biological studies. As a reference, a rutile TiO_2(110) single crystal has been analyzed without any treatment (cycles of beam sputtering and thermal annealing) to reduce surface contamination.

In Table 5.3 are shown the observed total atomic percentages of carbon, oxygen and titanium. Only in 1.0% sample deposited on glass has been observed also a 2% fraction of silicon, while in all other film the only detectable species where C, O and Ti.

	TiO_2 on Pt substrate			**TiO_2 on glass substrate**			**TiO_2(110) single crystal**		
O_2 %	**C**	**O**	**Ti**	**C**	**O**	**Ti**	**C**	**O**	**Ti**
1.0%	40.9	44.6	14.5	37.9	45.6	14.5	-	-	-
0.1%	51.0	37.3	11.7	41.7	17.8	40.5	45.1	42.9	12.0
0%	38.1	45.5	16.4	37.2	19.7	43.1	-	-	-

Table 5.3: Total atomic percentage (from XPS analysis) of TiO_2 thin films deposited by PMCS samples on Pt and glass substrates. Results from a rutile TiO_2(110) single crystal is also shown as reference. It is worth noting the presence of a 2% Si fraction on the 1.0% thin film deposited on glass.

As can be seen, the O/Ti signal ratio considering all oxygen species is by far higher than 2 suggesting a significant presence of contaminants from water, CO_x and others. This is in agreement with the large percentage of carbon-based species, around 40% in all samples. It is worth noting that also results from rutile single crystal are similar: being the typical amount of contamination from atmosphere around 10-20%, this suggests a particularly efficient chemical reactivity of titanium dioxide surface with water and CO_x, rather than speculating about the creation of carbon- or oxygen-based aggregates during PMCS synthesis. Indeed, by comparing carbon C1s core levels from all samples (see Figure 5.14), apart from some binding energy (BE) shifts due to charging effects (related to the insulating character of the different substrates), the shape of main structure around 285-286eV is similar for all surfaces, thus suggesting same chemical properties of carbon-based species. Only for films on glass, there is a second band around 282eV, but it is due to contaminants on the substrate and not on the titanium oxide surface.

An important drawback of such a high concentration of carbon-based pollutants on the metal oxide surfaces is the absence of a significant and reliable valence band signal. In fact, the 40% value means surface is covered by about 0.5-1.0nm of pollutants and every UPS analysis would result in a band structure typical of amorphous carbon aggregates and not of TiO_2 (as was indeed verified), with impossibility to properly evaluate also system work function. For these reasons, UPS analysis will not be presented here.

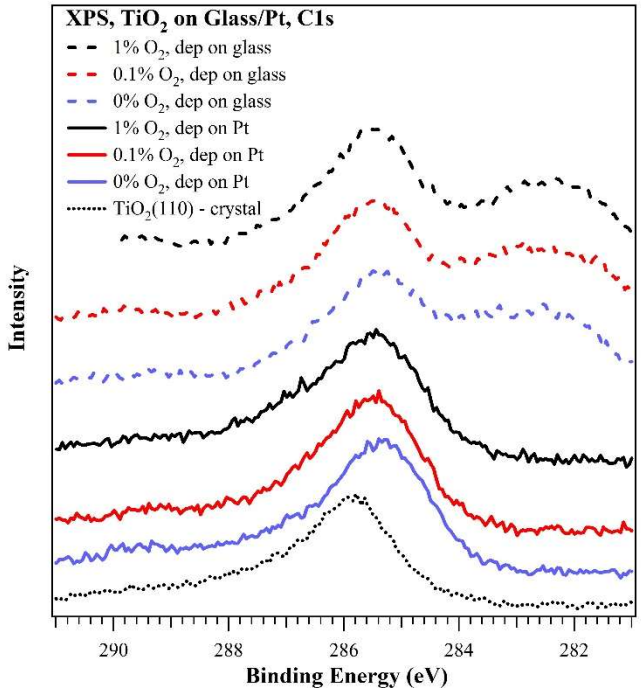

Figure 5.14: C1s core levels from all analyzed TiO_2 thin films deposited by PMCS. Results from a rutile TiO_2(110) single crystal (not treated) are shown for reference. Spectra are normalized in height.

O1s and Ti2p core levels are shown in Figure 5.15 and Figure 5.16, for TiO_2 films deposited on Pt and glass substrates respectively. While O1s typically shows a main feature around 530.5eV, with a broadening on the high binding energy side, Ti2p is characterized by a double peak structure related to the $L_{2,3}$ spin orbit coupling, with main peak at ~459eV and the second structure at ~465eV. As already seen for C1s, film deposited on glass as well as the TiO_2 single crystal are affected by BE shifts due to the insulating character of the substrate, while TiO_2 film deposited on conducting Pt are located at the same BEs.

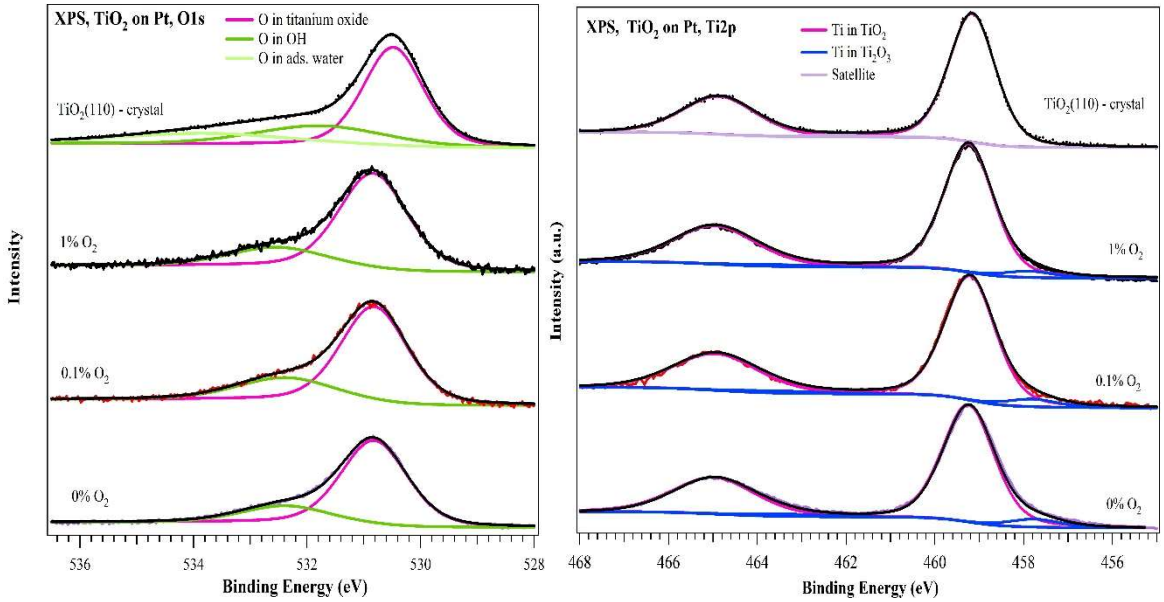

Figure 5.15: O1s (left) and Ti2p (right) core level from TiO_2 thin films deposited on Pt substrates. Results from a rutile $TiO_2(110)$ single crystal (not treated) are shown for reference. Spectra are normalized in height.

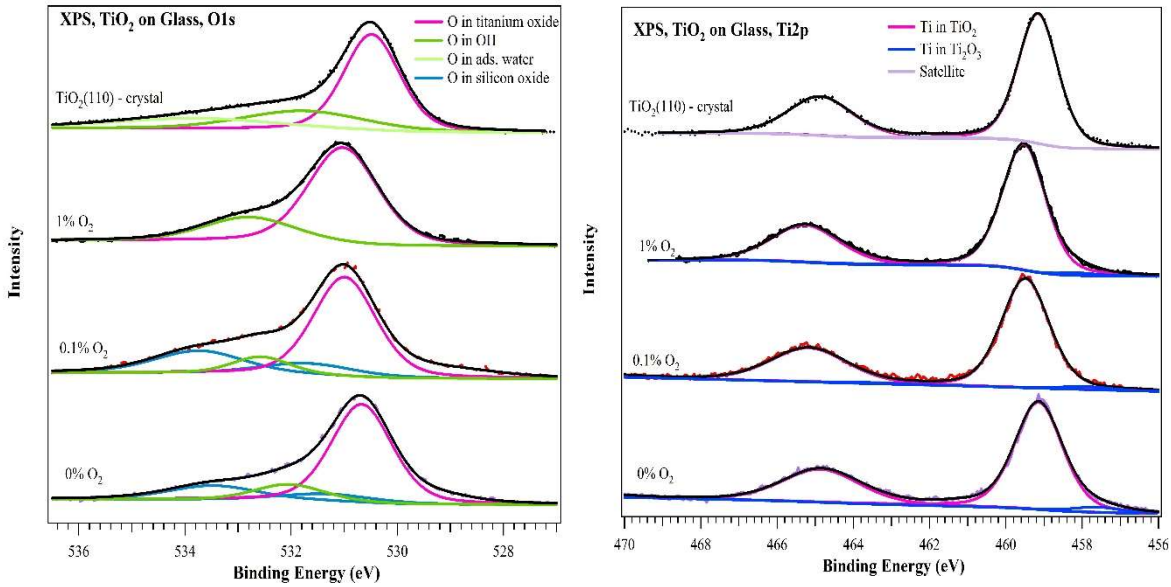

Figure 5.16: O1s (left) and Ti2p (right) core level from TiO_2 thin films deposited on glass substrates. Results from a rutile $TiO_2(110)$ single crystal (not treated) are shown for reference. Spectra are normalized in height.

The deconvolution and detailed analysis of all core levels puts in evidence the presence of different chemical species.

Spectra from rutile TiO_2(110) surface can be considered as a good reference, as rutile and anatase have strictly similar core level values for Ti2p and O1s. Results for the single crystal show presence of a single chemical component for Pt, with Ti2p 3/2-1/2 at 459.2-464.9eV, while O1s main peak is located at 530.5eV and related to TiO_2 species in good agreement with expected experimental values [104,105] of 458.5÷458.7eV and 529.8÷530.0eV, provided BE shifts are taken into account due to the insulating nature of TiO_2 single crystal. The energy difference between main Ti and Oxy components is about 71.3eV, in good agreement with 71.1÷71.5eV theoretical value for TiO_2 [104,105]. Other broader peaks are present at 462.2-467.9eV and are related to Ti loss structure, at 531.8 and 533.8eV and are due to presence of OH groups and water on the surface.

In PMCS films on Pt (Figure 5.15, right) Ti2p 3/2-1/2 features are located at 459.2-464.9eV for TiO_2 and 457.8-463.5eV for Ti_2O_3, with the Ti2p 1/2 band significantly broader than 2/3 one, as often found for oxides [104]. Small satellites, related to electron loss processes, are also present. Regarding titanium, it is present only Ti^{IV+} and Ti^{III+} oxidized forms, i.e. TiO_2 and Ti_2O_3 . We observe a rigid +0.7eV shift in analyzed film, a difference that can be due to the absence of charge compensation in our analysis and is not related to any chemical shift.

Concerning analysis of O1s core level in titanium oxides, it is worth noting the difficulties in properly identifying the different chemical species and thus stoichiometries. Due to the intrinsic large width of O1s core level, the small differences in terms of BE between TiO_2 and Ti_2O_3 species [106], as well as the presence of pollutants from water and OH groups worsening the peak deconvolution [107], this task has been often solved using a unique main peak including all oxide types [107-109]. Nevertheless, also if some interpretations are still controversial [110] and presence of Ti^{3+} in TiOH groups are suggested [111,112], it is accepted that O1s BE in Ti_2O_3 compound is located at 531.5eV, about 74.4eV far from Ti2p 3/2 feature at 457.1eV [105,113,114].

Going back to O1s analysis, the main feature is located at about 530.7eV, i.e. 71.5eV from the corresponding Ti2p 3/2 peak and is thus representative of Ti^{4+} oxide. Other two peaks are present at 532.2eV and at 532.3eV, with the former located at 74.4eV from the Ti2p 3/2

peak of Ti_2O_3 and representative of the sesquioxide, the latter related to oxygen in OH groups. If the O/Ti atomic percentage ratio is evaluated from the relative metal oxide peak (see Table 5.4), for TiO_2 compounds it is observed an oxygen overstoichiometry for 1.0% PMCS films, while the expected ratio is found for 0.1% film. The 0% film is not understoichiometric, as seen in the past [80,115]. This could be unlikely, since oxidation for this film occurs by exposing a metallic film to air, however it can be attributed to the different PMCS working conditions used for this work that led to a great reduction of mean grain size in the film, as shown in paragraph 5.1. This means there is a higher surface to bulk ratio here, improving any oxidation process in atmosphere at room temperature. Indeed, by using old PMCS deposition protocols oxygen understoichiometric film have been achieved. On the contrary, results for 0.1% and 1.0% films are the same as observed in the past. This is expected, since for these films oxidation occurs inside the PMCS source, during the ablation process thanks to the presence of oxygen in the gas mixture.

	TiO_2 on Pt substrate		**TiO_2 on glass substrate**		**TiO_2(110) single crystal**	
O_2 %	**O/Ti in TiO_2 (2.00)**	**O/Ti in Ti_2O_3 (1.50)**	**O/Ti in TiO_2 (2.00)**	**O/Ti in Ti_2O_3 (1.50)**	**O/Ti in TiO_2 (2.00)**	**O/Ti in Ti_2O_3 (1.50)**
1.0%	2.16	1.55	2.40	1.57	-	-
0.1%	2.00	1.54	1.98	1.49	2.02	-
0%	1.97	1.53	1.98	1.51	-	-

Table 5.4: ratio between atomic percentage of Oxygen and Titanium in Ti_xO_y compounds for TiO_2 thin film deposited by PMCS samples on Pt and glass substrates. Results from a rutile TiO_2(110) single crystal is also shown as reference.

	TiO_2 on Pt substrate		TiO_2 on glass substrate		TiO_2(110) single crystal	
O_2 %	**TiO_2**	**Ti_2O_3**	**TiO_2**	**Ti_2O_3**	**TiO_2**	**Ti_2O_3**
1.0%	96.2%	3.8%	96.1%	3.9%	-	-
0.1%	97.1%	2.9%	96.4	3.6%	100%	0%
0%	94.5%	554%	95.1%	4.9%	-	-

Table 5.5: percentage of TiO_2 and Ti_2O_3 oxides for thin film deposited by PMCS samples on Pt and glass substrates. Results from a rutile TiO_2(110) single crystal is also shown as reference.

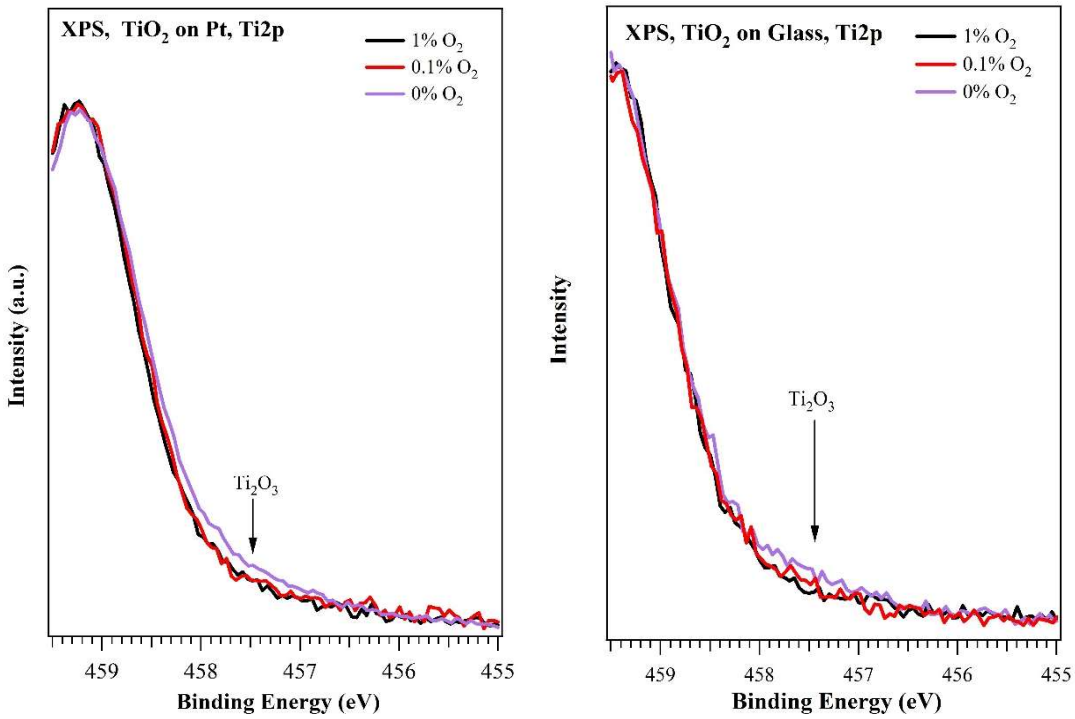

Figure 5.17: Comparison of Ti2p spectra in the Ti2p 3/2 region, to enhance the differences in presence of Ti_2O_3 specie between all PMCS films, deposited on Pt (left) and glass (right) substrates.

If the weight of each of the two titanium oxides is evaluated, it can be seen that there is a marked increase of the sesquioxide by reducing the O_2 content in the gas mixture. This can be seen in Table 5.5 and also by comparing spectra in the Ti_2O_3 Ti2p 3/2 region, as shown in Figure 5.17. This is an interesting behavior, since it is known that this kind of titanium

oxide can improve the surface wettability [116], an important aspect for all biological experiments that will be done (see paragraph 7.2).

Results for films deposited on glass substrate are highly similar from both a qualitative and quantitative point of view (see Figure 5.16), apart from the observed shift toward higher BEs. Briefly, Ti2p 3/2 features (Figure 5.16, right) are located in the 462.7-463.3 BE range for TiO_2 and 461.2-461.8 for Ti_2O_3, with satellites related to electron loss processes. O1s core level has a main peak in the 534.2-534.8eV BE range, with other components in the higher BE region related to OH groups, water and O1s component for the sesquioxide. Concerning stoichiometries, the same trend is observed as for film deposited on Pt, with an overstoichimetric 1.0% film and an increase of Ti_2O_3 weight for the film at 0% (Table 5.4 and Table 5.5). The presence of components from SiO_2 (external to the film) induce a higher error in determining quantitative values, however the trend is the same as previously observed.

NEXAFS experiments on PMCS TiO_2 grown on 1.0cm square silicon wafer were performed at BEAR beamline at ELETTRA synchrotron, Trieste. In Figure 5.13 is shown the Ti $L_{2,3}$ edge spectra from the three different types of TiO_2 from PMCS. The valence band is mainly formed by O 2p (mostly O 2p-derived) levels hybridized with Ti 4s and 4p orbitals [117]. The conduction band (probed by the XAS experiment presented here) is formed by Ti 3d, 4s and 4p, and O 2p orbitals. The crystal field induced by surrounding oxygen atoms splits Ti 3d orbitals in two sub-bands, namely *t2g* and *eg*. Due to the specific orientation towards O 2p orbitals of the surrounding oxygen and larger hybridization with O, the *eg* transition peak is slightly more intense than the *t2g* transition peak and highly sensitive to the crystal structure and coordination. The transitions in the Ti $L_{2,3}$-edge spectra involve excitations from Ti 2p levels to Ti 3d states of a conduction band, leading to the observed complex structure [118,119]. Due to the spin orbit coupling of Ti 2p orbitals, two main groups separated by ~ 5.5 eV are present, L_3 at 456-462eV and L_2 at 462-2659eV. In addition to the spin orbit coupling, the crystal field splits the 3d level into two sub-bands t_{2g} and e_g., giving rise to the structures in each L_3 and L_2 group at lower and higher energy, respectively.

The peak positions, relative intensities of all NEXAFS features of Ti $L_{2,3}$ edge are almost identical for all the studied stoichiometies, and are typical of an anatase TiO_2 phase,

confirming the previous micro-Raman analyses [120,121]. The interpretations of the spectra suggest the (electronic) structure of the three TiO_2, so the dominant phase is the anatase. It is worth noting how the different amount of oxygen employed in the growth process does not seem to deeply influence the final crystalline phase.

Together with the previous XPS results, this suggests that the observed oxygen excess does not change the crystalline phase or, unlikely, being confined on the more external and surface part of the film, or on the grain borders. This is difficult to understand, due to the intrinsic characteristics of the PMCS process leading to an efficient synthesis of TiO_2 clusters not only confined to external parts of cluster itself. More probably, we are dealing with structural defects distributed in the lattice, not affecting the anatase crystal structure but that could be important when studying memristive properties, where oxygen presence plays a crucial role.

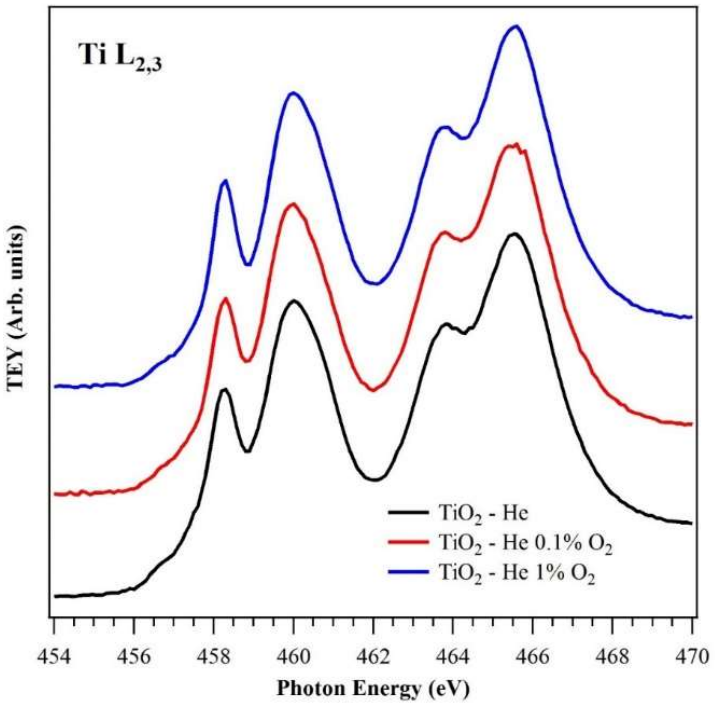

Figure 5.18: NEXAFS spectra of TiO_2 thin films grown using different gas carrier by PMCS deposition setup.

SEM and AFM measurements were performed to evaluate the morphological properties of the TiO_2 thin films. At first, SEM investigation was carried on to evaluate the thickness of the thin films grown on the platinum substrates. The found values confirmed the significant

reliability of the deposition process on the control of the thickness by quartz microbalance. Indeed, 52nm ±3nm was the expected thickness.

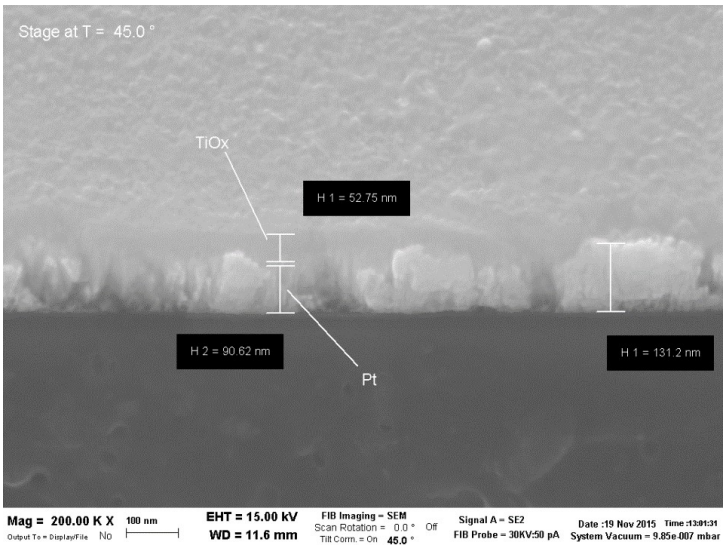

Figure 5.19: SEM image of PMCS TiO_2 on platinum substrate (cross section).

Moreover, the surface observations of all the stoichiometries have confirmed the micro Raman conclusions that the average grain size is in nanometric range. In Figure 5.20, Figure 5.21 and Figure 5.22 it is evident that the average size of the grain was smaller than 20nm and the roughness was lower than 3nm for all the stoichiometries. Moreover, the distribution of the size of the grain managed to be very narrow around its mean, thanks to the developments of the deposition setup, already described in the paragraph 5.1.

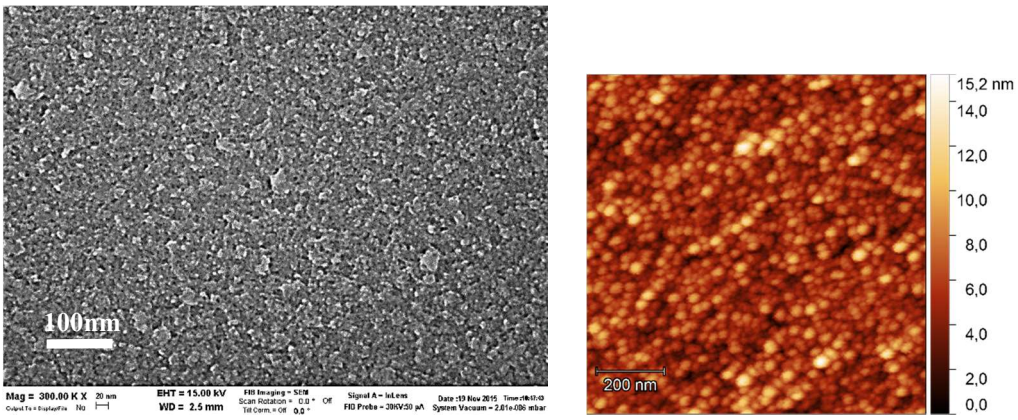

Figure 5.20: SEM and AFM images of TiO_2 on Pt substrate grown using 0% O_2 carrier gas.

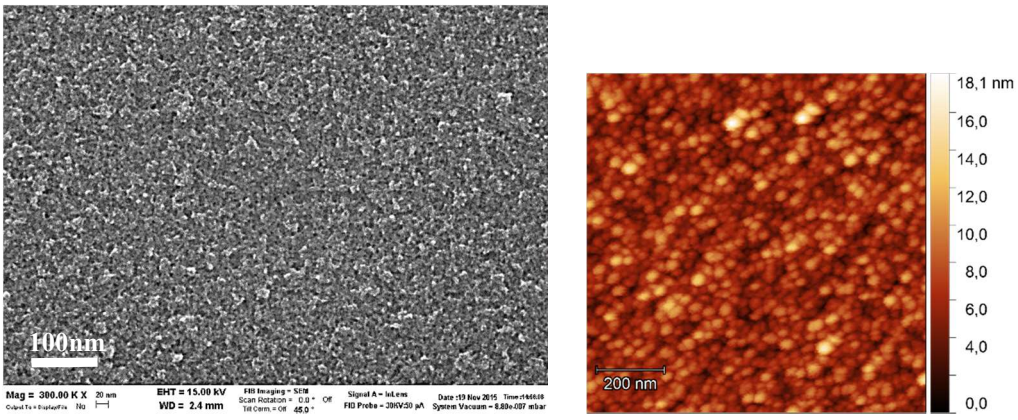

Figure 5.21: SEM and AFM images of TiO_2 on Pt substrate grown using 0.1% O_2 carrier gas.

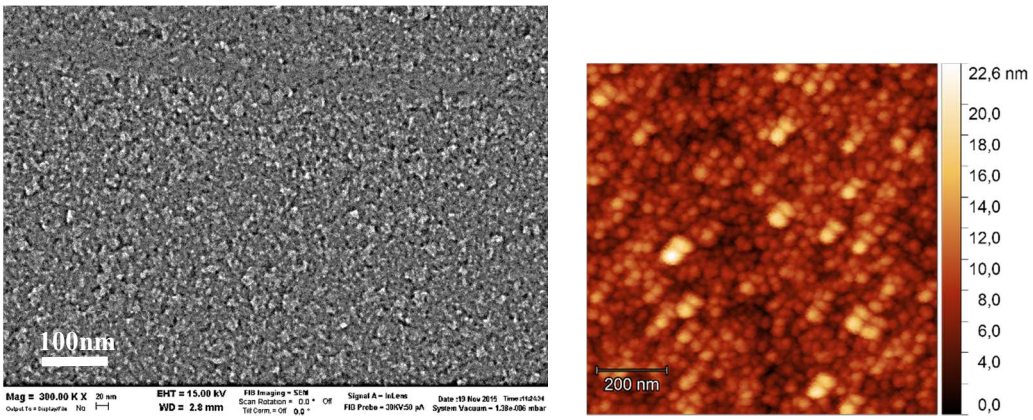

Figure 5.22: SEM and AFM images of TiO_2 on Pt substrate grown using 1.0% O_2 carrier gas.

Concerning the biological applications, the TiO_2 thin films deposited by PMCS on coverslips glass were analysed by a different AFM machine (see paragraph 4.2.4). Also in this case, three different films were produced by depositing the TiO_2 films with increasing percentages of oxygen in the mixture carrier gas: pure helium, helium with 0.1% and 1% of oxygen, respectively. The surfaces were characterized by the presence of some particles, which are visible also on the glass substrates that are used for the film deposition. Figure 5.23 shows a typical AFM image acquired on the film produced using a gas carrier with 0.1% of oxygen (right) compared with bare substrate (left).

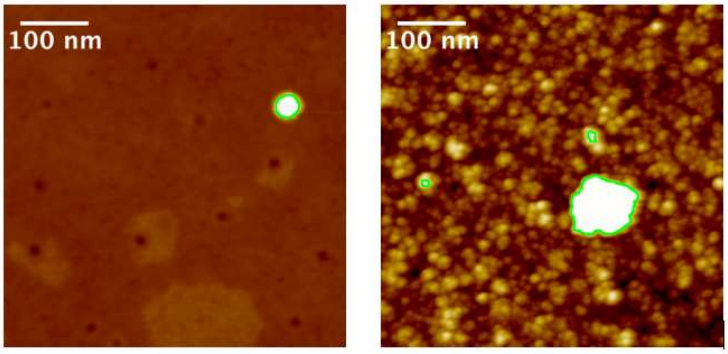

Figure 5.23 AFM scans showing the bare substrate (left) and a film obtained when depositing under 0.1% oxygen in the gas carrier.

The roughness of the films in the three deposition conditions are shown in Table 5.6

Film	**Roughness [nm]**
Substrate (bare glass)	0.83 ± 0.21
TiO_2 deposited with 0% O_2	2.9 ± 0.1
TiO_2 deposited with 0.1% O_2	3.0 ± 0.1
TiO_2 deposited with 1.0% O_2	2.8 ± 0.1

Table 5.6: Roughness values computed by AFM analysis on several AFM scans (at least 12).

It was computed discarding the contribution given by disperse particles (as those highlighted in green in Figure 5.23) and considering only the contribution due to the film growth on the glass. An average over at least 12 films for each type has been considered to achieve the final roughness value. These values clearly show an increase of the roughness when compared with the value measured on the bare substrate (0.83±0.21 nm). Being the latter a reference substrate for any kind of cell and neuronal growth, the higher roughness values for TiO_2 films must be taken into account when comparing the organic tissues activity in Chapter 7. Interestingly, the three deposition conditions results being almost equivalent from a morphological point of view.

5.4 Conclusions

In this chapter, the synthesis and the study of TiO_2 thin film grown by PMCS deposition technique were described in details. By a long optimization of the deposition setup it is possible to synthesize TiO_2 thin films having suitable, controlled and reproducible properties.

With respect to previous studies of TiO_2 from PMCS, roughness, porosity and grain mean size has been significantly reduced. This is fundamental for the final application in electronic devices like memristor, in particular in terms of smaller grain size, absence of debris and film structural homogeneity. All TiO_2 films shows an anatase structure, confirmed by chemical analysis where also a fraction of Ti_2O_3 was found, particularly higher for the 0% oxide. The observed oxygen overstoichiometry for the 1.0% film is probably related to presence of oxygen interstitials in the main lattice structure, and the expected O/Ti ratio for TiO_2 found in the 0.1% PMCS film suggests that this gas mixture is the proper one to achieve the anatase stoichiometry. Any oxygen excess is not lost in the PMCS synthesis but included in the metal oxide in form of atomic interstitials, leading to the observed superstoichiometry.

The small differences in chemical character, i.e. we are always dealing with an anatase structure, lead to presence of defects distributed in the oxide structure and surface and in

form of sesquioxide or oxygen interstitials, located inside the structure but, it supposes, also in grain borders.

We can conclude that morphological and chemical properties are promising for realization of memristive devices: the low surface roughness will help any electrical analysis, while the presence of a typical anatase oxide, possibly with oxygen overstoichiometries are a good starting point to control memristive properties. Finally, the presence of a significant amount of Ti_2O_3 could be useful for any biological application, where a good wettability is obviously required

Chapter 6
Electrical characterization of TiO_2 thin films

In the previous chapter, structural, chemical and morphological properties have been analyzed for the TiO_2 thin films deposited by PMCS technique. These studies are propaedeutic and necessary to better evaluate and discuss the memristive response of these films, thus hereafter focus will be pointed to its study and optimization, being a fundamental aim of this work.

A systematic investigation was performed as a function of the different types of TiO_2 PMCS films in order to evaluate possible differences in the memristive response. The electrical measurements were carried on TiO_2 thin films deposited on a platinum film (the bottom electrode, BE) on glass substrate, using a Ø50µm platinum wire as top electrode (TE). For all the measurements a 0.1V/s voltage rate was kept.

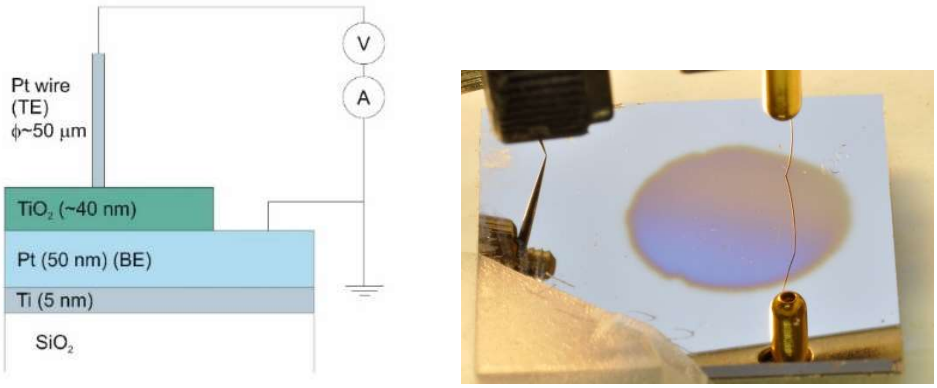

Figure 6.1: Experimental setup for electrical characterization by platinum wire.

6.1 Electroforming process

A voltage-controlled electro-forming procedure was established to induce the formation of conductive filament (CF), thus of the memristive property in the PMCS TiO_2 thin film (Figure 6.2). The procedure described in the following is the result of several experiments, where the final goal was to improve the device performances, finding the best compromise between electrical properties, ON/OFF ratio and life. It was reliable for all three types of TiO_2 film by PMCS.

As described in Figure 6.2, in the first step (black curve), the application of a negative loop voltage from 0V to -10V (line 1 and 2) was employed to form the CF. In this step, a compliance current I_{compl} was maintained at 500μA during the electroforming. The next stage, a voltage loop from 0V to 1.5V (line 3 and 4), without any current compliance, was necessary to bring the device in a higher resistance state (red curve). In fact, the application of an opposite voltage is necessary to break the conductive path, bringing the resistance of the device in OFF state (high resistivity). In particular, the chemical reaction for the rupture process of the CF can be represented by the oxidations of Ti^{3+} ions to Ti^{4+} ions, and the accompanying transition to the insulating TiO_2 phase by a thermo-chemical reaction caused by electro-migrated oxygen ions. The value of the resistance after the rupture of the CF was around 10-100kΩ (curve 5). This wide range of high resistance values reflects how the formation of the CF is not a precise and unique process, leading to CF dimensions (and thus final resistance) that spam in a certain range of values. Interestingly, this is not dependent on the evaluated stoichiometry. Considering that the resistance in OFF state was much smaller than that of the pristine material ($R > 10G\Omega$), this suggests the formation of a CF having probably a defined rupture mechanism, without completely degrading the conductive channel.

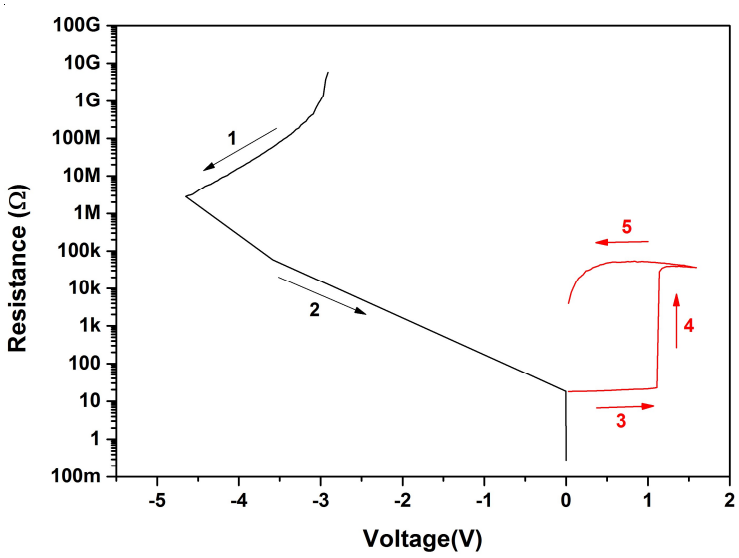

Figure 6.2: Representative electroforming curve.

Generally, it was observed how the applied voltage necessary to electroform TiO_2 thin film increases (in absolute value) with the increasing film thickness (Figure 6.3). This behavior suggested how in thicker films the driving force to move the oxygen vacancies/oxygen ions had to be higher in order to form a stable CF [122]. Surprisingly, after CF formation the memristive response of the metal oxide has no reminiscence of the electroforming process.

As already described, during the electroforming, great energy is applied in the system in order to move the specific ions towards one electrode. In particular applying a negative voltage, the oxygen ions tend to be repulsed from the pristine TiO_2 film to the grounded bottom electrode, and consequently the new created vacancies form localized conducting channels between the two electrodes. When a positive voltage is applied, the filament rupture process occurs close to the interface with the BE, i.e. an intermediate region between the BE and the residual filament is formed, characterized by a higher oxygen vacancy concentration and thus higher resistance [45].

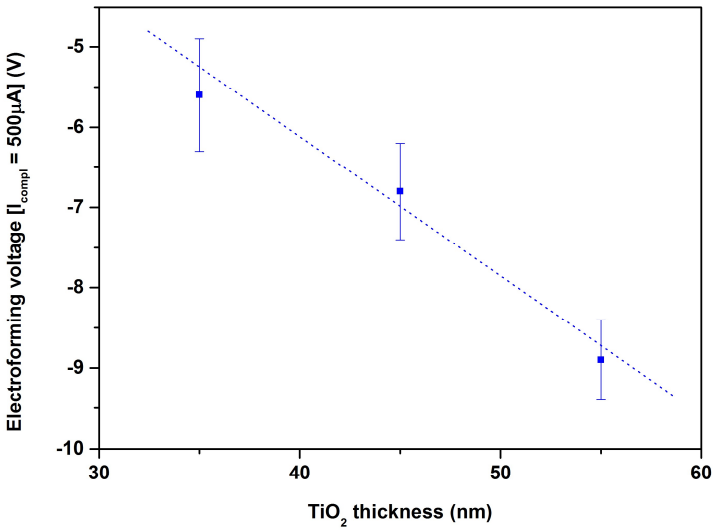

Figure 6.3: Electroforming voltage vs PMCS TiO_2 thin film thickness.

6.2 Memristive response of PMCS TiO_2 thin films

After the electroforming phase, the system was able to show a memristive behavior. By carefully controlling the parameters, such as the sweep voltage range and the compliance current (I_{compl}), all the films with different stoichiometries have shown good and interesting memristive responses. In consideration of the intrinsic and random structure of PMCS thin films, where TiO_2 grows with subsequent agglomeration and densification of material clusters, the memristive responses should be characterized by an intrinsic variability and the optimum values of the applied voltage and current compliance were not known a priori, but had to be properly tuned. Also considering other state-of-the-art memristors, the incredibly high variability of this kind of device is a common task, and also PMCS films seems to obey to this rule.

In Figure 6.4, Figure 6.5 and Figure 6.6 representative memristive behaviors for the three stoichiometies are shown.

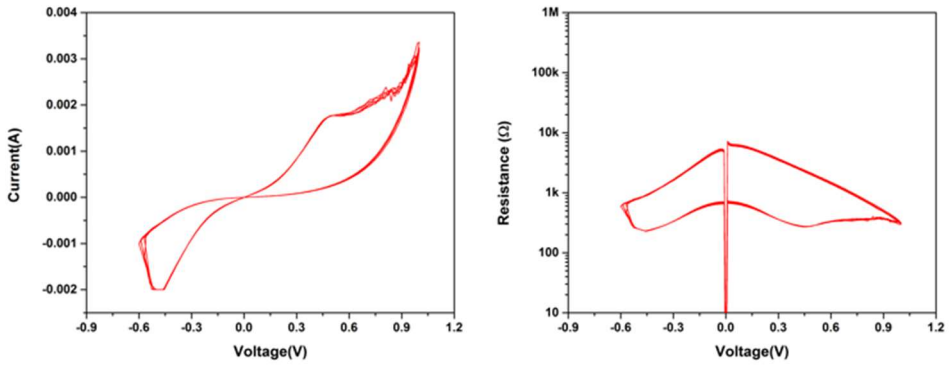

Figure 6.4: Memristive behavior (current vs voltage on the left, resistance vs voltage on the right) of PMCS TiO_2 grown using 0% O_2 carrier gas, 10 representative cycles are shown.

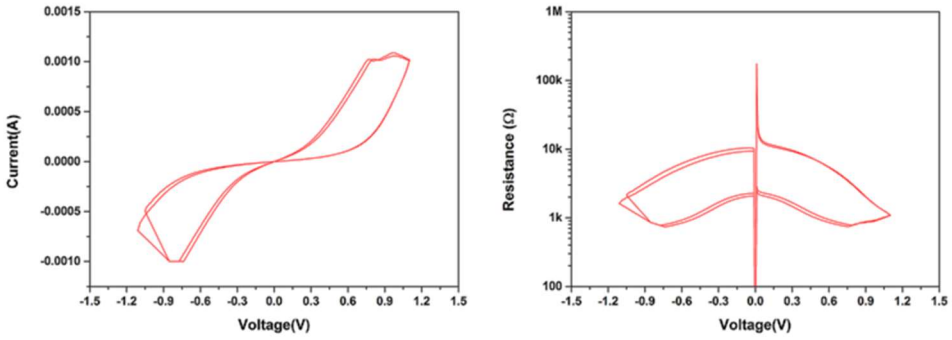

Figure 6.5: Memristive behavior (current vs voltage on the left, resistance vs voltage on the right) of PMCS TiO_2 grown using 0.1% O_2 carrier gas, 5 representative cycles are shown.

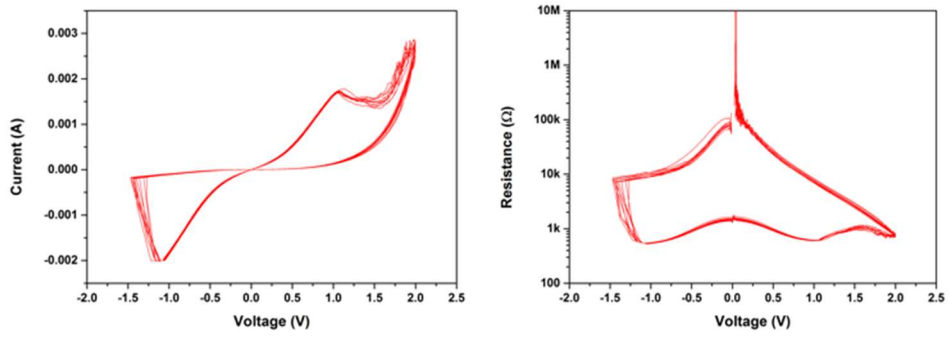

Figure 6.6: Memristive behavior (current vs voltage on the left, resistance vs voltage on the right) of PMCS TiO_2 grown using 1.0% O_2 carrier gas, 10 representative cycles are shown.

It is possible to evaluate how all the three types of TiO_2 films showed a significant memristive response in terms of ON-OFF ratio (higher than one order of magnitude) and stability of the voltage switch during the measurements (less than 0.1V, after 100 cycle). As mentioned, the great fluctuation of the memristive behaviors permitted a limited statistical study and a fully proper comparison among the stoichiometries, easy to understand. Despite the limitations about the measurement method, due to the use of a wire instead of a standard pin, three precise trends were observed with respect of the different film types. In particular, by increasing the percentage of oxygen in the TiO_2 thin films, the negative voltage to change the resistant state becomes higher. A similar behavior was observed on the resistance value in OFF state, that increases with O_2 content in the gas mixture. These two attitudes reflect how the movement of oxygen ions was more difficult in a system where the presence of defects or vacancies was lower, as in stoichiometric TiO_2, or where there is an excess of oxygen interstitials. Moreover, the comparable values of ON/OFF ratio for all the stoichiometries suggest a strong similarity of the involved mechanisms in the resistance switching, despite of the different resistance values involved.

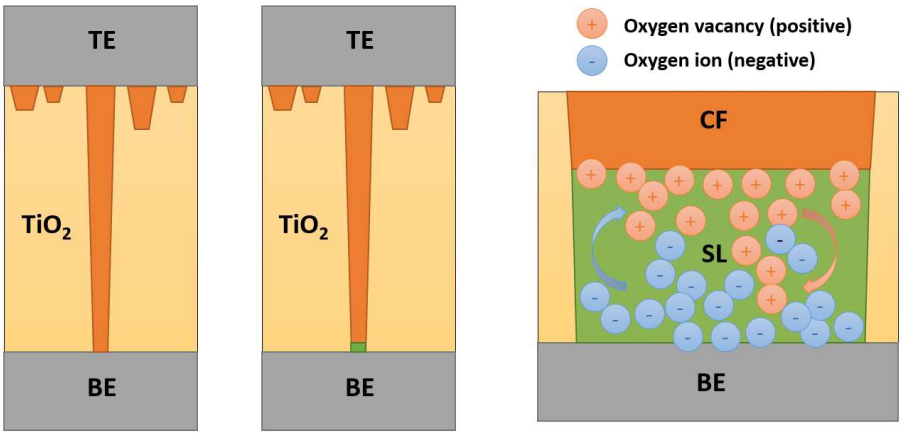

Figure 6.7: Scheme of the memristive response in TiO_2 thin films grown by PMCS deposition technique.

A possible interpretation of the memristive response in PMCS TiO_2 thin films is sketched in Figure 6.7. It shows how the electrical behavior could involve a first formation of strong stable CF and the creation of a switching layer (SL, green area in Figure 6.7) between the final portion of the CF and the BE, in which actually the change of the resistance occurs.

It can be supposed that the SL was formed during the second step of the EF, where the rupture of the CF occurred (line 4 and 5 in Figure 6.2). In this condition, a Schottky barrier (SB) can be formed in the narrow gap region between the end of the CF and the electrode. As known, the width of this barrier is inversely proportional to the square root of the dopant concentration. In TiO_2 system, the oxygen vacancies act as donors and any change in their concentration within the SB affects the barrier width. Resistance switching can be achieved by modulating the SB using the motion of the oxygen vacancies [5]. Indeed, when a negative voltage is applied to the TE, positively charged oxygen vacancies are attracted toward the electrode, thereby narrowing the SB width and inducing HRS to LRS switching. On the contrary, a positive voltage repelled oxygen vacancies from the electrode, thereby recovering the original width of the SB and inducing LRS to HRS switching.

Moreover, the modulation of the Schottky barrier by oxygen vacancy can validate another interesting behavior observed during the electrical characterization of PMCS TiO_2 thin films, or rather the possibility to switch on the device both in positive and in negative voltage. For simplicity, we will label the first mode as positive mode (PM) and the second as negative mode (NM).

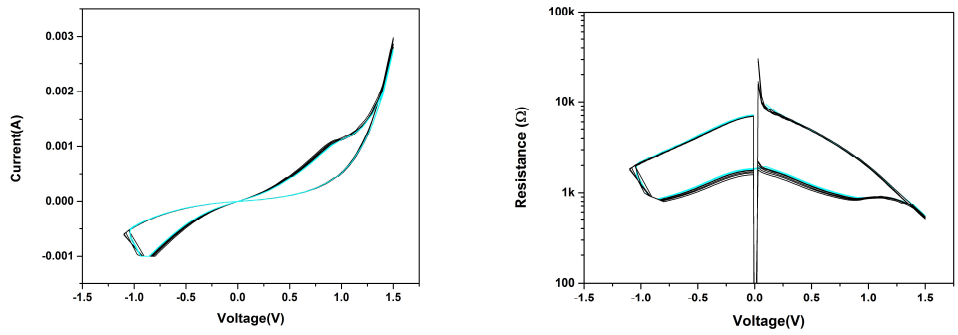

Figure 6.8: Example of PMCS TiO_2 thin film switching in NM, negative mode (current vs voltage on the left, resistance vs voltage on the right).

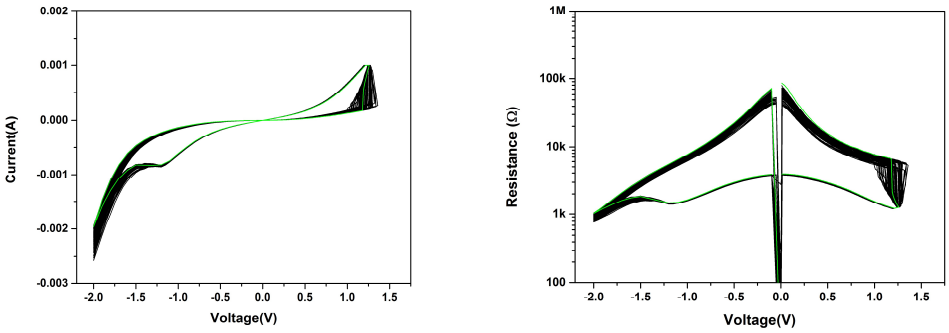

Figure 6.9: Example of PMCS TiO_2 thin film switching in PM, positive mode (current vs voltage on the left, resistance vs voltage on the right).

Several works [50,60,123,124] proved that the switching between NM and PM depends on the modulation of the SB in the different active interfaces. As described in the introduction of this work, the simple consideration that one single interface (for instance close to the BE) is active and the other one acts as starting point for the CF, the switching polarity is well defined to be NM, assuming that the active interface is biased (TE) and the other interface is grounded (BE). However, it is possible to observe in Figure 6.9 , that the resistance switching occurs also in the opposite side. This observation implies that the active interface can change, and it could be correlated to the slight changes in the width of SB due to a different oxygen vacancies distribution at the interface.

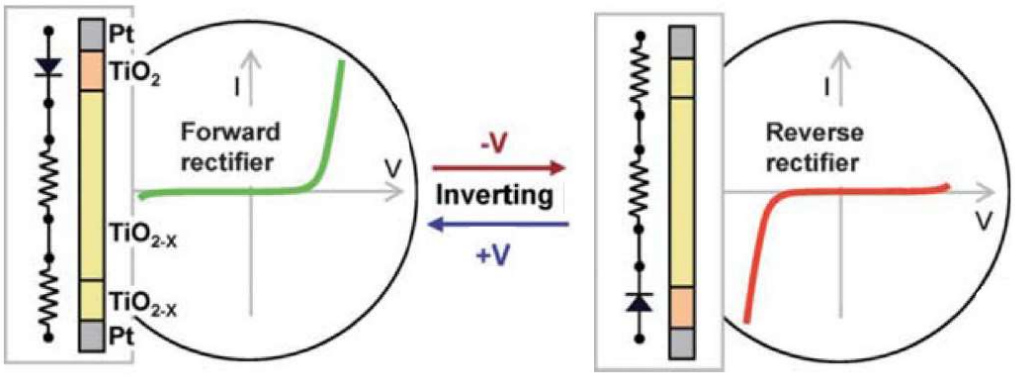

Figure 6.10: Change of active interface in a Pt/TiO_2/Pt device [124].

In literature, the polarity conversion was observed in a Pt/TiO_2/Pt cell [124], built similar of the device studied in this work. In this configuration, a SB can be formed at both interfaces and either height or width can be controlled by the density of the oxygen vacancies. A metal/semiconductor interface under heavy doping typically exhibits ohmic behavior, whereas low doping results in rectifying (Schottky) behavior. A lightly doped layer becomes an active layer, which dominates the resistance of the cell, because the largest voltage drop occurs across the Schottky barrier. Therefore, the resistance of the device is determined by the oxygen-vacancy density at the interfaces. When the oxygen-vacancy density is large at the bottom (top) interface, the top (bottom) interface becomes the active electrode and the cell functions as a forward (reverse) rectifier. These different oxygen-vacancy configurations lead to different polarities when oxygen vacancies move in the interfacial layers in response to an applied bias. When the top interface is the active electrode, the application of a negative (positive) bias to the top electrode attracts (repels) oxygen vacancies toward (from) the active electrode, which decreases (increases) the resistance of the cell. Thus, this configuration generates a NM. When the bottom interface is the active electrode, a positive effect occurs; thus the reverse rectifier generates a PM. Conversion between the two different polarities can be realized by applying a large electric field. When a sufficiently large negative voltage is applied to the top electrode of the forward rectifier, oxygen vacancies will be attracted to the top interface. Through this process, the cell changes to become a reverse rectifier; the top interface becomes a highly doped layer, whereas the bottom interface becomes lightly doped. The opposite transition, from a reverse to a forward rectifier, is also possible when a large positive voltage is applied to the top electrode. To confirm this scheme, it was easily evaluated how the range of resistance in NM and PM are different (see Figure 6.11), proving two different activations of the interface to switch the device.

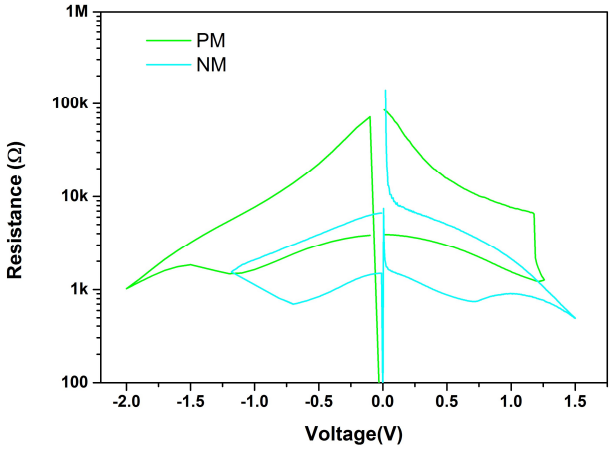

Figure 6.11: Comparison of resistance range of PM and NM behavior.

Interestingly, in TiO_2 systems grown by PMCS technique, NM was the most frequent behavior observed.

6.3 Modulation of the memristive properties

Important information were collected in order to explain the memristive mechanism of these materials and in its control by managing of the experimental parameters. During the electrical characterization of the TiO_2 thin films, two parameters have an essential role in determining the final memristive response: the current compliance (I_{compl}) and the switch reset voltage (V_{reset}). By properly changing these two variables, ON-OFF ratio and SET transition can be modulated.

The I_{compl} is mandatory to limit the current in ON and avoiding a hard breakdown of the insulator, during both electroforming process and in the transition from OFF state to ON state. It was observed that by increasing the I_{compl} the value of the resistance in ON state becomes lower. In Figure 6.12 several examples are shown.

This phenomenon can be explained considering how an extra accumulation of oxygen vacancies in the interface layer before the applied voltage was stopped. By increasing the

I_{compl}, a longer time has given to the system to repulse oxygen ions and increase the conductivity of the switching layers [125,126].

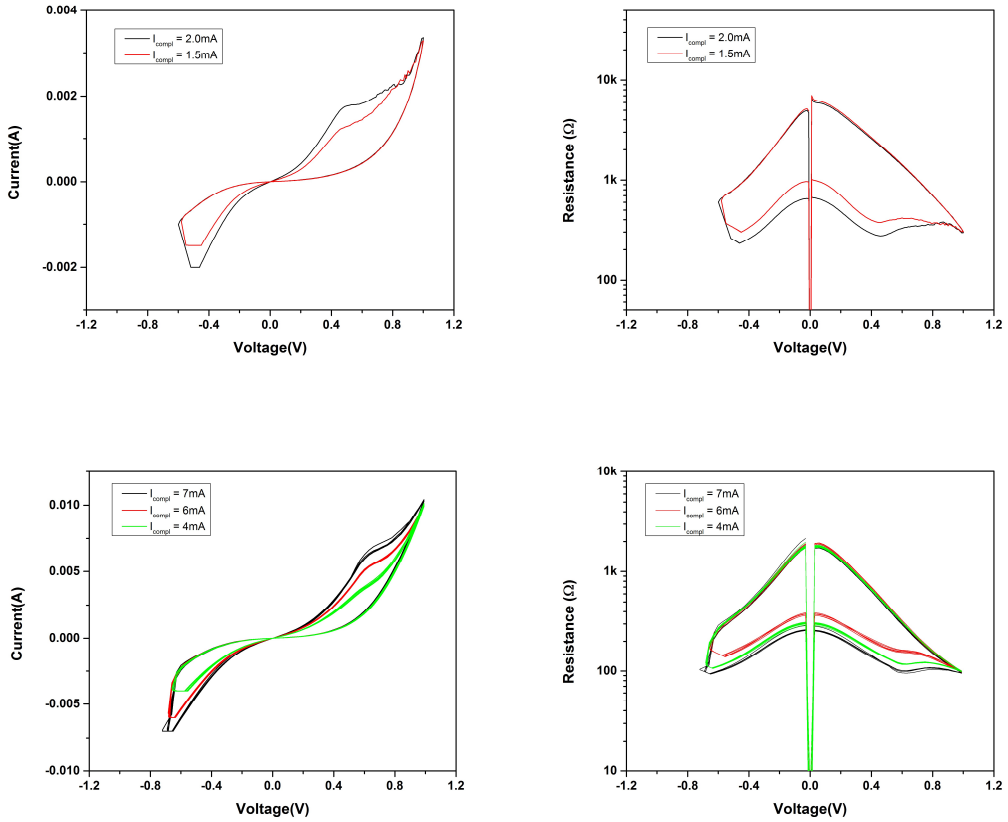

Figure 6.12: Examples of current compliance-controlled multi level resistive switching in PMCS TiO_2 thin films (current vs voltage on the left, resistance vs voltage on the right).

However, the voltage to switch the device OFF resulted to be important as well. Indeed, it was observed how by increasing of V_{reset} several changes in the memristive response were evident (Figure 6.13). First, the resistance in OFF state resulted to be higher, a phenomenon that can be explained by an extra accumulation of oxygen ions in the SL or directly an extended oxidation of the stable CF. Moreover, for the same reason, the voltage needed to switch the device on resulted to be higher at increasing of V_{reset} [127,128].

Finally, the transition from OFF state to ON state was sharper if the value of V_{reset} was greater in the previous cycle. Considering the memristor like a capacitor, an application of higher

positive voltage can create an accumulation of charge at the interface of CF and BE, like they were two electrode plates. If the dielectric constant becomes higher due to the higher presence of oxygen ions, the "discharge" that occurs when the right value of voltage is reached and the switch will be less graduated. Observing Figure 6.7, it is clear that if the amount of oxygen ions is intrinsically higher, due to the growth conditions, the thermodynamic effort to remove part of them will be greater.

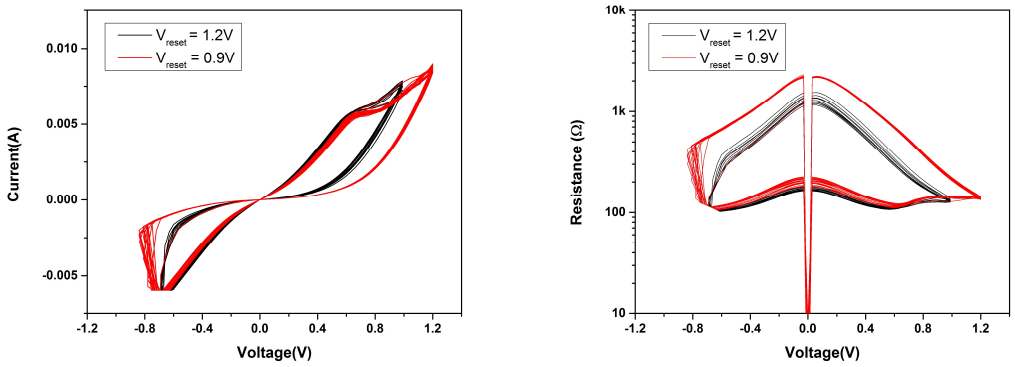

Figure 6.13: Examples of voltage switch off-controlled multi-level resistive switching in PMCS TiO_2 thin films (current vs voltage on the left, resistance vs voltage on the right).

The study of these parameters is fundamental for a perfect control of the memristive response of the TiO_2 thin films. Nevertheless, the measurement protocol employed in this work cannot be considered totally reproducible and reliable. Apart from the intrinsic memristor variability, the platinum wire could lead several problems concerning the stable position of the TE, as well as the possible mechanical deformation of the TiO_2 thin films during the characterization. Nevertheless, device life of more than 1000 cycles have been achieved also in these conditions, as shown in Figure 6.14.

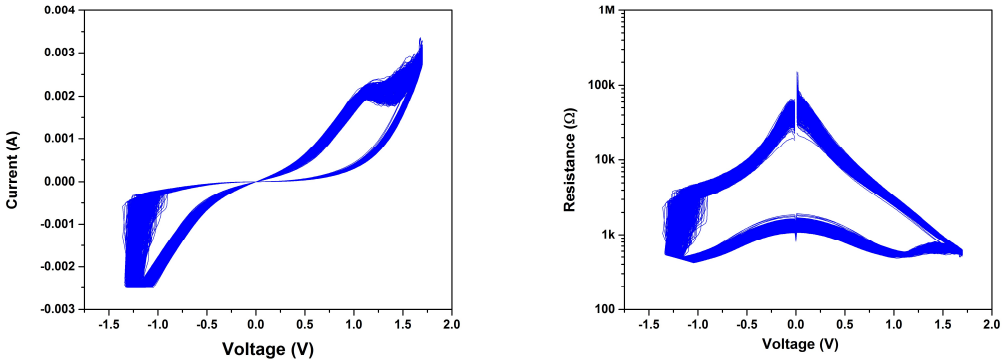

Figure 6.14: Examples of resistive switching in PMCS TiO_2 thin films for over 1000 cycles (current vs voltage on the left, resistance vs voltage on the right).

A possible solution is, of course, the creation of a top electrode made by platinum coating. To this end, several TE platinum deposition were carried out the PMCS TiO_2 thin films in order to increase the reliability of the study. However, a presence of small but not negligible porosity of the metal oxide did not allow the realization of standard sandwich structure composed of two fix metallic electrodes and the active layer (TiO_2), leading to formation of shorts between TE and BE[129]. Only in one case a successful device was achieved and will be described in the following.

6.4 PMCS TiO_2 memristive device prototype

The structure of the PMCS film, being achieved by deposition and agglomeration of clusters, give rise to a certain degree of porosity. Even if it has been highly reduced, considering PMCS films used for gas sensing where porosity was an advisable property [80,36], the formation of an interconnected pore network in the thin film structure can not be completely avoided. This leads to migration of hot metal atoms during TE deposition, with the formation of a platinum path, promoting short circuits in the sandwich structure. This electrical behavior became more self-evident when the resistance of the device in pristine state was less than 20Ω. However, despite the limitation concerning the porosity of the thin film, a first PMCS TiO_2 device prototype has been realized.

A 60nm PMCS TiO_2 was grown using a 0.1% O_2 in the carrier gas. Then, circular platinum dots have been deposited by electron beam evaporation to create top electrodes having a thickness of 50nm, using a hard mask with Ø275µm hole. Clearly, the presence of a fix TE allowed the use of a standard steel spring contact tip and the bottom electrode was grounded, as usual.

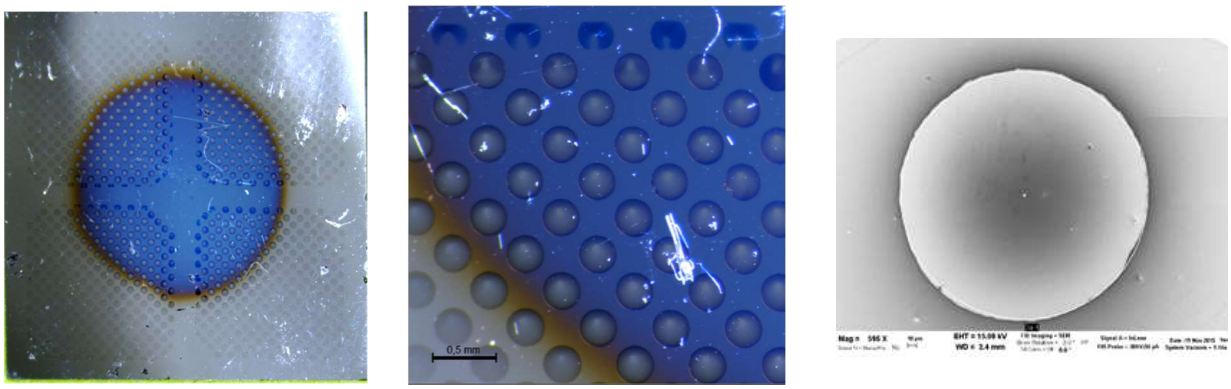

Figure 6.15: The PMCS TiO_2 prototype: increasing magnification of the platinum TE.

After a mandatory electroforming process, the device has shown a good memristive response, as following:

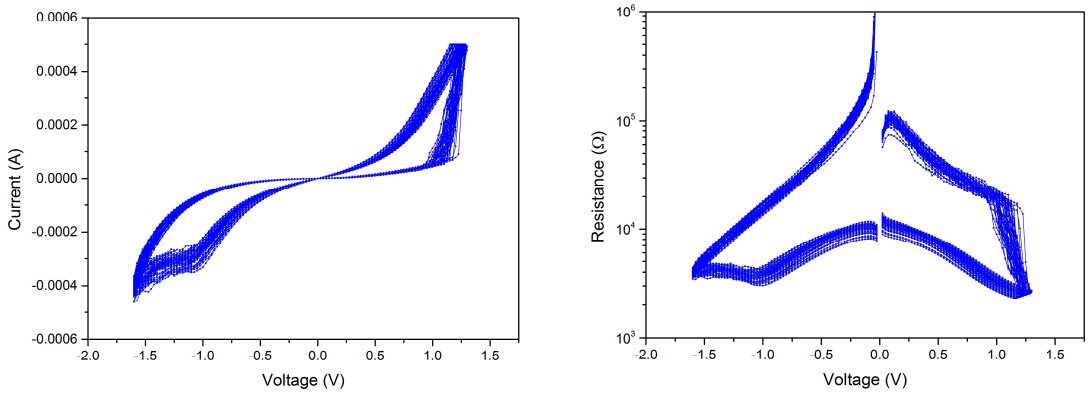

Figure 6.16: Memristive response of first PMCS TiO_2 prototype, with Pt film as both TE and BE (current vs voltage on the left, resistance vs voltage on the right).

Both the voltage switch (V ≈ 1.1V) and ON-OFF ratio (1 order of magnitude) were stable in time up to 200 cycles. In a longer range of the cycles (more than 1000 cycles) the ON-OFF ratio tends to reduce and final ON-OFF ratio is stabilized at 0.7. This behavior could be due to excess of oxygen ions in the switching layer that led towards an higher values of the resistance both in OFF and in ON state [130,131].

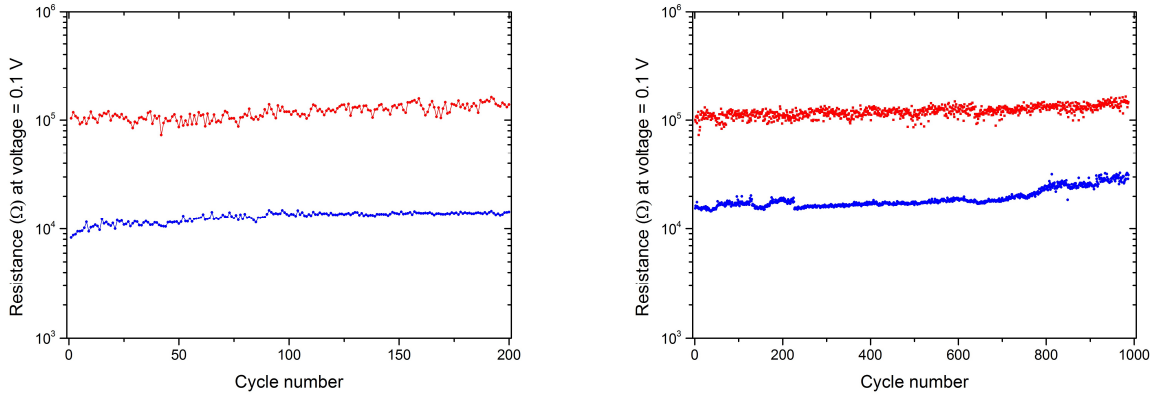

Figure 6.17: Evolution of the ON and OFF resistance values @ 0.1V vs cycle number.

6.5 Conclusions

For the first time, the PMCS deposition technique was employed for the synthesis of nanostructured TiO_2 thin films for memristive applications. A consistent study was carried on to optimize and understand the best experimental conditions concerning the electrical characterizations. It was established a suitable protocol to electroform the material and make it memristive. Using a Pt wire like TE, all the metal oxides studied in paragraph 5.3 have shown a very interesting memristive response, modulated by the intrinsic chemistry of the material. In particular, by increasing the oxygen percentage in the matrix, both resistances (ON state and OFF state) and the voltage switch increase. Moreover, it was possible to control the final response by changing two main parameters such as the I_{compl} and V_{reset}. Finally, despite the limitation in the creation of a device in MIM configuration, a first prototype was proposed showing same main electrical properties, with device life as long as 1000 cycles.

Chapter 7
PMCS TiO_2 thin film for biological application

In the following chapter, an important study was carried on to evaluate the realization of a hybrid system where the electronic device (memristor) and the biological environment (neuronal tissue) are able to communicate with each other by electrical signals is one of the most challenging task of Madelena project, and thus also of this thesis work. The PMCS TiO_2 thin films are a priming candidate to fulfill this role thanks to their memristive response, evaluated in paragraph 5.3, and to the tendency to form active interfaces with organic molecules [93]. However, the biological and neurological compatibility of the TiO_2 thin films deposited by PMCS is a fundamental step to achieve the final issues, and for these reasons, has been studied in detail.

After a brief introduction to the concepts leading the researches presented in this chapter, the biocompatibility of the PMCS TiO_2 films will be investigated, as well as the film stability after organic tissues growth. Finally, the neuronal activity and response for neuronal networks grown on inorganic films will be shown.

Introduction

The nervous system is composed by neurons, specialized cells that are characterized by three parts: *i*) the soma, which is the central body of the cells containing the nucleus; *ii*) numerous dendrites, which propagate from the soma and are committed to receive stimuli from other neurons; *iii*) a single axon, the longer neurite that transmits the electrical signal to other neurons. At the end of the axon, the electrical stimuli activate the release of molecules that are secreted to transmit the signal to the successive neuron. These molecules will trigger an electrical

discharge at the dendrite level of the second neuron, which will propagate towards the soma and successively, if strong enough, to the axon to continue the signaling chain. If this electrical discharge does not overcome a determined threshold, the signal will stop its propagation through the neural network. The threshold is variable and is greatly influenced by the activation history of the neuron itself. Neurons are very delicate cells and they need special attentions and care to be cultivated *in vitro* after the extraction from (typically) mouse embryos.

Neuronal cells can form very complex communication networks, characterized by a marked redundancy and with the possibility to store, maintain, evaluate and move information by using the same system. Indeed, the high degree of interaction allows neural cells to constitute "computing units" with a large parallel processing power able to greatly overcome the capacity of Von Neumann based computing devices [4]. Computing ability of "inorganic electronics" is based on processing units different from memory units and using specific paths to exchange communication. Even if the overall architecture can be parallel in concept, most of the ability to achieve performances of an adaptive neuronal network concerns software and not hardware.

To overtake this limit, new architectures are being investigated by the scientific community. In fact, the proposed similarity of a memristor with an axon [27] is introducing new paradigms toward realization of adaptive systems based on hardware, rather than on software. A synapse is essentially a two-terminal device and bears striking functional resemblance to a memristor. Neurons modify their conductive and resistive capacity depending on their previous "stimulatory experience", allowing the information to proceed only when the received stimuli exceed the voltage threshold of the axon hillock. The electrical resistance of a memristor is not constant but depends on the history of current that had previously flown through the device. By retaining the charge, this lead to formation of a dynamic threshold that has to be surpassed by the input for signal transmission. Processors built with memristors will vary their physical characteristics according to their "experience", progressively developing features such as learning and decision making at the hardware and not software level [17]. Besides, devices with these characteristics could potentially be able to "communicate" with neurons themselves, sensing their electrical activity and adapting to it. The application of this technology could be endless, from the modelling of artificial neural networks to the construction of novel surgical devices.

Such a fascinating scenario is characterized by an intrinsic and highly structured interdisciplinarity, from materials science to electronics, computing up to biology and medicine. This means that most of players are not completely aware of all requirements of such a complex system. In this framework, before proceeding towards more sophisticated applications, the first step to be considered is the biocompatibility of the memristive substrates with neuronal tissues, since the anchoring to the surface is a fundamental issue that could have a great impact on the overall functionality of neurons, starting from their vitality.

7.1 Film thickness and mechanical stability in biological environment

As shown in Figure 5.11, the morphology of all titanium oxide films grown on glass substrates show a mean roughness of ~3nm, i.e. three times higher than the substrate itself that is typically used for standard biological growth. The chemical properties are different in terms of oxygen stoichiometries and surface pollutants, however considering that all films are strongly chemically treated before each biological analysis it is reasonable that all differences in OH or carbon contaminations are lost. XPS analysis have been performed on treated films to check this issue, but presence of post treatment pollutants (due to atmosphere exposure) made this check not reliable.

A systematic study was performed in order to properly evaluate the biocompatibility and final stability for organic cells and tissues grown on TiO_2 films by PMCS.

The inorganic film stability after the previously mentioned chemical treatments, and in typical experimental conditions used for biological tissues growth has been checked by evaluating the film thickness. It was analysed using a P-6 profilometer (KLA Tencor, USA) immediately after film its deposition, after a sterilization step in 100% ethanol and after 14 days at 37°C in phosphate buffer, in order to simulate a neuronal culture.

Several batches of samples (of all titanium oxide types, i.e. 0%, 0.1% and 1.0%) were produced to verify the reproducibility of the deposition process, with satisfactory results. The film thickness for 0% films (shown for example) is reported in Figure 7.1 (vertical bars

for new protocol) and was negligibly different after both treatments, within the typical errors of this kind of analysis, thus suggesting a good stability of TiO_2 PMCS films.

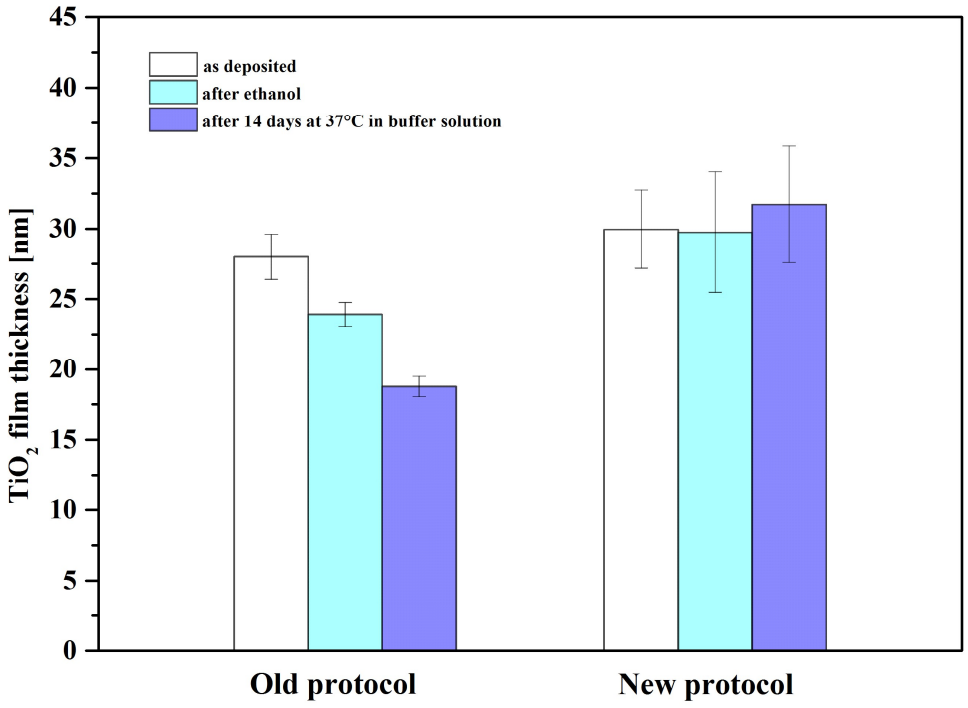

Figure 7.1: Mechanical stability of TiO_2 film grown using old and new synthesis protocols for PMCS approach. Analysis by means of a profilometer in different conditions: as deposited, after ethanol washing and after incubation in phosphate buffer for 14 days at 37°C.

Interestingly, analysis of 0% TiO_2 films realized before the optimization of the PMCS deposition process (Figure 7.1, old protocol bars) has shown poor mechanical stability, with a marked thickness reduction after both treatments. Such a difference is probably related to a lower film density, higher porosity or lower cluster aggregation in the growing film with respect to titanium oxide layers grown using the new and optimized synthesis protocols.

7.2 Wettability

The wettability of PMCS TiO_2 films grown using the three different gas mixtures (0%, 0.1%, 1.0%) were analyzed by a static contact angle measurement. Moreover, using two probe liquids, it was possible to estimate the surface energy, its polar and dispersive components, according to Owens Wendt's method [132]. The polar components are related

to the polar groups, electric charges and free radicals on the surface. The dispersive components are due to the London force and take into account non-polar interactions between the material and the dispersive liquid. They are determined by the roughness, unevenness and branching level of the surface.

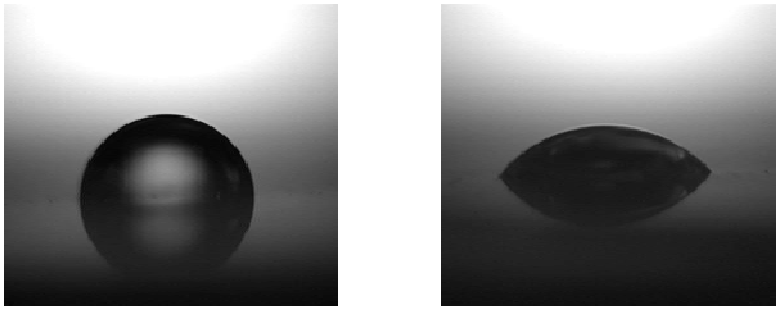

Figure 7.2: Contact angle images of water drop (left) and diiodomethane droplet (right) of TiO_2 on glass grown using 0% O_2 carrier gas.

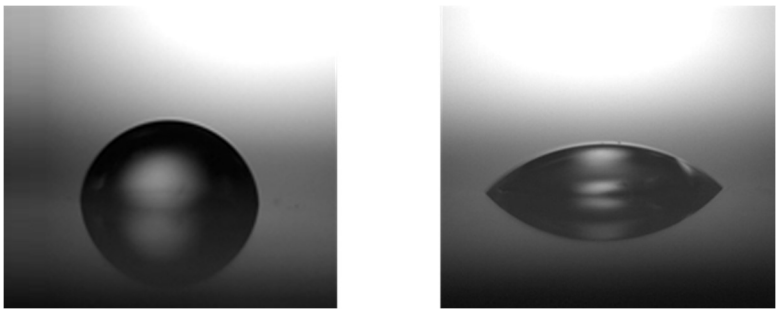

Figure 7.3: Contact angle images of water drop (left) and diiodomethane droplet (right) of TiO_2 on glass grown using 0.1% O_2 carrier gas.

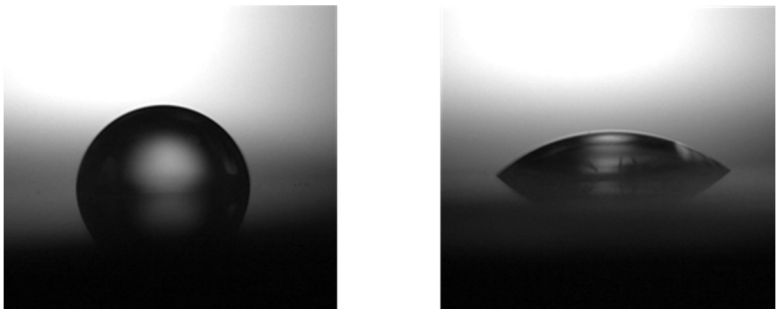

Figure 7.4: Contact angle images of water drop (left) and diiodomethane droplet (right) of TiO_2 on glass grown using 1.0% O_2 carrier gas.

The static contact angle is measured using a custom made system. For each measurement 2µl of deionized water or diiodomethane droplets were placed on the substrate. The images were acquired with CMOS camera and analyzed by Drop-Analysis software [133]. For each sample, the images of 5 drops placed in different zones were observed to improve statistics (Figure 7.2-7.4).

The surface free energy values, calculated in dispersive and polar contributions for all TiO_2 stoichiometries are reported in Figure 7.5**:** where each value represents the average of five measurements and the errors are estimated as the standard deviations.

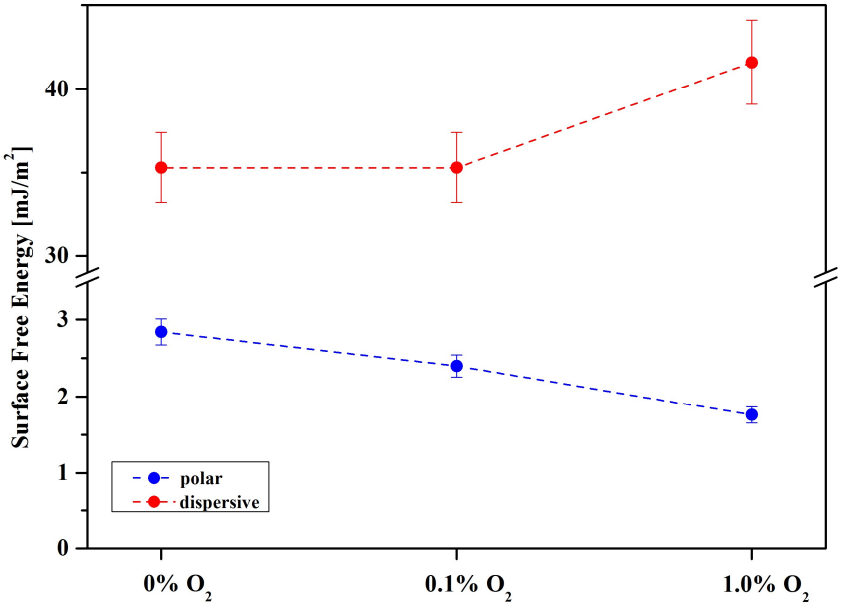

Figure 7.5: Surface free energy calculations on the three different TiO_2 PMCS films.

The polar component is decreasing from stoichiometric 0% and 0.1% films to the over-stoichiometric 1.0% film. This behavior could be correlated to the presence of extra-oxygen on the surface and a lower percentage of Ti_2O_3 in the film synthesized at 1.0% gas mixture. These two parameters could increase the interaction with a polar liquid as water and thus the hydrophobicity of the system. A different behavior in the wettability proprieties could also lead different growth condition in biological environment.

7.3 Biocompatibility and neurocompatibility of PMCS TiO_2 thin films

As observed in paragraph 6.2, PMCS TiO_2 nanostructured films display an interesting memristive behavior, making TiO_2 films suitable candidates for bio-interfaced memristors/neurons. Nevertheless, a necessary condition for neurocompatibility of TiO_2 is its basic biocompatibility in biological environments, which can be proved with the growth of cell lines less demanding with respect to management of neurons. In these experiments, PMCS TiO_2 thin films were deposited on glass coverslips using helium as carrier gas (0%). HeLa and MCF7 cells, derived respectively from cervix and breast cancers, were used. Coming from cancerous tissues, these cells adapt easily to different growth substrates, and for such reason are generally selected to test biocompatibility. For more details, see Appendix B and C. The cells were grown on the slides for 48 hours and were counted after the staining of the nuclei (Figure 7.6).

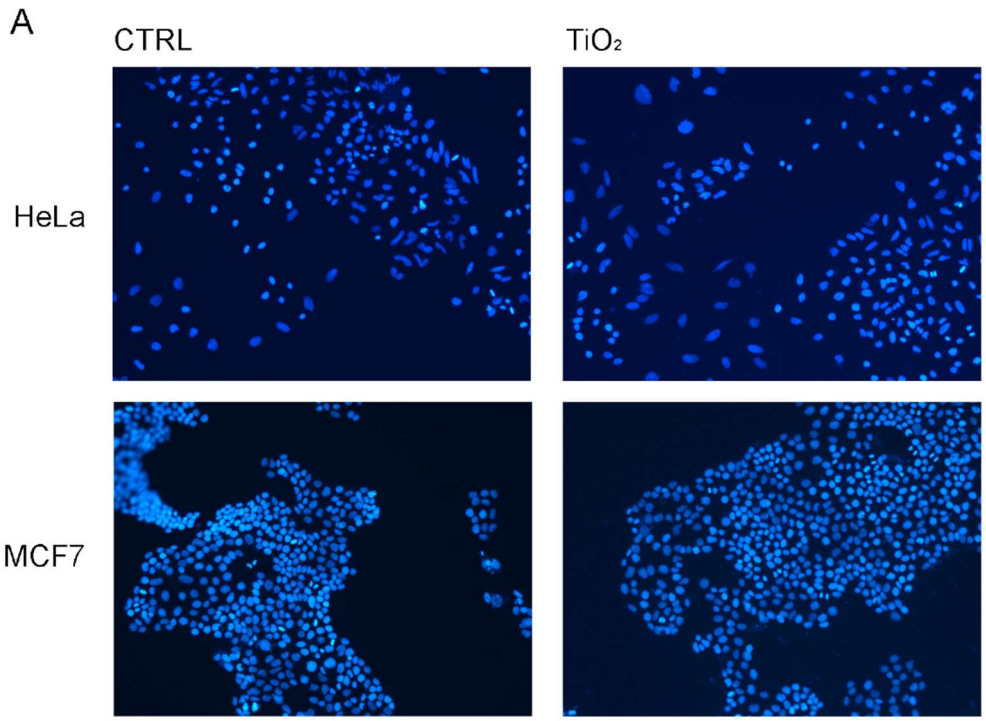

Figure 7.6: Representative image of cells grown on control glass slides (CTRL - left) and TiO_2 coated glass slides (right).

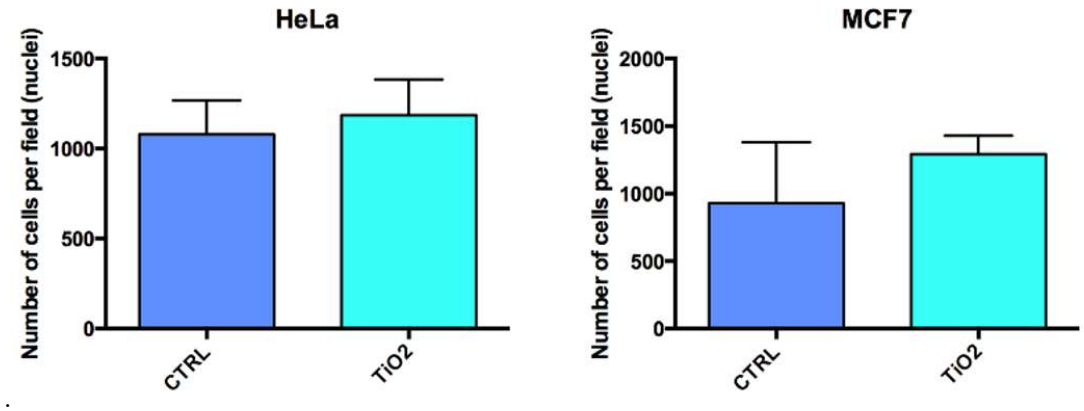

Figure 7.7: Viability evaluation of HeLa and MCF7 cells on TiO_2 coated (0%) glass slides compared to controls. Values express the number of cells and error bars show the standard deviation of the mean.

As shown in Figure 7.7, number of cells on TiO_2 films and glass controls have shown no statistical differences, thus, films grown by PMCS can be considered biocompatible. No further tests have been made with the other two types of TiO_2, i.e. 0.1% and 1.0%, considering that results for the 0% surface where representative enough for the biocompatibility check purpose, as suggested by biologist. In fact, also considering the high number of TiO_2 films necessary for these analysis, it was preferred to develop more significant (and time consuming) tests for neuronal growth efficiency.

The next step was to grow a neuronal culture. As described in the Appendix C, primary neurons were obtained from murine embryos. Compared to tumor cell lines, neurons require more specific and demanding conditions to be efficiently kept in culture, especially regarding adhesion to the surface and the presence of neuro-specific growth factors in the media. To fulfill the latter need, specific media formulations (see Appendix A) have been produced, while regarding the substrates, surfaces are usually coated with a layer of poly-D-lysine (PDL). PDL is a specific polyamino acids, which facilitate the attachment of cells and proteins to solid surfaces in biological applications. It enhances electrostatic interaction between the negatively-charged ions of the cell membrane and the positively-charged surface ions of coated surface. In fact, when adsorbed to the substrate, PDL increases the number of positively-charged sites available for cell binding.

As a preliminary control, to check for any specific neurocompatibility of 0% TiO_2, neurons were seeded on TiO_2 without any poly-D-lysine coating. In contrast with the previously used

tumor cell lines, the neuronal culture showed a very low attachment and no neurite growth after 14 days *in vitro*, as shown in Figure 7.8.

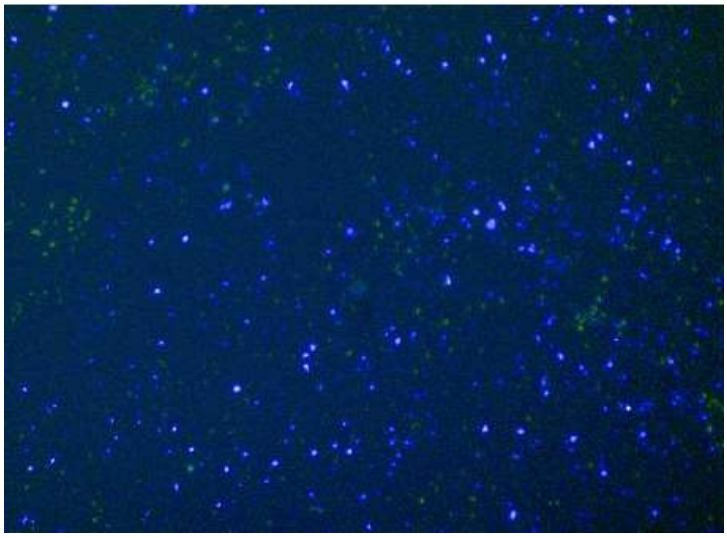

Figure 7.8: Neuronal culture on PMCS TiO_2 thin film, without PDL layer.

Since uncoated TiO_2 thin films gave negative results, PDL coating was evaluated for the successive experiments.

The first test was to verify the efficiency of the adsorption process of PDL on 0% TiO_2 thin film surface. For that purpose, a fluorescein-labeled Poly-L-lysine (PLL-FITC) incubation was performed in order to measure the spontaneous adsorption of poly-D-lysine on these films by optical analysis. The coated was done incubating PDL with the surfaces at 0.01 mg/ml concentration in 0.1 M phosphate buffer pH 7.4 at 37°C for different time periods. After washing, the surfaces were analysed through fluorescence microscopy and the results are reported in Figure 7.9. A high fluorescence signal was observed right at the shortest incubation time (15 minutes), with no further increases up to three hours of incubation. The adsorption on a standard coverslip was also measured in order to have a reference (dashed line in Figure 7.9) with a standard surface.

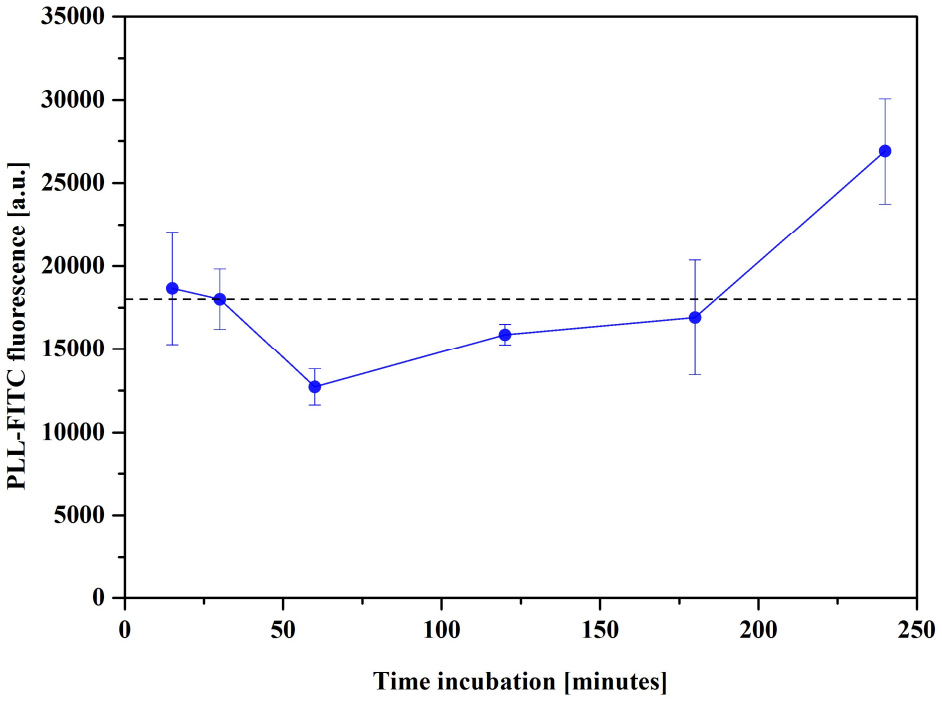

Figure 7.9: Kinetic of adsorption of 0.01 mg/ml PLL-FITC on TiO_2 films (0%) as a function of time. Data are reported as mean values of three areas and the error bars represent the standard deviations. The dashed line represents the PLL-FITC adsorption on a standard microscope coverslip treated for neuronal cell growth.

These films seem to be prone to naturally adsorb polylysine without the need for any specific functionalization process. Thus, after this reliability check with the 0% TiO_2, films with the three different stoichiometries were produced, and PLL-FITC was used to check the spontaneous adsorption on the three different films. A 0.01 mg/ml PLL-FITC solution in 0.1 M phosphate buffer pH 7.4 was incubated on the films for 45 minutes at 37°C (according to the biological protocol used for neuronal seeding). After a washing step, the samples were measured using a fluorescence microscope.

The three films showed a different behaviour. In Figure 7.10 the fluorescence intensity of poly-D-lysine is reported and compared with a standard substrate (quartz).

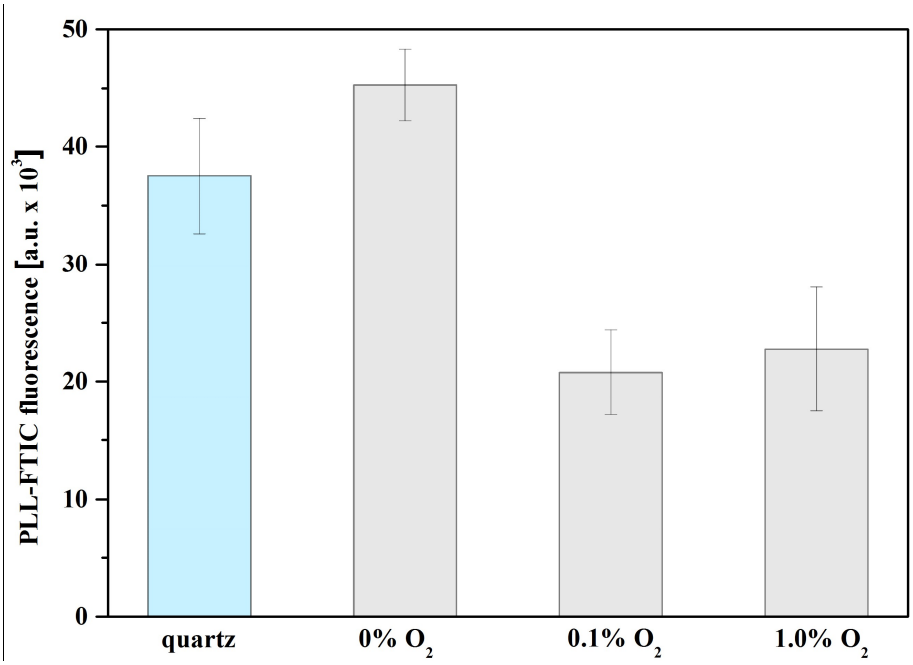

Figure 7.10: PLL-FITC adsorption on TiO_2 films deposited in helium atmosphere with different oxygen content (gray bars) and quartz substrate as reference (red bar). The values are reported as mean values of five areas on three different samples and error bars represent the standard deviation.

The PLL-FITC fluorescence signal is higher on the 0% O_2 film, surprisingly higher than the control surface. This better performance is in good agreement with the observed properties from contact angle investigations (Figure 7.5**:**), suggesting that the 0% O_2 film shows properties that can, in principle, better emphasize the neuronal growth.

Indeed, from this point of view , the presence of PDL on TiO_2 (0% type PMCS) promotes clearly a higher attachment and better growth of the neuronal culture, as can be seen by comparing Figure 7.8 and Figure 7.11. PDL was therefore considered as mandatory and used for all experiments.

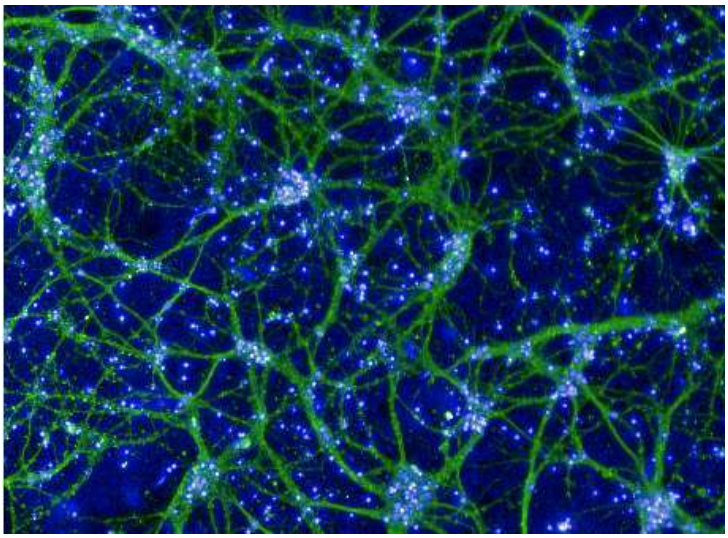

Figure 7.11: Neuronal culture on PDL coated PMCS TiO_2 thin film.

.

Considering these results, neuronal growth studies were extended to all TiO_2 PMCS film types in order to check the influence on neuronal growth. The substrates and the control glass slides were treated accordingly to the protocol previously described. At 14 days in vitro (DIV14), neurons were fixed and analyzed. By day 14, neuronal processes should be properly grown and differentiated, forming a functional network. Different parameters were selected to evaluate the state of the cells. More in detail, it was assessed:

1. the average number of processes;
2. the area of the nuclei on the slide;
3. the average number of extremities per neuron;
4. the average maximum as well as the total length of neurites per cell.

Altogether, the above parameters can be used to describe different morphological aspects to evaluate the development of neurons *in vitro*. All the collected data were compared to controls, namely neurons grown on PDL coated glass slides (Figure 7.12). As can be clearly seen, from a statistical point of view the three TiO_2 surface are equivalent and strictly similar to the reference glass substrate. The number of nuclei and their area, of extremities and maximum neurite length are similar for the four surfaces. Such an efficient neuronal growth is also confirmed by the quality of the developed network, as shown in Figure 7.13.

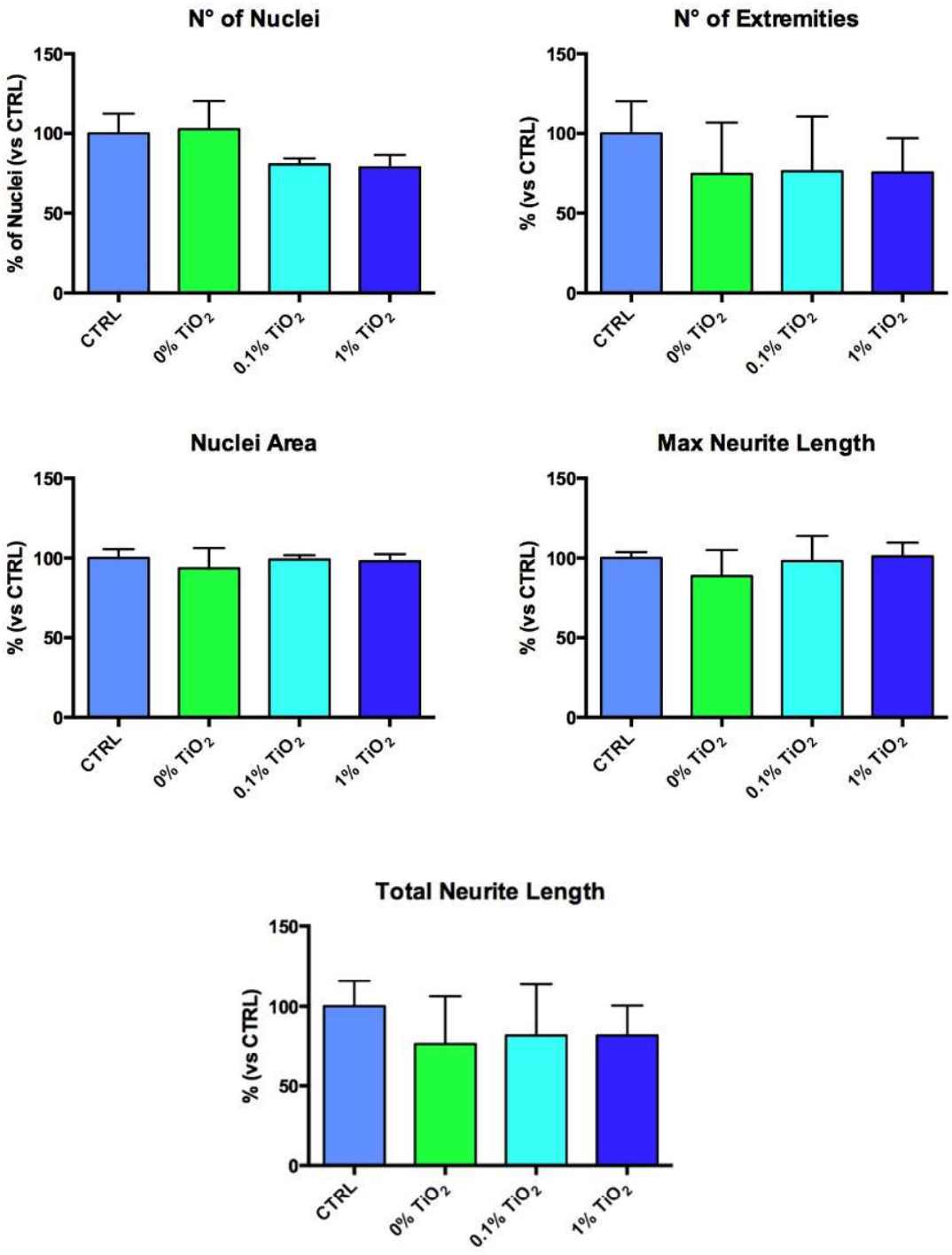

Figure 7.12: Murine cortical neurons were seeded on PMCS-derived TiO_2 films coated glass slides and were compared with glass slides controls at 14DIV. The mean of controls was scaled to 100 and the bars represent the standard deviation of the mean.

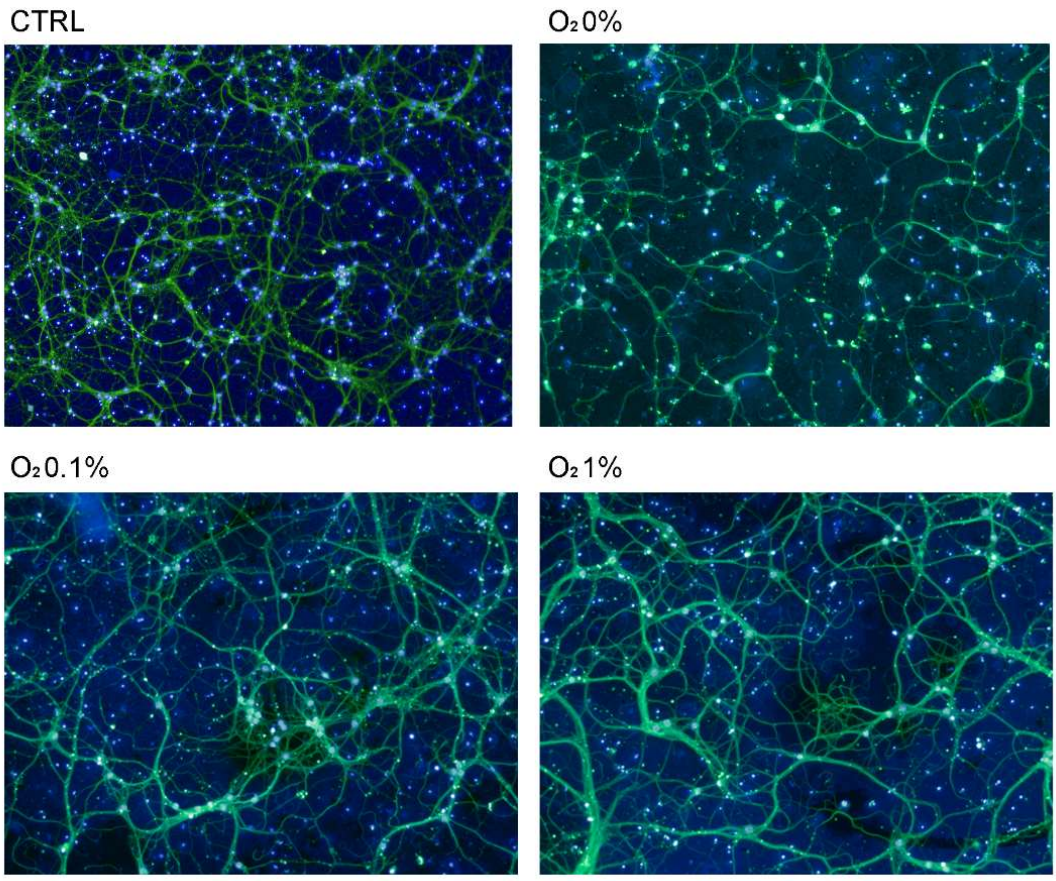

Figure 7.13: Representative images of neuronal growth on controls and TiO_2 coated glass slides.

The different types of TiO_2 PMCS films did not affect neuronal attachment and growth on the substrates, if compared to the control substrate. Also viability (number of nuclei counted) as well as process development of neurons grown on TiO_2 are comparable with controls.

Once verified the influence of the different TiO_2 surfaces in neuronal network growth, it is worth noting the necessity to evaluate a further parameter, element that is necessary when electrical analysis are required. Having in mind the proposed coupling between neurons and memristive devices, the presence of a metallic electrode is mandatory in bottom contact or both bottom and top contacts. Thus, we analyzed the influence of the presence of a platinum surface for the neuronal growth. The substrates and the control glass slides were produced accordingly to the protocol previously described. For this reason, a set of experiments was performed to compare the culture of murine cortical neurons on 0% TiO_2 thin films deposited on platinum slides with those cultured on either normal glass slides or uncoated platinum

(Figure 7.14). All samples were PDL coated. Results shown in Figure 7.14 clearly show that platinum seems to negatively affect the neuronal attachment and development, but the presence of the TiO_2 thin films coating by far improves neurons number.

Thus, it can be concluded that the presence of TiO_2 on the platinum substrate is able to mitigate the negative effects of the metallic electrode.

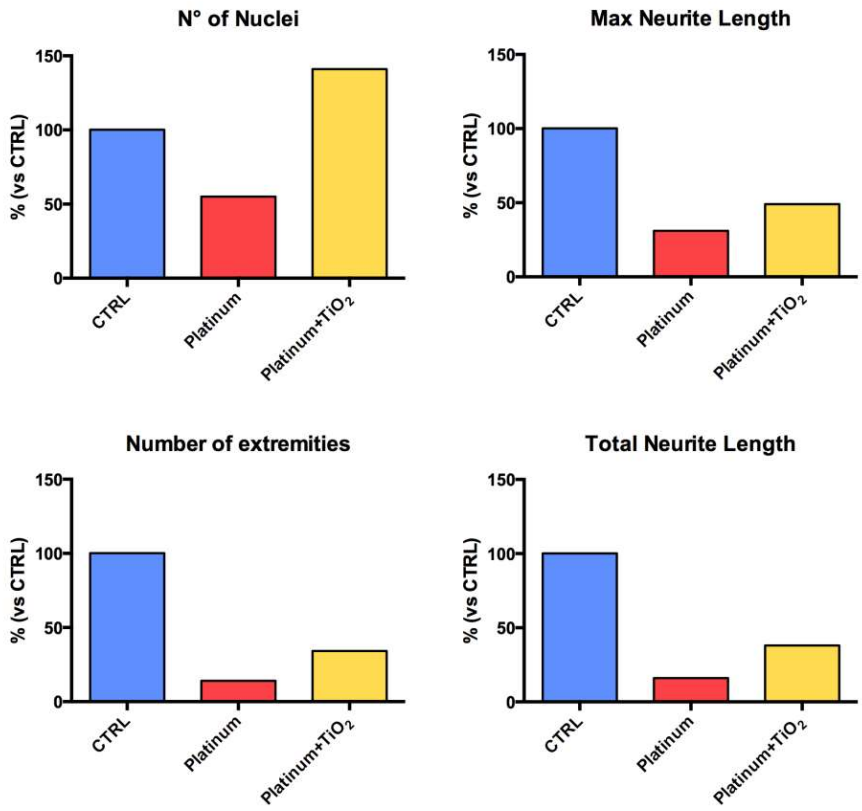

Figure 7.14: Murine cortical neurons seeded on TiO_2 coated platinum slides compared to glass slides controls and uncoated platinum slides at 14DIV.

These results provided promising indications towards the realization of a hybrid system, in which the neurons and the memristive devices could communicate by electrical signals. In particular, the presence of a top platinum electrode should be avoided.

A further step was the evaluation of the electrical activity of the neuron culture grown on PMCS TiO_2 thin films.

7.4 Electrophysiology test

The following evaluation for the assessment of the viability of the cultured neuronal cells consisted in the measurement of their electrical activity through a patch clamp. In electrophysiology, the patch clamp technique is a particular method that allows the study of single or multiple ion channels in cells. It can be applied to a wide variety of cells, but is especially useful in the study of excitable cells such as neurons. Figure 7.15 shows the experimental setup for the electrophysiological tests.

Patch-clamp recordings in whole-cell configuration [134] were performed at non-sterile conditions and at room temperature (~20 °C). To record total membrane currents, in each experiment the culture medium of a dish was exchanged with a bath solution and a patch pipette previously filled was approached to a selected cell. Patch-clamp recording micropipettes were fabricated from GB150-8p (OD 1.5 mm, ID 0.86 mm) borosilicate glass capillaries (Science Product, Hofheim, Germany) using a PIP6 temperature controlled pipette puller (HEKA, Lambrecht/Pfalz, Germany). The current at the pipette tip was reset before establishing the seal by injecting tension via the amplifier circuitry. Bioelectric signals were picked up using a universal voltage/current clamp amplifier (ELC-03XS, npi, Tamm, Germany) connected to a PC computer via a breakout-box interface (INT-20X, npi, Tamm, Germany). As shown in Figure 7.16, a high-precision positioning was provided by a piezo-drive micromanipulator (Sensapex, Oulu, Finland). Instant patch-clamp parameters (e.g., $R_{pipette}$, R_{seal}, etc…) were monitored with the signal acquisition software (WinWCP Electrophysiology Software). A voltage command generated by the computer was responded by the cell as current value, storing both values in the PC's memory. Each stimulation window had 1024 fixed data points with a sampling frequency dependent on time's window. Signal filtering was set using the rule of thumb. Once stored, signals and monitored parameters were processed off-line and current/voltage relationships (IV curves) were calculated (MATLAB, MathWorks, USA). Current–voltage (IV) curves permitted the comparison between cell types adhering to TiO_2 thin film grown by PMCS and controls (cellular culture grown on bare coverslips).

The recordings were performed in the whole cell configuration under standard conditions, mimicking the normal intracellular and extracellular ionic concentrations in order to elicit whole currents. The first step consisted in the evaluation of the currents after seven days (7DIV), since the electrical activity could be influenced by the different degree of adaptation and maturation of the neuronal network on the new surfaces. Once attached to the membrane, whole-cell configuration was obtained accessing to the cell's interior after the rupture of the patch seal (electric resistance R>1GΩ) by glass. To test the voltage activation, the membrane potential was set to a holding level of −40 mV, then starting from −100 mV two alternating stimulation protocols (1 Hz frequency) were used, consisting of 15 pulses of +20mV steps with different temporal durations: short pulses (10 ms) followed by long pulses (100 ms).

Figure 7.15: Experimental setup for electrophysiological tests.

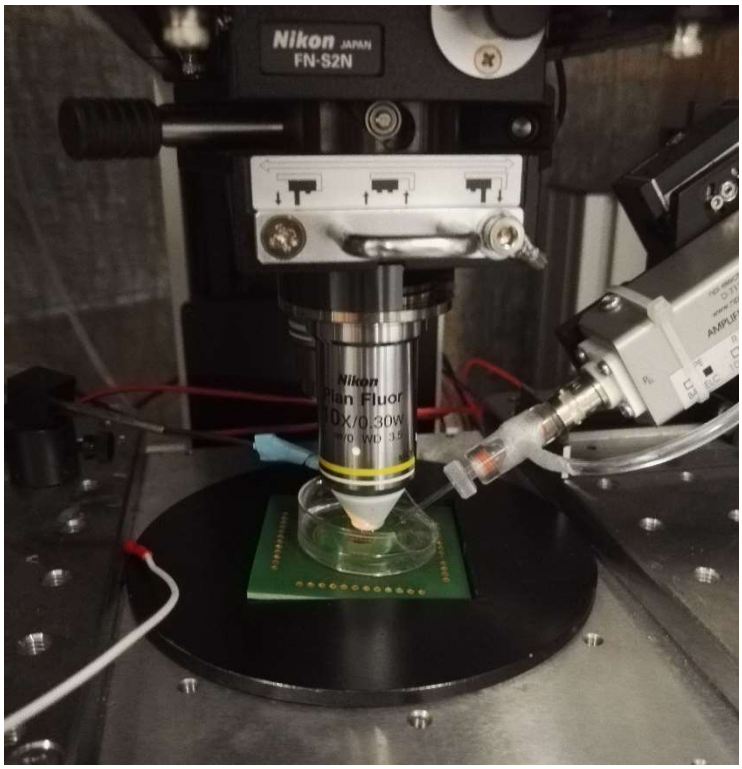

Figure 7.16: Microscope setup and the glass capillary moved by micromanipulator.

The evaluated surfaces consisted in TiO_2 surfaces obtained under different deposition conditions, namely 0%, 0.1% and 1.0% O_2 gas mixture with He. All the TiO_2 different film types were investigated to evaluate a possible role of the surface chemistry in the cellular response. It has to mention that the environmental conditions were dramatically different with respect to the incubator parameters. In particular, the percentage of CO_2 (5.0% and 0.03% respectively) and the temperature (36°C and 20°C respectively) could modify the viability of the neuronal culture. However, this effect is appreciable only after a long time (around 60 minutes) and for this session of experiments was considered negligible.

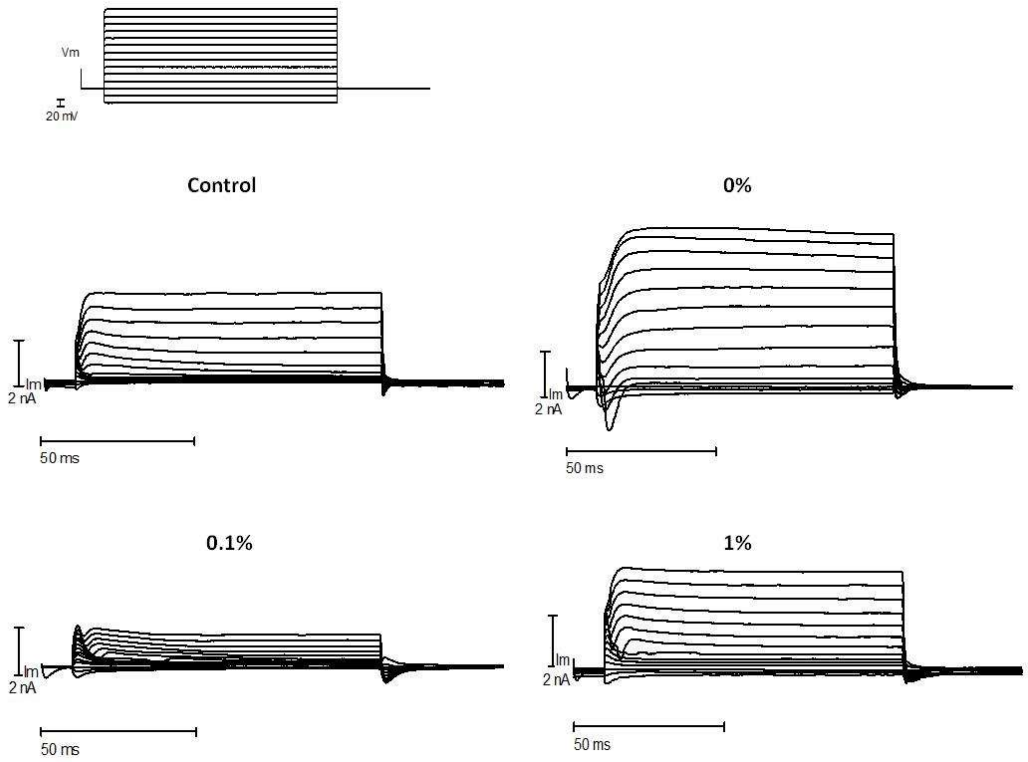

Figure 7.17: Representative current recordings of 7DIV neurons on the different TiO_2 surfaces. Voltage Clamp mode with a voltage step stimulus of 14 steps from -150mV to 110mV for 100ms.

Figure 7.17. shows representative current recordings in the voltage-clamp mode of neurons on control and on the different TiO_2 surfaces. The main differences consisted in the value of currents in the steady state period and in the voltage at which the activation occurred. Therefore, the analysis was focused on the maximal current in the steady state period ($I_{maxSteady}$) and on the evaluation of the membrane potential.

Indeed, the statistical analysis of $I_{maxSteady}$ (see Figure 7.18) showed how elicited currents higher than the control were observed for the 0% TiO_2, lower for the 0.1% while no significant differences were observed for the 1.0%.

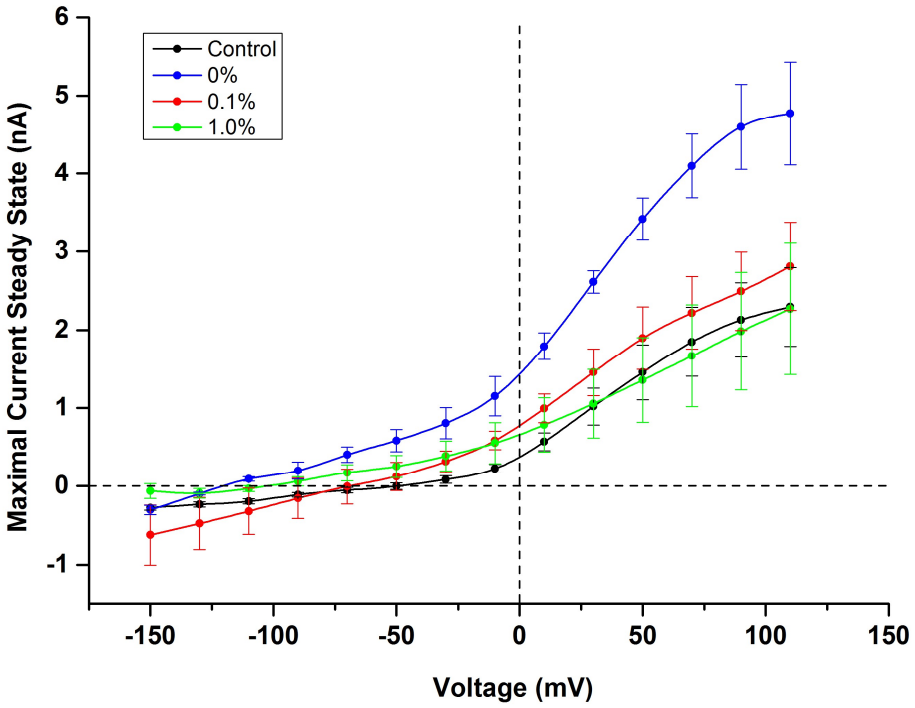

Figure 7.18: 7DIV neurons on the different TiO_2 stoichiometric surfaces (I-V graph of the steady state currents).

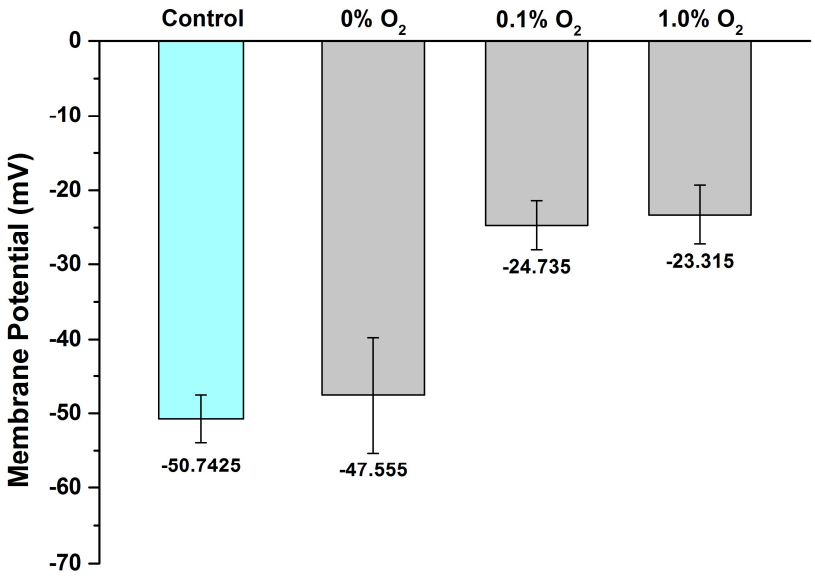

Figure 7.19: 7DIV neurons on the different TiO_2 stoichiometric surfaces (Membrane Potential)

Regarding the membrane potential (Figure 7.19), the 0% TiO_2 showed no statistical differences (mean=47.55mV) compared to the control (mean =50.75mV), but was significantly higher than the other two TiO_2 PMCS films.

A lower negative membrane potential could explain the higher excitability of the neurons and therefore, the increased elicited currents. Thus, considering the higher $I_{maxSteady}$ and the low membrane potential, the 0% TiO_2 surfaces demonstrated the best performances for the bio-hybrid system. For these reasons, the 0% TiO_2 film was chosen as the surface of choice for all further experiments.

Finally, for the evaluation of the spontaneous electrical activity, the action potentials without any kind of stimulus in the current clamp mode was recorded. Figure 7.20 shows that both, control and 0% TiO_2 neurons, have comparable spontaneous activity.

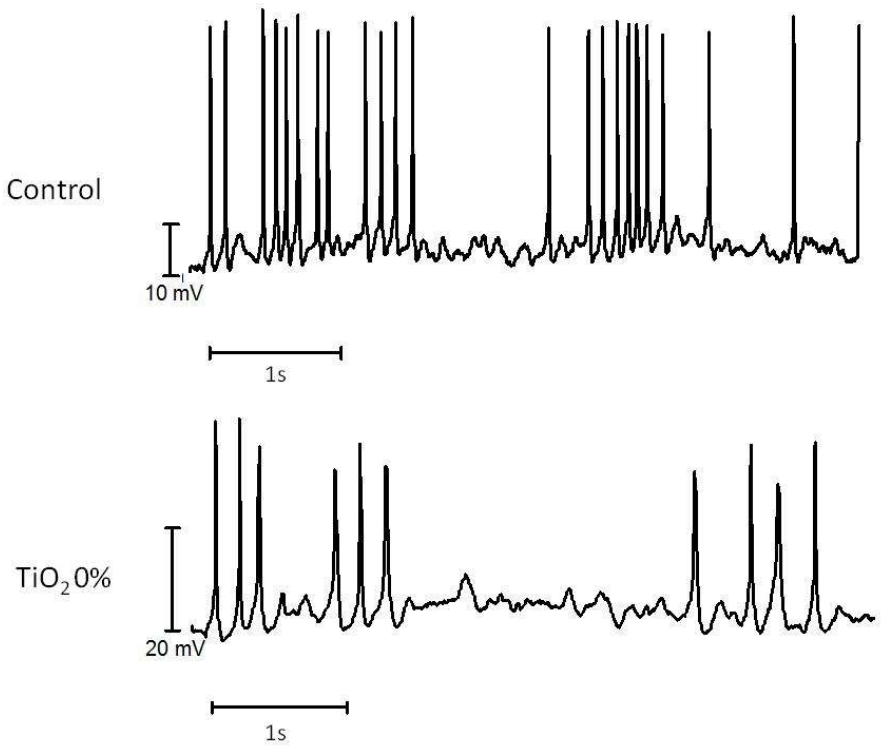

Figure 7.20: Representative recordings of the spontaneous electrical activity in 7DIV neurons on control and 0% TiO_2 surfaces.

7.5 Conclusions

An important study on over 100 TiO_2 thin films has been carried on the biocompatibility and neurocompatibility of TiO_2 grown by PMCS. The films have shown a very good mechanical stability in biological environments for time compatible with standard cellular culture. Moreover, the surface investigations proved how the wettability of the films was inversely proportional with the increasing of percentage of oxygen in the mixture gas using during the growth. This is probably related to the greater presence of the sesquioxide in this type of PMCS film. Even if this feature did not affect the quality of the culture with both standard cellular lines and neurons, the latter electrical activity seems to be higher for the 0% TiO_2 film. A possible explanation could be in the greater adhesion of PDL on this surface, leading to a stronger interaction with the extracellular membrane of the neurons.

Finally, it is worth noting the low biocompatibility vs. neuronal growth of metallic platinum surfaces. This could be a great deal for the realization of the hybrid memristor-neuronal tissue system if necessity of both bottom and top electrode device are required. The use of a different metal for top electrode would lead to different memristive properties, an unacceptable condition that would further widen the research activities. However, the ability of TiO_2 film by PMCS to work properly and reliably also without deposition of a top electrode is the best feature to solve this problem.

Starting with these significant and promising results, the realization of a hybrid memristor-neuron system can be carried on.

Chapter 8
Study of PMCS TiO_2 – neuronal culture hybrid system

The most challenging and fascinating goal of this thesis work is the realization of a hybrid system, in which a neuronal culture and an array of TiO_2 memristors could actively communicate each other. In particular, the idea is that the electrical stimuli from the biological system could be able to modify the memristive behavior of the TiO_2 thin film and/or induce adaptation of neurons by pulses given through the memristor channel. In literature, Gale et al. [32] proposed an unconventional electronic system where memristive devices and neuronal culture were able to communicate each other. However, starting from a Multi Electrode Array (MEA) where neurons are grown, memristors are connected in an external circuit where electrical stimuli occur (Figure 8.1), and not directly interfaced with the organic tissue.

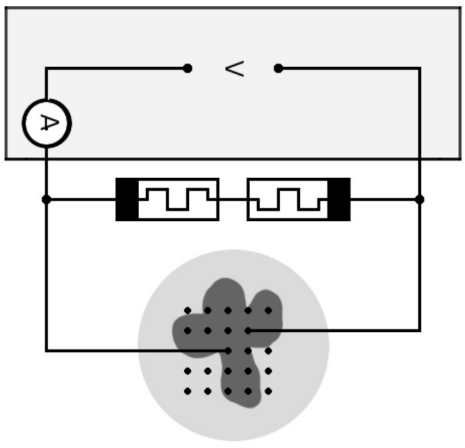

Figure 8.1: Experimental scheme for studying of neuronal networks and memristors using MEA [32].

We propose an innovative system where electronics and neuronal culture are integrated, creating an active inorganic/organic interface where neuronal tissues are grown on memristive devices, previously prepared and electroformed. Here it will be described the main steps for the realization of the device and the first preliminary test, useful to evaluate the feasibility of the hybrid system.

8.1 Design of the hybrid system

A deep study was performed in order to realize a suitable system, where both electrical response of the memristors and the neurocompatibility behavior of the neuronal cells were ensured. The challenging and final purpose was to evaluate if and how an electrical stimulation from the neuronal culture grown on the memristive material could change/switch the electrical state of the device (from higher resistivity or lower resistivity o vice versa), and conversely if electrical stimuli coming from the memristor device are able to be read by the neurons.

A PMCS TiO_2 thin film grown using 0% O_2 mixture gas was chosen due to better features obtained by the first electrical physiological tests (see Chapter 7) and the good memristive response (see Chapter 6). The building of the hybrid system required different phases that will be described in the following.

8.1.1 Memristive material

For this experiment, it was used a specific 10mmx10mm quartz substrate, on which 32 Cr/Au/Pt dots (300µm diameter) were deposited by evaporation, as showed in Figure 8.2. Each dot had a passivated gold guide that permits the collection of the signals far from the main electrode area, avoiding formation of further electrical contacts with every kind of tissue or material deposited on the top of the substrate.

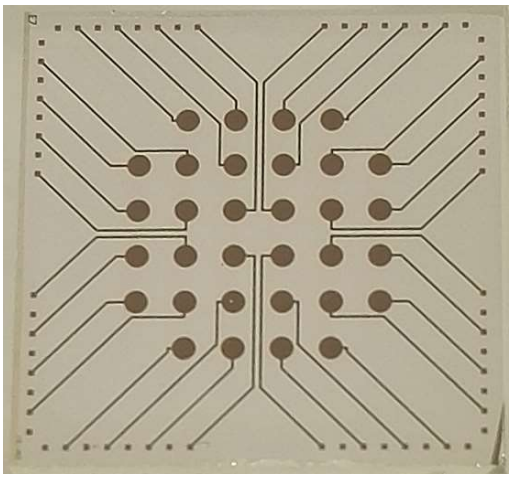

Figure 8.2: 10mmx10mm quartz substrate, on which 32 large dots Cr/Au/Pt are deposited.

A 50nm TiO_2 thin film was then grown by PMCS technique on the previously shown substrate, using the carrier gas mixture with 0% of oxygen and coating part of the patterned circuits, in particular the dots (Figure 8.3).

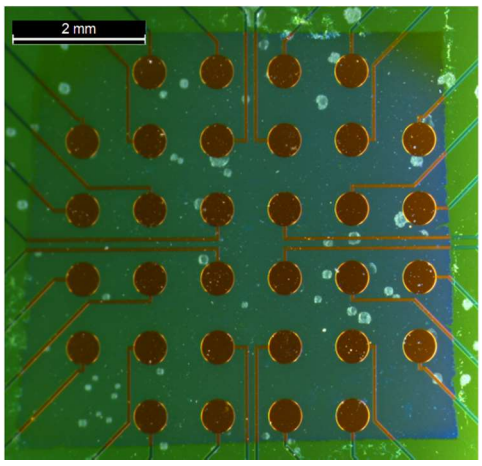

Figure 8.3: PMCS TiO_2 on Pt dots array.

As described in Chapter 6, PMCS TiO_2 thin films do not allow the reliable realization of a standard MIM memristive structure due to the formation of shorts with the bottom electrode.

This, in turn, resulted in being an advantage for the application pursued in this last chapter: the realization of memristor properly working also without any top metal electrode has been possible, a metal electrode that should have been removed in order to grow neuronal tissues after electroforming and I/V testing measurements. In fact, platinum biocompatibility does not enable neuronal growth, as described in paragraph 7.3.

Hence, in order to achieve the desired and necessary memristive properties, a single memristor was realized on each dot using the electroforming procedure described in paragraph 6.1. Every memristor was characterized and left in a specific resistivity states: high resistance state (R = 10-100kΩ), low resistance state (R= 0.1 -1kΩ), short circuit state (R = 12-15Ω), with the first and second ones corresponding to OFF and the ON memristor conditions (see Figure 8.4), the last to the resistance value right after the electroforming.

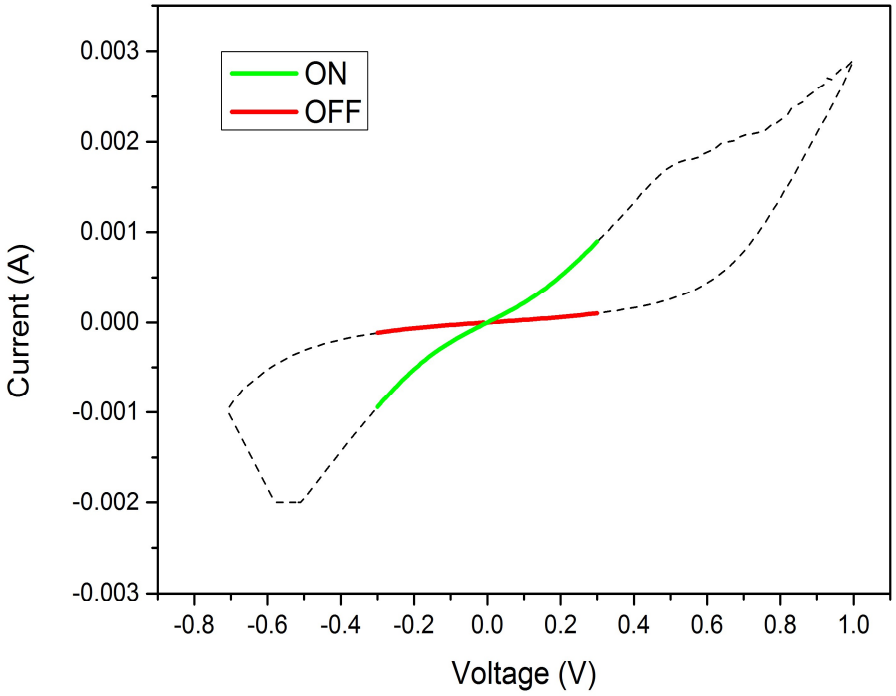

Figure 8.4: Representative I-V curve of PMCS TiO_2 for hybrid system.

To make the electrical activation procedures easier, the substrate was installed on a specific larger chip holder and each memristor/dot was bonded to an external electrode by using a gold wire.

8.1.2 Preparation of the substrate for the neuronal culture

A homemade petri was designed and applied on the surface of the chip, as shown in Figure 8.5. The petri structure was composed of a first polymeric cylinder, with a height of about 4mm and empty internal part leaving exposed the PMCS film on the dots chip. It was bonded by PDMS directly to the main chip surface, a polymer normally used in biological environment for absence of toxicity effect for the cells, in order to grant the water tightness for future neuronal growth without altering the TiO_2 film biocompatibility. Than a larger one, with a shape of a perforated normal petri with a height of about 15mm and external diameter of 30mm was stuck together with the polymeric cylinder, always by using a small amount of PDMS. Moreover, the external part of the polymeric petri was cut to simplify the electrophysiological tests by patch clamp. In this way, it was possible to properly create the best environment for neuronal growth as well as be able to perform electrophysiological experiments on the same chip.

It is worth noting how the chip holder (green square in Figure 8.5) was previously drilled in the center, in order to enable illumination from the bottom side to properly observe the quality of the neuronal culture by standard microscope.

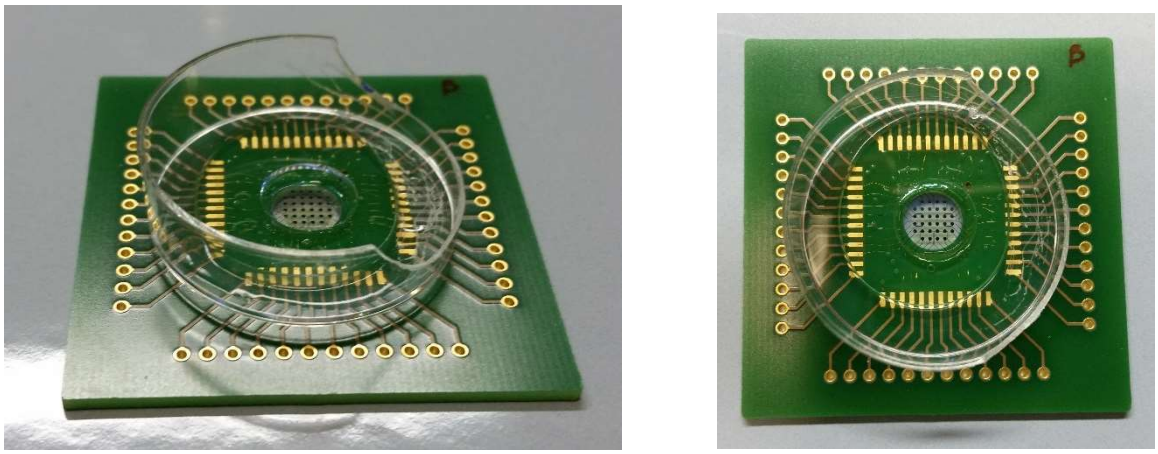

Figure 8.5: Hybrid system device.

8.1.3 Neuronal culture for the hybrid system

For the neuronal growth on PMCS film, the same protocol proposed in Chapter 7 was adopted. A neuronal culture was grown on the poly-D-lysine (PDL) coated PMCS TiO_2 in the homemade petri. As was expected from the previous neurocompatibility, also in this new configuration the viability and the proliferation of the culture turned out to be high and promising for this purpose. Indeed, after only 5 days it was possible to observe a good neuronal network. Figure 8.6-8.8how the progressive increasing of connections at 2, 3 and 5 days respectively. In order to further improve the interconnection of the neurons and consequently the intensity of the electrical activity of the neuronal network, the cellular growth was prolonged up to 21 days. As can be clearly seen in figures, the back illumination enable easy optical imaging around the dots, but not on them due to the metal coating darkening light.

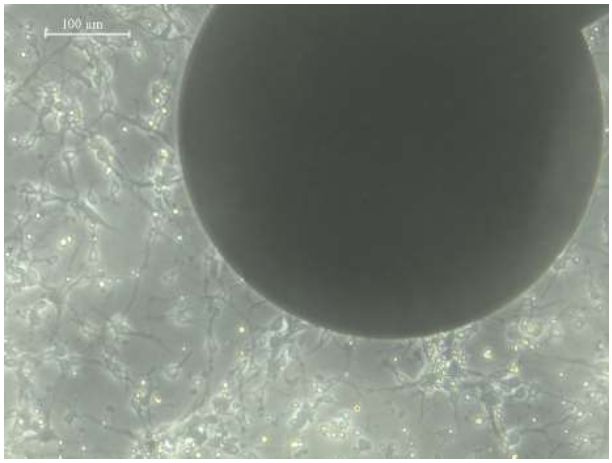

Figure 8.6: Neuronal cell grown on hybrid device (2DIV).

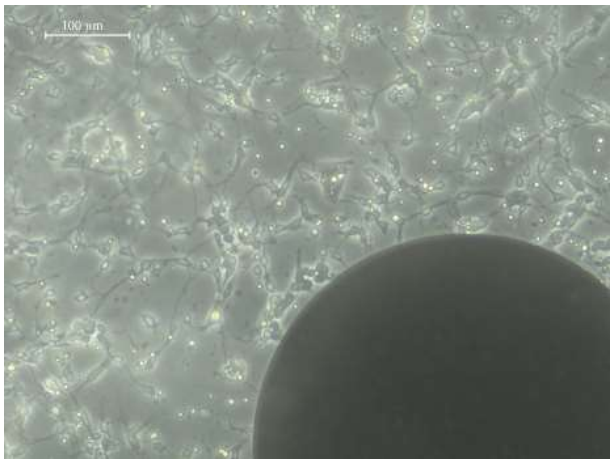

Figure 8.7: Neuronal cell grown on hybrid device (3DIV).

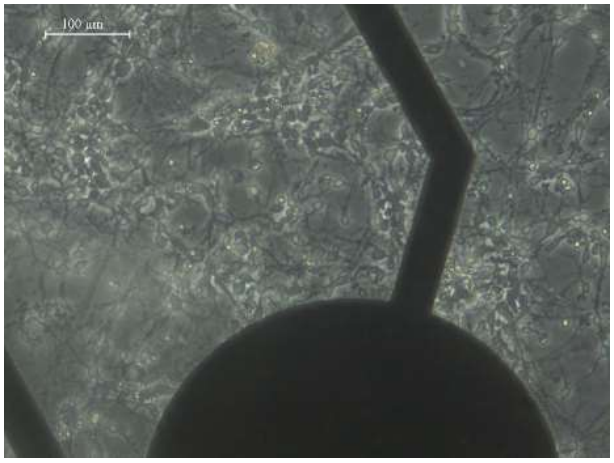

Figure 8.8: Neuronal cell grown on hybrid device (5DIV).

8.2 Preliminary tests

The preliminary tests on the innovative hybrid system were performed by patch clump in standard air (CO_2 = 0.03%) at room temperature (20°C), in an environment that is not the one used for the tissues growth. As already mentioned in paragraph 7.4, the temperature and the CO_2 percentage in the atmosphere are by far lower than the 37°C and CO_2 = 5%, unfortunately leading to a progressive inactivity of the neuronal cells. Thus, all measurements had to be carried on within 90 minutes after the extraction of the hybrid

system from the standard culture environment. Obviously, after two hours all neuronal tissues are lost and dead. This is a related to the difficulties in joining different research activities that need highly different working conditions, difficulties that have been overcome by a precise organization and time scheduling of all activities.

Two different methods can be employed to test the active communication between the memristive system and the neuronal culture:

1. the activations of the bottom electrode by increasing voltage and the relative measurement of the neuronal activity of the cells grown on that specific dot, by collecting signal from the patch clamp probe;
2. the excitation of the neuronal system by chemical or electrical stimuli, as the patch clamp probe, and the measurement of electrical signals through the memristor by collecting signal from the bottom electrode

As suggested, the preparation of this set up required involvement of all group in the Madelena project and several researches before defining the best TiO_2 materials, the proper chip design, memristor preparation and final neuronal culture. This is indeed the final step of three years of activities in different science fields, that will go on also during 2017. Here will be presented the first preliminary results.

In this test, the first method was used, in order to obtain also reliable information concerning the feasibility of the hybrid system. The experiment was performed on three dots chosen for the particular good quality of neuronal culture grown on them. As a control, the same procedure was applied on the neuronal culture grown on chip without the presence of the PMCS TiO_2 thin film.

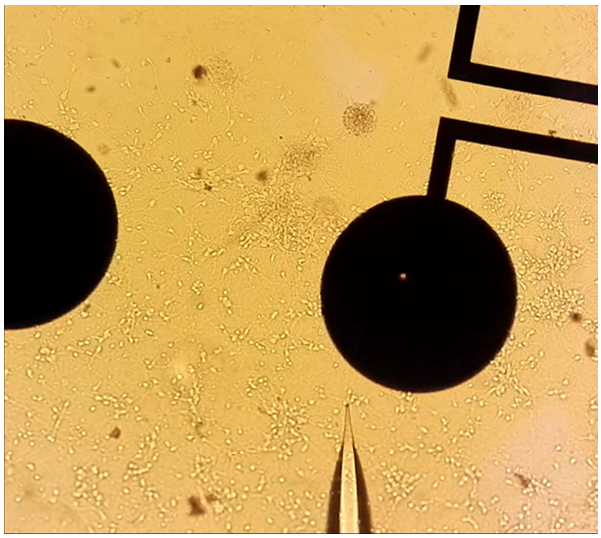

Figure 8.9: Configuration of the experiments. The patch clump (pipette on the bottom) collects the signal of the neurons excited by external stimuli from the electrode (black dot).

The whole cell culture of one neuron was measured through the patch clamp technique (Figure 8.9). An external stimulus protocol from + 100mV to -2V was applied on the nearest electrode (Figure 8.10), where a memristor left in the ON state was present.

First results showed an interesting behavior (Figure 8.11). The presence of a PMCS TiO_2 thin film in the hybrid device induced a train of spontaneous activity of the neuron excited by an external application of voltage. In particular, it was observed in a detailed view the action potential current of the cells. This phenomenon was not recorded in the control chip, where TiO_2 was not present.

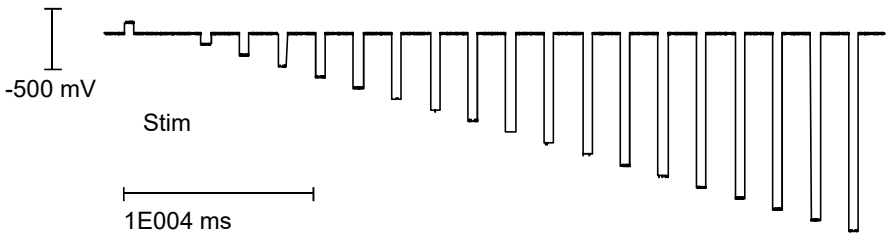

Figure 8.10: Sequence of applied pulse.

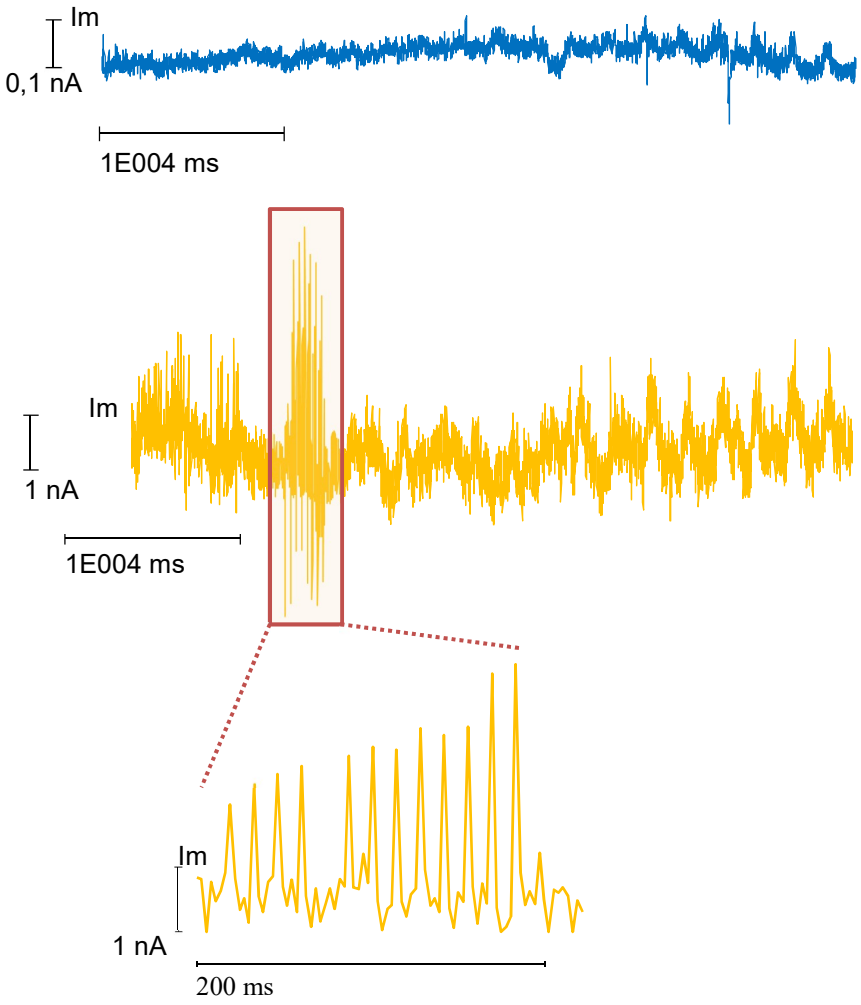

Figure 8.11: Neuronal response activated by external stimuli through the PMCS TiO_2 thin film. On device without TiO_2 (Blue line). On device with TiO_2 (yellow line).

Unfortunately, the time required to properly set the patch clamp system was higher than expected, and no further reliable data have been achieved. This means that the influence of the memristor state cannot be discussed, as well as the possibility to work in a different stimulating approach.

As a preliminary experiment, these promising results make this hybrid device an effective system for the realization an active interface between memristive inorganic world and biological environment.

8.3 Conclusions

The realization of a hybrid device where memristor devices can actively send and collect signal, stimuli from a neuronal tissues has been achieved. Exploiting all results achieved in this work, described in the previous chapters, a system based on a suitable MEA structure with platinum dots with a 50nm TiO_2 0% PMCS film deposited on the top has been used as substrate for neuronal tissue growth. This has been achieved after electroforming (and characterization) of one single memristor on each dot. Leaving the devices in three different conditions, namely ON and OFF memristive states and very low resistance, typical of the conductive channel after electroforming step, an electrical impulse has been applied to the bottom electrode. The electrical signal has been successfully recorded from the patch clamp probe, located on neurons close to the electrode itself where a memristor in the ON state was present.

The time required to properly set the whole experimental apparatus was higher than expected, and no further data have been achieved. What is clear is that the proposed scheme for the hybrid system is viable and suitable for further experiments, as well as that information acquired in this first fundamental analysis will help also in improving the overall reliability.

Chapter 9
Conclusions and perspectives

The main aims of this work were to evaluate TiO_2 thin films, synthesized by Pulsed Microplasma Cluster Source (PMCS), for realization of devices showing memristive response and that could be used in a neuron-memristor hybrid system, where biological system and electronics could interact each other. Undoubtedly, to reach these goals, a multidisciplinary approach was mandatory in order to understand all the scientific aspect involved in this work, starting from the synthesis of the material to its final application. This work has been developed within the first part of Madelena, a four years project where different partners are involved, with skills from materials science to electronics and biology. There is a coincidence of purposes between Madelena and this thesis work, but of course, the project will produce the final results during 2017. As described in the previous chapters, important objective have been achieved that are propaedeutic for the Madelena aims and have clearly shown the feasibility of the most challenging issue, the realization of a hybrid neuronal system.

In order to achieve the necessary reliability and reproducibility to synthesize TiO_2 films for electronic devices, important development of the PMCS deposition technique was carried out at IMEM-CNR of Trento. This PMCS used supersonic pulsed beams seeded by clusters of the metal oxide synthesized in a plasma discharge. The study of the pulsed beam showed how it was intrinsically inhomogeneous, a feature that led to film with noticeable inhomogeneity too. By a tough optimization of the deposition process, based on an great number of tests and several changes in the hardware and the parameters of the deposition, it has been possible to synthesize TiO_2 thin films having suitable, controlled and reproducible properties. In particular, roughness, porosity and grain mean size has been significantly reduced with respect to previous studied led by the same deposition machine.

The choice of the carrier gas employed during the deposition process resulted to be crucial. In this work, three helium mixture gases were used with increasing percentage of oxygen (0%, 0.1% and 1.0% O_2). The final stoichiometry of the TiO_2 thin films can be tuned with the gas mixture, achieving stoichiometric for 0% and 0.1%, overstoichiometric for 1.0%. In general, all PMCS thin film showed an anatase TiO_2 structure, grain dimension size lower than 20nm and average roughness of about 3nm. The chemical properties clearly show that when oxidation occurs during the synthesis process inside the PMCS source, TiO_2 is formed also with presence with oxygen overstoichiometry, probably related to interstitial oxygen atoms. Also, when oxidation of a metallic film occur in atmosphere a stoichiometric TiO_2 is achieved, but there is a significantly higher presence of the sesquioxide, Ti_2O_3.

Concerning the memristive application, this is the first work in which PMCS nanostructured TiO_2 thin films were employed. After a long testing period, it was established a suitable protocol for electroforming (EF) the material and make it memristive. Using as top electrode (TE) a Pt wire, all the PMCS TiO_2 have shown a significant memristive response, modulated by the intrinsic chemistry of the material. In particular by increasing of the percentage of oxygen in the matrix, both resistances (ON state and OFF state) and the voltage switch increases. Moreover, the I_{compl} and V_{reset} were evaluated being the two main parameters to modulate and control the memristive response. The realization of a standard metal-insulator-metal (MIM) structure, with platinum dots as TE deposited on the TiO_2 films resulted to be a hard task, due to formation of electrical shorts related probably to a residual porosity in the film, an intrinsic characteristic of PMCS approach. Nevertheless, a device has been realized showing same main electrical properties, with device life as long as 1000 cycles.

An important study on over 100 thin films has been carried on the biocompatibility and neurocompatibility of TiO_2 grown by PMCS, in collaboration with two important partner of the MaDEleNa project, such as FBK labs and CiBIO labs. In the preliminary biological test, all the films grown adopting the optimized deposition process have shown a very good mechanical stability in biological environments. The surface investigations proved how the wettability of the films was inversely proportional with the increasing of percentage of oxygen in the mixture gas using during the growth. This is probably related to the greater presence of the Ti_2O_3 in this type of PMCS film, especially in the 0% O_2. Furthermore, all the PMCS TiO_2 thin films guaranteed consistent biocompatibility. As expected,

neurocompatibility has been achieved only after surface coating with poly-D-lysine (PDL), a specific polyamino acid facilitating the attachment of cells and proteins to solid surfaces. All surfaces have shown good results, but best were for the 0% film. The electrophysiological measurements demonstrated how electrical activity of the neuronal culture grown on TiO_2 films, after seven days, seems to be higher for the 0% TiO_2 film. A possible explanation could be in the greater wettability and adhesion of PDL on this surface, leading to a stronger interaction with the extracellular membrane of the neurons.

In this thesis, both of the most important requirements for the realization of a memristor-neuron hybrid device were reached. Starting with these significant and promising results, a prototype of PMCS 0% TiO_2 hybrid device was designed and realized. It is based on a multi electrode array (MEA) on top of which a 0% TiO_2 film has been deposited by PMCS. Each MEA dot had a memristor, left in different resistance states. A modified petri positioned on top of the MEA chip enabled the neuronal culture. As expected from the previous studies, also in this case both the memristive response and the neural culture showed interesting results. In the preliminary electrophysiological tests, it was possible to observe how the presence of TiO_2 increases the spontaneous electrical activity of the neuronal network when the memristor is activated by external applied voltage. However, the time required to properly set the patch clamp system was higher than expected and no further reliable data have been achieved. This means that the influence of the memristor state (ON, OFF, low resistance) cannot be discussed, as well as the possibility to work in a different stimulating approach.

In conclusion, in this thesis it was demonstrated the possible use of the PMCS deposition technique as a valid method to grow nanostructured TiO_2 thin films for memristive and biological applications. Additionally, a first prototype of hybrid device based on this metal oxide was proposed as an important first step towards the realization of a neuromorphic bio-inspire system.

The relevant results achieved give answers to scientific problems that were known, but not still solved. First, in order to realize a memristive device based on MIM structure several further improvements in the control of the thin film porosity will be necessary.

Consequentially, a more accurate and systematic study of the memristive response can be performed. Moreover, new different studies on the electrical behaviors of different PMCS TiO_2 thin film have to be carried on by using, e.g., conductive AFM, that can give a great contribution on the comprehension of the mechanism involved in the resistance switching. In the same direction, the use of planar structure of the electrode in the PMCS memristive devices could give significant information about the formation of CF during the EF, indicating possible improvements towards the realization of a more reliable and precise TiO_2 device.

Finally, a series of more significant analysis of the described hybrid system are already planned, to prove how PMCS memristive material is a suitable candidate for the realization of bio-inspired devices.

Appendix A: List of materials for biological tests

15mm diameter microscope glass slides (Marienfeld 01 115 50).

1X PBS (Phosphate Buffer Saline) pH7.4 (LifeTechnologies 10010-015).

Coating solution: 10µg/ml poly-D-Lysine hydrobromide (Sigma Aldrich P6407) in PBS.

1X EBSS: dilute 10X Earle's Balanced Salt Solution (Sigma Aldrich E7510) added with 2.2g/l of Sodium Bicarbonate (Sigma Aldrich). Filter 0.22µm to sterilize.

Protease inhibitor solution: 500mg of BSA (Sigma Aldrich A9418) 500mg Trypsin Inhibitor Chicken Egg White (Sigma Aldrich T9253). Dissolve in 50 ml EBSS. Filter 0.22µm to sterilize.

Plating Media: MEM+GlutaMax (LifeTechnologies 41090-101) completed with 10%FBS (LifeTechnologies 16140-071) and 1% PenStrep (LifeTechnologies 15140-163).

Dissociation Solution (papain solution): 30U of papain suspension (Worthington) diluted in 30mL of EBSS supplemented with 30µL of 0.5M EDTA and 50µl of 1M cystine HCl (Sigma Aldrich C8786) solution. The prepared mix has to be activated at 37°C for at least 20 minutes immediately prior to use.

DNase solution (Sigma Aldrich D5025).

Appendix B: Cell count and morphological analysis

All the steps are performed at room temperature and in each step a double washing with PBS has to take place. Coverslips and supports with 14 days in vitro neurons were washed with pre warmed HBSS (Sigma Aldrich) and cell were fixed in PFA 4% for 15 minutes at room temperature. Cells are treated with 0.1% TritonX100 in PBS for 5 minutes to permeabilize the membrane. Unspecific antibody binding sites are blocked by incubating the slides for 30 minutes in blocking solution 100X (2% FCS, 2%BSA, 0.2% fish skin gelatin, 10X PBS).

The samples are then incubated for 2 hours with the neuron specific anti-βIII-tubulin primary antibody (Sigma Aldrich T8578) diluted in blocking solution 10X. After this step, the slides are incubated with the anti-mouse IgG Alexa Fluor® 488 (LifeTechnologies A11017) fluorescent secondary antibody for 1.30 hours. To stain nuclei for counting, the cells were incubated for 5 minutes with DAPI and then mounted on microscope slides with Mowiol.

The images are acquired with a Zeiss Observer.Z1 microscope equipped with the Apotome module using the Zen Blue imaging software (Zeiss). The images are processed with the imaging software Columbus 2.4.2 (Perkin Elmer) to analyze the parameters used for the evaluation of neurocompatibility.

Appendix C: Cultures of primary murine neurons on PMCS TiO_2 films

The TiO_2 was deposed on glass microscope coverslips in order to test biocompatibility. The control for each analysis were neurons derived from the same tissues grown directly on glass coverslips. Prior to the seeding of cell lines and primary murine neurons, the PMCS-derived TiO_2 films and glass controls were washed with absolute ethanol, dried, rinsed with sterile deionized water and kept in sterile PBS from 5 to 10 minutes.

Cell lines were directly seeded on the sterile TiO_2 coated slides in DMEM medium supplemented with FBS, Glutamine and a mixture of Penicillin and Streptomycin. For murine cortical neurons, PBS was replaced with freshly made poly-D-Lysine coating solution and coating was finalized by incubating the samples for 30 minutes at 37 °C. The poly-D-Lysine solution was successively removed by washing several times with PBS, obtaining samples ready to host neuronal cultures.

Cortices were extracted from mouse embryos at stage E15.5 (15.5 days after mating), operating inside laminar flow hood to maintain sterility. Dissected cortices were kept in ice cold PBS solution to preserve neurons. The brain tissue was enzymatically and mechanically dissociated incubating with papain solution for 20 minutes at 37°C and gently pipetting up and down to separate the different components of the organ.

DNase solution was added to clear cell suspension from DNA contamination and cellular suspension was centrifuged at 1200 g per 5 min to pellet the cells. The dissociating solution was replaced with protease inhibitor solution to stop all proteolytic reactions. After a final centrifugation at 1200 g per 10 minutes, the cells were resuspended in plating medium pre-warmed at 37°C, counted to assess cell density and diluted to $3x10^5$ cell/ml. Neurons were then seeded on the substrates at a final density of 100×10^3 cell/cm^2 and kept in incubator at 37°C and 5% CO_2.

The following day the samples were inspected for cell adhesion and 50% of plating media was replaced with Neurobasal (LifeTechnologies 21103-049) supplemented with B27 (LifeTechnologies 17504-044) to support neuronal growth.

Partial medium replacement was performed twice a week. Within 14 days neurons grew and differentiated forming a fully-developed and physiologically active neuronal network. In order to obtain a neuron-enriched culture, Cytosine β-D-arabinofuranoside (Sigma Aldrich C1768) was added to the culturing medium at final concentration of 1μM: this reagent interferes with DNA replication and eliminates proliferating cells (e.g. glia and astroglia) leaving post-mitotic neurons unaffected.

Bibliography

[1] L. Chua: "Memristor - The Missing Circuit Element," IEEE Trans. Circuit Theory 18, 07, (1971).

[2] L. Chua: "Resistance Switching Memories Are Memristors," Appl. Phys. A – Mater. 102, 765, (2011).

[3] L. Chua and S. M. Kang: "Memristive Devices and Systems," Proc. IEEE 64, 209, (1976).

[4] D. Strukov *et al*: "The missing memristor found", Nature, vol. 453, pp. 80 – 83, 1154, (2008).

[5] J. J. Yang *et al*: "Memristive switching mechanism for metal/oxide/metal nanodevices", Nature Nanotechnology, vol. 3, pp. 429 – 433 (2008).

[6] L. Chua: "The fourth element", Proc. IEEE 100, 1920 (2012)

[7] L. Chua: "Memristor, Hodgkin–Huxley, and Edge of Chaos", Nanotechnology 24, 383001 (2013)

[8] L. Chua: "If it's pinched it's a memristor", Semicond. Sci. Technol. 29, 104001 (2014)

[9] Y.P. Ho *et al*: "Nonvolatile memristor memory: device characteristics and design implications", Proc. IEEE ACM. 485 (2009)

[10] D.H. Kwon *et al*: "Atomic structure of conducting nanofilaments in TiO_2 resistive switching memory". Nat. Nanotechnol.5(2), 148–153 (2010)

[11] C. Nauenheim *et al*: "Investigation of the electroforming process in resistively switching TiO_2 nanocrosspoint junctions", Appl. Phys. Lett.96(12) (2010)

[12] S.J. Song *et al*: "Identification of the controlling parameter for the set-state resistance of a TiO_2 resistive switching cell", Appl. Phys. Lett. 96(11) (2010)

[13] T.A. Wey and S. Benderli: "Amplitude modulator circuit featuring TiO_2 memristor with linear dopant drift". Electron. Lett.45(22), 1103-U8 (2009)

[14] X. Cao *et al*: "Forming-free colossal resistive switching effect in rare-earth-oxide Gd_2O_3 films for memristor applications". J. Appl. Phys.106(7) (2009)

[15] T. Driscoll *et al*: "Phase-transition driven memristive system", Appl. Phys. Lett.95(4) (2009)

[16] S.H. Jo *et al*: "Nanoscale memristor device as synapse in neuromorphic systems", Nano Lett.10(4), 1297–1301 (2010)

[17] M.D. Pickett *et al*: "A scalable neuristor built with Mott memristors", Nat Mater 12, 114–117 (2013).

[18] F. Pincella *et al*: "Electrical properties of an organic memristive system", Appl Phys A, 104:1039–1046 (2011)

[19] T. Berzina, et al: "Optimization of an organic memristor as an adaptive memory element", Journal of Applied Physics 105 (12) 124515 (2009)

[20] T.W.K. Dong Ick Son *et al*: "Flexible organic bistable devices based on graphene embedded in an insulating poly(methyl methacrylate) polymer layer", Nano Letters 10 (7) 2441(2010)

[21] A. Chanthbouala *et al*: "A ferroelectric memristor", Nat. Mater. 11, 860 (2012)

[22] D.J. Kim *et al*: "Ferroelectric Tunnel Memristor", Nano Lett. 12, 5697 (2012)

[23] X.B. Wang *et al*: "Spintronic Memristor Through Spin-Torque-Induced Magnetization Motion", IEEE Electron Dev Lett. 30, 294 (2009)

[24] M. Elshamy *et al*: "Comparative review of the TiO_2 and the spintronic memristor devices", CCECE Tech Dig. 1 (2014)

[25] B. Linares-Barranco and T. Serrano-Gotarredona: "Memristance can explain spike-timedependent-plasticity in neural synapses", Nature Precedings, 1–4 (2009)

[26] L. Chua *et al*: "Hodgkin-Huxley axon is made of memristors", Int. J. Bifurcat. Chaos 22 (3), 1230011 (2012)

[27] L. Chua *et al*: "Neurons are poised near the edge of chaos". Int. J. of Bifurcat. Chaos 11, 1250098 (2012)

[28] T.Prodromakis and L. Chua: "Two centuries of memristors", Nature Materials 11, 478–481(2012)

[29] H.Kim *et al*: "Memristor bridge synapses", Proceedings of the IEEE 100(6), 2061–2070 (2012)

[30] I. Ebong and P. Mazumder: “Memristor based STDP learning network for position detection” In Proceesings of 2010 International Conference on Microelectronics (ICM), pp. 292–295 (2010)

[31] G. Howard *et al*: “Evolution of Plastic Learning in Spiking Networks via Memristive Connections”, Evolutionary computation 22(1), 79–103 (2014)

[32] E. Gale *et al*: “Connecting Spiking Neurons to a Spiking Memristor Network Changes the Memristor Dynamics”, IEEE ICECS conf. proc. (2013)

[33] S. Girish Kumar: “Review on Modified TiO_2 Photocatalysis under UV/Visible Light: Selected Results and Related Mechanisms on Interfacial Charge Carrier Transfer Dynamics”, J. Phys. Chem. A, 115, 13211–13241 (2011)

[34] K. Zakrzewska: “Gas sensing mechanism of TiO_2-based thin films”, Vacuum, Volume 74, Issue 2, Pages 335–338, (2004)

[35] S. Iannotta *et al*: “Novel nano-hybrid gas sensor based on n-TiO_2 functionalized by phthalocyanines via supersonic beam co-deposition: performance and application to automotive air quality”, Proceedings of IEEE Sensors 2008, Article number 4716730, Pages 1498-1500 (2008)

[36] F. Siviero *et al*: “Hybrid n-TiO_2-CuPc gas sensors sensitive to reducing species, synthesized by cluster and supersonic beam deposition”, Sensors and Actuators B 126 214–220 (2007)

[37] A. J. Frank *et al*: “Electrons in nanostructured TiO2 solar cells: transport, recombination and photovoltaic properties”, Coordination Chemistry Reviews, Volume 248, Issues 13–14, Pages 1165–1179 (2004)

[38] N. Coppedè *et al*: “Solid state dye sensitized solar cells based on supersonic beam deposition of organic, inorganic cluster assembled, and nanohybrid materials”, Journal of Renewable and Sustainable Energy Volume 2, Issue 5, , Article number 053106, (2010)

[39] M. D. Earle: “The electrical conductivity of titanium dioxide”, Phys. Rev., vol. 61, pp. 56-62, (1942)

[40] D. C. Cronemeyer: “Infrared absorption of reduced rutile TiO_2 single crystals” Phys. Rev., vol. 113, pp. 1222-1226 (1959)

[41] N. Yu and J. W. Halley: “Electronic structure of point defects in rutile TiO_2” Phys.Rev. B, vol. 51, pp. 4768-4776 (1995)

[42] R. Williams: “How we found the missing memristor”, Spectrum, IEEE, 45(12):28-35 (2008)

[43] G. Park *et al*: “Observation of electric-field induced Ni filament channels in polycrystalline NiO_x film” Appl. Phys. Lett. 91, 222103 (2007)

[44] K. H. Choi *et al*: “Cost-effective fabrication of memristive devices with ZnO thin film using printed electronics technologies” Appl Phys A 106:165–170 (2012)

[45] R. Waser *et al*: “Redox-Based Resistive Switching Memories – Nanoionic Mechanisms, Prospects, and Challenges”, Adv. Mater., 21, 2632–2663 (2009)

[46] D.H. Kwon *et al*: “Atomic structure of conducting nanofilaments in TiO_2 resistive switching memory”, Nat. Nanotechnology. 5, 148–153 (2010)

[47] J.P. Strachan *et al*: “Direct identification of the conducting channels in a functioning memristive device”, Adv. Mater. 22, 3573–3577 (2010)

[48] B.J. Choi *et al*: “Resistance switching mechanism of TiO_2 thin films grown by atomic-layer deposition”, J. Appl. Phys.; 98-033715 (2005)

[49] J.J. O’Dwyer: “The theory of the electrical conduction and breakdown in solid dielectrics”, Clarendon press (1973)

[50] J.S. Lee *et al*: “Resistive switching phenomena: a review of statistical physics approches” Appl. Phys. Rev. 2, 031303 (2015)

[51] R. Waser *et al*: “Nanoionics-based resistive switching memories” Nat. Mater. 6, 833, (2007)

[52] T. W. Hickmott: “Low-Frequency Negative Resistance in Thin Anodic Oxide Films”, J. Appl. Phys. 33, 2669 (1962).

[53] A. Rose: “Space-Charge-Limited Currents in Solids”. Phys. Rev., 97, 1538–1544 . (1955)

[54] Y. Seo *et al*: “Conduction mechanism of leakage current due to the traps in ZrO_2 thin film”, Semicond. Sci. Technol Vol.24, Num.11 (2009)

[55] S. Kim *et al*: "Comprehensive modeling of resistive switching in the Al/TiO_x/TiO_2/Al heterostructure based on space-charge-limited conduction". Appl. Phys. Lett. 97, 2–4 (2010)

[56] K. Zheng *et al*: "TaO_x Based Resistive Switching Random Access Memor", ECS Solid State Lett. 3, Q36–Q39 (2014)

[57] R. Waser *et al*: "Redox-Based Resistive Switching Memories – Nanoionic Mechanisms, Prospects, and Challenges", Adv. Mater. 21, 2632 (2009)

[58] K. Nagashima *et al*: "Intrinsic Mechanisms of Memristive Switching", Nano Lett. 11, 2114 (2011)

[59] S.C. Chaw *et al*: "Random Circuit Breaker Network Model for Unipolar Resistance Switching", Adv. Mat. 20,1154 (2008)

[60] F. Miao *et al*: "Observation of two resistance switching modes in TiO_2 memristive devices electroformed at low current", Nanotechnology; 22:254007 (2011)

[61] E. Gale *et al*: "Aluminium Electrodes Effect the Operation of Titanium Oxide Sol-gel Memristors," arXiv:1106.6293v1

[62] C. Yoshida *et al*: "High speed resistive switching in Pt/TiO_2/TiN film for non volatile memory applications", Appl. Physic. Lett; 91:223510 (2007)

[63] W.G. Kim *et al*: "Effect of post annealing on the resistive switching of TiO_2 thin film", Microelectron Eng, 86:2153 (2009)

[64] W.G. Kim *et al*: "Effect of the top electrode material on the resistive switching of TiO_2 thin film", Microelectron Eng, 87:98 (2010)

[65] E. Gale: "Drop-coated titanium dioxide memristor", Material chemistry and physics, (2014)

[66] D. Navaneethan *et al*: "Fabrication of TiO_2 thin film memristor device using electrohydrodynamic inkjet printing ", Thin Solid Films 520 5070–5074 (2012)

[67] E. Verrelli *et al*: "Forming-free resistive switching memories based on titanium-oxide nanoparticles fabricated at room temperature", AIP vol. 102, 2 (2013)

[68] J. D. Kim *et al*: "Investigation of analog memristive switching of iron oxide nanoparticle assembly between Pt electrode" AIP vol. 114, 22 (2013)

[69] H.Y. Jeong *et al*: "A low-temperature-grown TiO_2-based device for flexible stacked RRAM application", Nanotechology , 21:115203 (2010)

[70] M.J. Cardillo: "Of Vacuum Science and Technology" 15, 423 (1978)

[71] G. Scoles: "Atomic and Molecular Beam Methods", Oxford University Press, Oxford (1988)

[72] P. Milani and S. Iannotta: "Cluster Beam Synthesis of Nano-structured Materials", Springer-Verlag, Berlin (1999)

[73] W. Gerlach and O. Stern: "Der experimentelle Nachweis der Richtungsquantelung im Magnetfeld" Z. Physic 8, 110, 9, 349, (1922)

[74] A. Kantrowitz and J. Grey: "A High Intensity Source for the Molecular Beam. Part I. Theoretical" Rev. Sci. Instr. 22, 328 (1951)

[75] E.W. Becker and K. Bier: "Zeitschrift Fuer Naturforschung A", 9, 975 (1956)

[76] E.W. Becker and W. Henkes: "Geschwindigkeitsanalyse vonLaval-Strahlen" Z. Physik. 146, 320 (1956)

[77] O. Hagen and W. Henkes: "Untersuchung der thermischen Relaxation bei Düsenströmungen durch Analyse der gaskinetischen Geschwindigkeitsverteilung", Zeitschrift Fuer Naturforschung A 15, 851, (1960)

[78] J.B. Anderson: "Molecular Beams and Low Density Gas dynamics", edited by P.P. Wegener, New York, Dekker (1974)

[79[A. Graham and J.P. Toennies: "Quasielastic Helium Scattering Studies of Surface Diffusion: The Diffusion Barrier", Surf. Sci. 427, 1 (1999)

[80] T.Toccoli *et al*: "Growth of titanium dioxide films by cluster supersonic beams for VOC sensing applications", IEEE Sensors Journal, 3:199, (2003).

[81] T. Toccoli *et al*: "Nanostructured TiO2 Thin Films Prepared by Supersonic Beams and their Application in a Sensor Array for the Discrimination of VOC", Proceedings of IEEE Sensors Volume 1, Issue 1, pages 647-650, (2002)

[82] O. Hagena and W. Obert: "Cluster Formation in Expanding Supersonic Jets: Effect of Pressure, Temperature, Nozzle Size, and Test Gas" J. Chem. Phys., 56:1793 (1972).

[83] K. Wegner *et al*: "Cluster beam deposition: a tool for nanoscale science and technology: J. Phys. D 39, R439-R459 (2006)

[84] L. Ravagnan *et al*: "Cluster-beam deposition and in situ characterization of carbyne-rich carbon films". Phys Rev Lett.; 89(28 Pt 1):285506 (2002)

[85] L. Diederich *et al*: "Supercapacitors based on nanostructured carbon electrodes grown by cluster beam deposition", Applied Physics Letters, 75, 2662 (1999).

[86] F. Bisio *et al*: "Optical properties of cluster-assembled nanoporous gold films", Phys. Rev. B 80, 205428 (2009)

[87] E. Barborini et al: "Nanostructured TiO_2 films with 2eV optical gaps", Advanced Materials, 17, 1842 (2005).

[88] S. Iannotta *et al*: "Organic, cluster assembled and nano-hybrid materials produced by supersonic beams: growth and applications to prototype device development", NSTI-Nanotech 2005, ISBN 0-9767985 1-4 vol. 2 (2005)

[89] T. Mazza *et al*: "Libraries of cluster-assembled titania films for chemical sensing", Applied Physics Letter 87, 103108 (2005)

[90] R. Carbone: "An Advanced Application of Protein Microarrays: Cell-Based Assay for Functional Genomics", Methods in Molecular Biology 570, Chapter 19. Humana Press (2009)

[91] R. Carbone *et al*: "Characterization of cluster-assembled nanostructured titanium oxide coating as substrate for protein arrays", Anal Biochem.; 394(1):7-12 (2009)

[92] L. Giorgetti *et al*: "Adsorption and Stability of Streptavidin on Cluster-Assembled Nanostructured TiO_x Films", Biophysical Journal, Volume 96, Issue 3, Pages 50a-50 (2008).

[93] R Carbone *et al*: "Biocompatibility of cluster-assembled nanostructured TiO_2 with primary and cancer cells", Biomaterials. (17): 3221-9 (2006)

[94] C. Ress *et al*: "Comparative Bioaffinity Studies for In-Vitro Cell Assays on MEMS-Based Devices", Sensors and Microsystems Volume 54 of the series Lecture Notes in Electrical Engineering pp 83-87 (2009)

[95] L. Abad *et al*: "Performance of a solenoid driven pulsed molecular beam source", Rev. Sci. Instrum. 66, 3826 (1995)

[96] S.Hüfner: “Photoelectron Spectroscopy”, Springer-Verlag, Berlin, 1995.

[97] J. Chastain and R.C. King: “Handbook of X-Ray Photoelectron Spectroscopy”, Ed. Physical electronics Inc., USA (1992)

[98] T.W. Collette and T.L. Williams: “The role of Raman spectroscopy in the analytical chemistry of potable water”, J. Environ. Monit. 4, 27 (2002)

[99] D.C. Koningsberger and R. Prins: “X-ray Absorption: Principles, Applications, Techniques of EXAFS, SEXAFS and XANES” ,Wiley, New York, (1988)

[100] G. Bunker: “Introduction to XAFS”, Cambridge University Press, Cambridge (2010)

[101] P. Piseri *et al*: “Manipulation of nanoparticles in supersonic beams for the production of nanostructured materials”, Solid state and Material Science 8, 195-202 (2004)

[102] P. Piseri *et al*: “Production and characterization of highly intense and collimated cluster beams by inertial focusing in supersonic expansions”, Review of scientific instruments volume 72, number 5 (2001)

[103] Y.L. Dua *et al*: “Variable-temperature Raman scattering study on anatase titanium dioxide nanocrystals”, Journal PCS (2006)

[104] M. C. Biesinger, et al: “Resolving surface chemical states in XPS analysis of first row transition metals, oxides and hydroxides: Sc, Ti, V, Cu and Zn”, Applied Surface Science 257, 887 (2010)

[105] M.V. Kuznetsov *et al*: “XPS analysis of adsorption of oxygen molecules on the surface of Ti and TiN_x films in vacuum” J. Electr. Spectr. and Relat. Phenom. 58, 169 (1992)

[106] N Bundaleski *et al*: “Adsorption dynamics of water on the surface of TiO_2 (110)”, Journal of Physics: Conference Series 257, 012008 (2010)

[107] B. R. Chrcanovic *et al*: “Chemical and topographic analysis of treated surfaces of five different commercial dental titanium implants”, Materials Research. 2012; 15(3):372-382 (2012)

[108] L. Wang *et al*: "Local Fine Structural Insight into Mechanism of Electrochemical Passivation of Titanium" ACS Appl. Mater. Interfaces 8, 18608 (2016)

[109] R.R. Mohanta *et al*: "Ion beam induced chemical and morphological changes in TiO_2 films deposited on Si (111) surface by pulsed laser deposition", Applied Surface Science 325, 185 (2015)

[110] G. Cappelletti et al: "Nano-titania assisted photoreduction of Cr(VI). The role of the different TiO_2 polymorphs", Applied Catalysis B: Environmental 78, 193 (2008)

[111] M. Roy *et al*: "Photofunctionalization of Titanium: An Alternative Explanation of Its Chemical-Physical Mechanism", Plos ONE 11, 0157481 (2016)

[112] H. Yaghoubi *et al*: "Nanomechanical Properties of TiO_2 Granular Thin Films" ACS Applied Materials and Interfaces 2, 2629 (2010)

[113] M. V. Kuznetsov *et al*: "XPS analysis of adsorption of oxygen molecules on the surface of Ti and TiN_x films in vacuum", J. Electron Spectrosc. Relat. Phenom. 58, 169–176 (1992)

[114] M. Grodzicki *et al*: "TiO_2 thin films grown on SiO_2–Si(111) by the reactive evaporation method", Optica Applicata 43, 99 (2013)

[115] F. Detto *et al*: "Excitonic recombination in superstoichiometric nanocrystalline TiO_2 grown by cluster precursors at room temperature", Phys. Chem. Chem. Phys. 14, 5705 (2012)

[116] D. Kuscer *et al*: "The effect of the valence state of titanium ions on the hydrophilicity of ceramics in the titanium-oxygen system", Journal of the European Ceramic Society 28, 577 (2008)

[117] D.O. Scanlon *et al*: "Band alignment of rutile and anatase TiO_2", Nat. Mater. 12 798–801 (2013)

[118] F.M.F. De Groot *et al*: " $L_{2,3}$ x-ray-absorption edges of d^0 compounds: K^+, Ca^{2+}, Sc^{3+}, and Ti^{4+} in O_h (octahedral) symmetry", Phys. Rev. B. 41 928–937 (1990)

[119] F.M.F. De Groot *et al*: "Oxygen 1s x-ray absorption of tetravalent titanium oxides: A comparison with single-particle calculations", Phys. Rev. B. 48 2074–2080 (1993)

[120] H. C. Choi *et al*: "Size effects in the Raman spectra of TiO_2 nanoparticles", Vibrational Spectroscopy, Vol.37, Issue 1 (2005)

[121] S. O. Kucheyev *et al*: "Electronic structure of titania aerogels Soft x-ray absorption study", Phys. Rev. B 69, 245102 (2004)

[122] I. H. Inoue *et al*: "Nonpolar resistance switching of metal/binary-transition-metal oxides/metal sandwiches: Homogeneous/inhomogeneous transition of current distribution", Phys. Rev. B 77, 035105 (2008)

[123] R. Bruchhaus *et al*: "Memristive switched with two switching polarities in a forming free device structure" MRS Online Proceeding Library, 1337, 73-78 (2011)

[124] J. J. Ynag *et al*: "A family of Electrically Reconfigurable Nanodevices", Adv. Mater., 21, 3754–3758 (2009)

[125] F. Nardi *et al*: "Resistive switching by voltage-driven ion migration in bipolar RRAM. Part I: Experimental study", IEEE Trans. Electron Devices 59, 2461–2467 (2012)

[126] D. Ielmini: "Filamentary-switching model in RRAM for time, energy and scaling projections", International Electron Devices Meeting – IEDM'11 pp. 17.2.1–17.2.4 (2011)

[127] S. Yu and H. Wong, "A phenomenological model for the reset mechanism of metal oxide RRAM". IEEE Electron Device Lett. 31, 1455–1457 (2010)

[128] B. Gao et al: "Oxide-based RRAM: physical based retention projection", Proceedings of the European Solid State Device Research Conference, ESSDERC 2010 pp. 392–395 (2010)

[129] G. Baldi *et al*: "Optimization of Synthesis Protocols to Control the Nanostructure and the Morphology of Metal Oxide Thin Films for Memristive Applications", AIP Conf. Proc. 1648, 280002-1–280002-4 (2015)

[130] B. Chen *et al*: "Physical mechanisms of endurance degradation in TMO-RRAM", IEEE International Electron Devices Meeting (IEDM) (2011)

[131] I. Valov *et al*: "Nanobatteries in redox-based resistive switches require extension of memristor theory", Nat. Commun. 4, 1771 (2013)

[132] D. K. Owens and R. C. Wendt: "Estimation of the surface free energy of polymers", Journal of Applied Polymer Science, 13 (8), 1741–1747 (1969)

[133] A. Stalder *et al*: “Low-bond axisymmetric drop shape analysis for surface tension and contact angle measurements of sessile drops”, Colloids and Surfaces A: Physicochem. Eng. Aspects286, 92–103 (2006)

[134] O.P. Hamill *et al*: “Improved patch-clamp techniques for high-resolution current recording from cells and cell-free membrane patches”, Pflugers Arch. 391 85–100 (1981)

Acknowledgments

Foremost, I would like to express my sincere gratitude to my supervisors DR. Salvatore Iannotta and DR. Roberto Verucchi, whose knowledge, guidance and patience deeply enriched the experience of preparing this thesis, from the first experiments to the final writing.

Special thanks go to all the teams of research at the laboratories of IMEM-CNR in Trento and Parma, for their precious advice and encouragement during these 3 years PhD program. Their expertise on synthesis and characterization of inorganic materials has been of invaluable help to reach the obtained results and survive in the hardest moments. In particular, a special mention goes to Lucrezia Aversa, Claudio Corradi, Marco V. Nardi, Roberta Tatti, Melanie Timpel and Matteo Tonezzer from IMEM-CNR Trento, Giacomo Baldi, Silvia Battistoni, Alice Dimonte and Marco Pola from IMEM-CNR Parma who most of all helped me in this long path.

Moreover, I would like to thank deeply all the people involved in the biologist and bio-physic part, without them no cell and biological test would have grown and carried out on my materials. In particular Nicola Cornella, Aura Matilde Jiménez Garduño, Lorenzo Lunelli, Laura Pasquardini, Cecilia Pederzolli, Cristina Potrich and Alessandro Roncador.

I cannot forget to thank Paolo Bettotti (UniTN), for the precious advice during the long AFM sessions, Cristian Collini and Leandro Lorenzelli (FBK labs) to support me in the realization of the memristive devices and Valentina Prusakova (UniTN) for the new interesting collaboration on SolGel-PMCS hybrid devices.

I would also like to express my loving gratitude to my parents, my sister and my fiancée Alessia for their constant support and understanding, and to my friends all around the world for their smile and the many beautiful hours spent together in Trento, Parma and Paris.

Last but not least, the financial support by MaDEleNa project and PAT (Provincia Autonoma di Trento) is greatly acknowledged.